Master of Science Thesis

Preliminary investigation on NS-DBD Plasma Actuator
for active Flow Separation Control

Giuseppe Correale

13th December 2011

Faculty of Aerospace Engineering · Delft University of Technology

TU Delft

Preliminary investigation on NS-DBD Plasma Actuator
for active Flow Separation Control

Master of Science Thesis

For obtaining the degree of Master of Science in Aerospace Engineering at Delft University of Technology

Giuseppe Correale

13th December 2011

Faculty of Aerospace Engineering · Delft University of Technology

Delft University of Technology

Delft University Of Technology
Department Of
Aerodynamics

The undersigned hereby certify that they have read and recommend to the Faculty of Aerospace Engineering for acceptance a thesis entitled **"Preliminary investigation on NS-DBD Plasma Actuator"** by **Giuseppe Correale** in partial fulfillment of the requirements for the degree of **Master of Science**.

Dated: 13th December 2011

Head of department: _____
prof.dr.F. Scarano

Supervisor: _____
dr.ir. L.L.M. Veldhuis

Reader: _____
dr. S.J. Hulshoff

Reader: _____
M.Kotsonis,Msc

Reader: _____
prof.dr.A.Yu. Starikovskiy

...to the memory of little Dario.
Our love for him will never leave our hearts.

Summary

The results of a preliminary experimental research on a Nanosecond Dielectric Barrier Discharge Plasma Actuator are presented in this document. For carrying out such a research, experiments were performed in the low speed facilities of Delft University of Technology. Four wind tunnels and several data acquisition techniques have been used in order to investigate the physical actuation mechanism that a NS-DBD plasma actuator is able to achieve. Leading Edge Flow Separation Control has been demonstrated at a Reynolds number up to 3.3 millions, and with a Mach number about 0.3. Set-ups of tests like Schlieren or PIV and results of such tests have been shown and discussed in this report.

For industrial application the issue of applicability rose up. A scalability study has shown the capability of the NS-DBD Plasma Actuator of working on different scales. From a phenomenological study several actuation principles have been derived. Moreover, from the large data set that was obtained possible physical mechanisms that underlay the NS-DBD plasma actuation have been proposed.

The most remarkable results achieved are: maximum lift coefficient increased about 20% with respect to its theoretical maximum, stall angle delayed about 5 degrees, drag due to the wake reduced about 300% in a leading edge flow separated condition.

Eventually possible outlook and future research aimed to get the plasma actuator at an "industrial" stage is proposed.

This experimental study has been carried out as a joined project between Delft University of Technology and NEQLab Research BV. The first one supported the project with knowledge and facilities, the second one with technology, equipments and manpower.

Contents

List of Figures

Chapter 1

Introduction

The world of the flow control has shown important improvements over the past century and a lot of new concepts and devices have been developed in order to achieve a valuable enhancement of the aerodynamics performance of any application dealing with a fluid (gas or liquid) flow.

Reason for pushing the envelope in this field is that, anyhow, any flow control technique, while dealing with a flow, usually archives positive and negative effects on the aerodynamics performances. So basically a flow control application is a trade-off between positive and negative effects. This is a reason why there is not an unique optimized working strategy for any flow control application.

Any Aerodynamic device, outside the range of conditions where the flow is controllable with an overall positive effect, will experience a drastic reduction of its aerodynamics performance.

The energy expense required by an aerodynamic device depends on the aerodynamics conditions of the flow which it is dealing with. The final goal of the flow control is to reduce the energy required for the application under consideration. On the other hand any flow control technique requires energy itself in order to control the flow. So a trade-off in terms of energy is the difference between the energy saved applying flow control and the energy required from the flow control technique itself.

Very often flow control techniques require to add structural elements to the aerodynamics device under control which may increase the aerodynamics resistance that the body offers to the flow. These structural elements represent a continuous energy loss and they dissipate energy also when the flow does not need to be controlled and even if the energy trade-off gives a positive energy saving, it is felt that more energy could be saved.

So, in order to reduce the energy expense due to any flow control technique and the parasitic extra drag induced by additional structural elements aimed to control the

flow, researchers about flow control have moved in the direction of the active flow control.

With "Active flow control" are meant all those techniques devoted to control the flow only when it is required so adding extra drag elements or spending energy only when necessary; these techniques differ from "Passive flow control" by the fact that for the latter ones the expenses in terms of induced drag and energy are higher since they can never be "switched off". The downside of the "active flow control" techniques is that very often they require additional mechanism for being actuated which increase the complexity of the aerodynamics device, sometimes drastically.

Among the several active flow control techniques, developed over the years, the Dielectric Barrel Discharge (DBD) Plasma Actuator is one of those considered very promising since:

- simple constructive requirements
- not expensive
- no moving elements
- fast reactivity
- low parasitic drag
- low energy consumption

Actually there exist basically two different kinds of DBD plasma actuators: the AC-DBD plasma actuator driven by AC voltage waveform, which is also the most well-known one, and the NS-DBD plasma actuator driven by high voltage nanosecond pulses. The latter is the one under study and discussion in this document.

First the state of art about DBD plasma actuator in general will be presented as well as the physical aspects and limits of applicability that researchers have found during the past years. Then, following a theoretical approach, the reason why this subject has been selected for this study will be introduced and a possible physical mechanism for the actuation will be hypothesized.

Afterwards, the results of an experimental study will be presented, carried out on high lift devices like wind turbine airfoils and a discussion about all the observed phenomena will be carried out. First the experimental set-up will be presented and all the required equipment will be shown in details, together with a brief description of the facilities used for the different experimental campaigns. Moreover possible data corrections will be proposed. Then the data acquired from the experimental study will be presented not as a whole, but going through the chronological history of the research. Time by time it will be make clear how new observations have brought to the light new characteristics of the device under study and it will be discussed.

It will be also shown, and proven experimentally, that the NS-DBD plasma actuator could be scaled, which thing is very important in order to get the research at an "application stage".

With "application stage" it is meant the stage of a project where the research is basically over and the development of the device for an industrial application is started.

A physical mechanism of actuation will eventually be proposed trying to explain all the phenomena observed during the experiments; moreover a theoretical approach will be undertaken in order to define a conceptual working principle for the NS-DBD plasma actuator.

Last but not least a series of comments and possible industrial applications will be given and an outlook of some of them will be discussed.

The research has been carried out as a join project where TUDelft and NEQLab Research BV have been collaborating: the first one supporting the work with knowledge and facilities and the second one providing technology, equipments and man power.

The research itself has been roughly one year long and a CFD simulation has been carried out in parallel about NS-DBD plasma actuator by PhD student Ilya Popov. This CFD simulations have shown a very good agreement with all the observed phenomena. The results of this experimental work have been supporting the CFD research as well as the CFD results have been supporting the experimental research.

It has been observed during the research that the NS-DBD plasma actuator is capable to actively control the flow on high lift element such as airfoils reattaching the flow when experiencing flow separation. An effect has been observed on the drag which, in the best case, achieved a reduction about 300%. The best result with respect to lift enhancement is an increase of the lift coefficient about 20% of the theoretical maximum for the airfoil under investigation, and the critical stall angle has been moved to one about five degrees higher. The highest Reynolds number at which NS-DBD plasma actuator has been investigated is about 3.3 millions, on a medium scale model, in a low turbulence wind tunnel, with a velocity of the free stream flow up to 80 m/s. The scalability has been proven through a Schlieren test campaign. The results have shown how increasing the number of actuators the observed effect actually increase. Moreover thanks to Schlieren tests also other phenomena have been observed: the formation of two counter rotating vortex forming into the shear layer. Those observed phenomena greatly helped figuring out a possible physical mechanism of actuation.

Afterwards a closer look at the discharge region has been felt necessary so a PIV test campaign has been carried out, not only on an airfoil immersed into a 30 m/s flow, but also on a flat plate in still air. The results of the PIV tests also helped a lot in the physical understanding of the device under study. Moreover it also showed new peculiar characteristics of the NS-DBD plasma actuator. With this

set of data several effects of NS-DBD plasma actuator have been recognized and a combination of two of them, working together, is the core idea of the proposed physical mechanism of actuation.

In chapter two a background about flow control, either steady/unsteady and active/passive, is given. Then AC-DBD Plasma Actuator is introduced and typical results and mechanism of such a device is presented. Eventually NS-DBD Plasma Actuator is introduced. The state of art of this device is presented in details and some typical result is shown. In paragraph 2.5.2 the phenomenology of the nanosecond-pulsed actuator is discussed. This paragraph requires some special attention: in this section is discussed what is thought to be the principal phenomenology of NS-DBD Actuator.

In chapter three the several set-ups, equipments and facilities are presented.

In chapter four all the test results are presented. In chapter five a summary of all the results obtained is presented and a discussion about them is carried out. Moreover some conclusion is drawn out.

Eventually, in the last chapter possible outlooks of NS-DBD Plasma actuator are given together with ideas for a further investigation about ND-DBD Plasma Actuator.

Chapter 2

Background

The term "flow control" is referred to all those techniques meant to affect the character or the natural behavior of a flow during its development along a smooth surface, changing the natural disposition of the flow field. In the 1904 Prandtl [1], investigating the behavior of viscous flows, introduced as first the concept of Boundary Layer (BL). He explained the mechanism of the steady separation, and he showed some result about the flow control around a cylinder by suction at the wall, achieving a consistent boundary layer separation delay.

Basically the BL is that region of the flow field where the viscous effect cannot be neglected anymore. Physically, when the momentum of the BL cannot overcome the energy lost due to the skin friction and the adverse pressure gradient it does separate from the surface. In general, regardless to the kind of motion, the BL will always have the same characteristics in terms of energy content but, since different concept for flow control are required for different kind of flow motion, it will be distinguished between flow control for internal flows and flow control for external flows. This work focuses on the flow control for external flows. The flow control can have different tasks and, based on what it is meant for, it can be split in different subparts as it is shown in Fig.2.1 . It can delay or advance transitions from laminar to turbulent flow, or perhaps it suppresses or enhances turbulence. It could be used in order to prevent or provoke separation of the flow from a surface. It could lead to drag reduction, lift enhancement and even noise suppression.

In this work the task of preventing or delaying the separation of the fluid wall-bounded flow will be studied. Among the several kinds of flow separation the one on which this work is focusing is the leading edge separation, restricted to the incompressible flows. Moreover, flow control may be further divided into two big categories: Active Flow Control and Passive Flow Control. The difference between these two categories is that for the latter one the flow control is actuated by devices that are continuously working on the flow, even if it is not required, so Passive

Flow Control techniques are those which are always "turned on" and they cannot be "turned off" during the operational period of the aerodynamics device they are working on. On the other hand, for the former one, the control on the flow is actuated by devices that do not work continuously but they are activated by an user only when it is required, so the Active Flow Control techniques are those which could be "turned on and off" by an user, or by any feedback loop control, and they could be optimized a way further with respect to the passive techniques, such that a bigger improvement of the aerodynamics performances may be achieved.

Anyway it is important to underline how much any possible task of the flow control could affect all the others. As Mohamed Gad-el-Hak[2], in his book (Flow Control: Passive, Active and Reactive) underlines, an ideal method to control the flow that is simple, effective and inexpensive does not exist, and he did produce a drawing that graphically shows how the different tasks of the flow control could interact with each other. Such a scheme is proposed hereafter in the Fig.2.1.

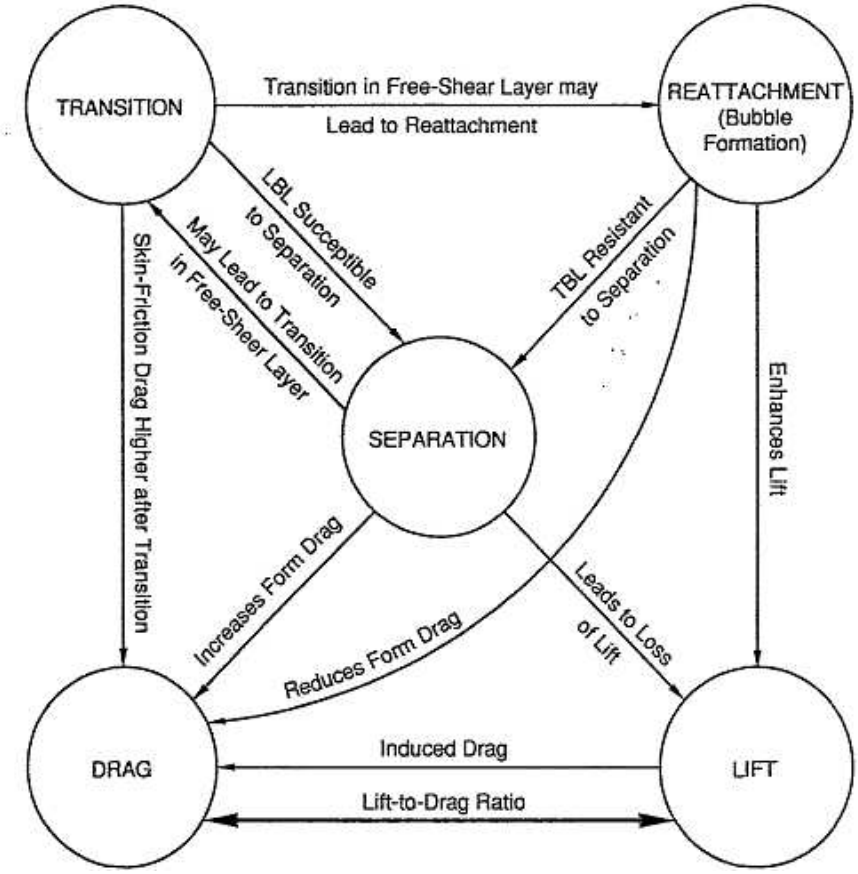

Fig. 2.1: Interactions of possible effects of any Flow Control technique[2]

As an example, BL of an external wall-bounded flow developing on a lifting surface, such as an airfoil, will be taken into consideration. If the BL is turbulent it will be more resistant to separation and then the incidence of the airfoil, with respect to the

free stream flow, could be increased thus enhancing the lifting performances. On the other hand the skin friction for a turbulent BL is a way bigger then a laminar one. The transition delay could lower the skin friction but it will keep the flow laminar for a longer period, and since the laminar BL can stand only to very small adverse pressure gradient the laminar BL will require a reduced incidence of the airfoil with respect the free stream direction. When the laminar BL separates, for a moderate Reynolds number, the free SL (Shear Layer) formed by the separation will experience transition to turbulent which may result in the reattachment of the separated flow and the consequent formation of a laminar separation bubble which reduces the possible optimal incidence of the airfoil and increase the drag, reducing also the lifting performance.

So the ultimate goal for the flow control in general is to be able to make a trade-off of all the interactions between the several effects of the actuation and eventually having as a result an effective increase of the lift-to-drag ratio.

2.1 Steady flow separation control

The research about the physical understanding of the phenomena that cause the separation of a wall-bounded flow have considerably advanced in the last 20 years. A detailed overview of all the techniques, active or passive, developed for Flow Separation Control is a massive task therefore, here in this document, it will be reported only about those devices consider related to the subject under study.

The main concept for controlling a wall-bounded external flow is that the velocity profile along the solid surface has to be kept "as full as possible", or mathematically it translate in keeping the second y-derivative of the velocity at the wall ($\frac{\partial^2 u}{\partial y^2}|_{y=0}$) as negative as possible.

Experimental studies have proved that methods using geometry modifiers, such as slats, flaps, or vanes, or perhaps constructing aerodynamics elements with special materials deformable under the action of pressure gradient, effectively affect the flow by a gradual mitigation of the adverse pressure gradient that the flow experiences moving downstream along the smooth surface, so basically archiving the goal of keeping the velocity profile "as full as possible", for example bodies can be designed for incipiently separated flow over large surface areas using the so called Stratford closure [3] [4].

A second technique that could be used in order to affect the velocity profile is based on suction at the wall or transpiration walls. As already mentioned, Prandtl [1] [5] put the basis for such kind of technique, developing also an approximation method to compute the amount of suction needed to prevent laminar separation. Other researcher over the years have improved the Prandtl method [7]. A particularly simple calculation, as an example, for a symmetrical Zhukovskii airfoil with uniform suction predicts a suction coefficient just sufficient to prevent separation of $C_q =$

$1.12Re^{-0.5}$ [6](where the Reynolds number is based on the airfoil chord and the free stream velocity). For turbulent BL semi-empirical methods have been found [8]. With such a method suction coefficients sufficient to prevent separation on a typical airfoil are in the range of $C_q = 0.002 - 0.004$.

Others techniques are based on thermal effect, since the temperature gradient in the flow field could affect the shape of the velocity profile. Such techniques are basically heat transfer at the wall. In a gas motions, subtracting heat from the fluid adds a negative contribution to the curvature of the velocity profile at the wall, so postponing the separation point. Nevertheless this method has been proved only for high-speed gaseous flows, analytically [9] [10] and experimentally [11] [12].

All the above mentioned methods are able to affect the velocity profile at the wall. This is clearly visible, from a theoretical point of view, just having a look at the stream-wise component of the momentum equation at the wall, in a steady case:

$$\rho v_w \frac{\partial u}{\partial y}|_{y=0} + \frac{\partial p}{\partial x}|_{y=0} - \frac{\partial \mu}{\partial y}|_{y=0}\frac{\partial u}{\partial y}|_{y=0} = \mu \frac{\partial^2 u}{\partial y^2}|_{y=0} \tag{2.1}$$

It is easy to recognize the first term on the left hand side of the equation 2.1 to be the suction-related term, the second one to be the pressure-related term and the third one the thermal-related term: as the equation shows that all these terms are able to affect the shape of the velocity profile.

If the fluid particles near the wall does not have enough momentum for continuing its motion it is brought to rest at its "Separation Point". This point is commonly recalled as the Goldstein's Singularity. In a steady situation a characteristic of this point is that both the velocity of the fluid and the shear stress at the wall are zero there.

2.2 Unsteady flow separation control

The unsteady separation is a much more complex phenomenon since it is characterized by different vanishing locations for the wall shear stress and the velocity at the wall [13] [14]. The concept to control this kind of flow separation is still the same with respect to the one used for steady separation case. The main difference with respect to the steady case is understandable just having a look at stream-wise component of the momentum equation at the wall, which reveals a time-related term, the unsteady term.

From this time-related term techniques are sought such that forcing disturbances are introduced in the flow motion, and, basing on the frequency of such forcing disturbance, flow control could be achieved.

Among the most used techniques it could be found pulsed suction/blowing systems, zero net mass flux systems, and more. The unsteady forcing has been proved to be more effective then the steady one [15] in fact an experimental study on different kind of airfoils has shown that an unsteady forcing is able to achieve an higher critical stall angle and a higher lift coefficient with respect to the case of steady forcing on the same models in the same aerodynamics conditions. A very important parameter for such kind of flow control is the operating frequency at which the technique works, the dimensionless number expressing such a frequency is the Strouhal number. It has been shown that the range of effective dimensionless frequencies related to the separation control is on the order of the unity. The Strouhal number is define ad:

$$St = f\frac{L}{U_\infty} \tag{2.2}$$

where f, L and U_∞ are respectively the forcing frequency, the characteristic length of the separated region and the free stream velocity [15] [16].

Physically, setting the Strouhal number to the unity means that a perturbation need to be introduced with a time scale such that it could be comparable to the time scale that the free stream needs in order to propagate along the separated region.

In an unsteady situation small disturbances introduced into the shear layer, produced by the separated BL, are amplified by nature if they are introduced very close to the receptivity point of the SL. This implies that the location of the actuator device could highly affect the result of the application. It has been observed that placing the actuator close to the separation point increases the chances to successfully introducing such perturbation, which provokes the formation of vortexes. Such three dimensional structures, developed as Kelvin-Helmholz instability, are able to transport momentum throughout the separated free stream region, therefore reattaching the flow [18].

For example a experimental study on forced reattachment of flow to an inclined flat surface, simulating a simple flap, shown that the excitation parameters determined the total duration of the reattachment process. Minimum reattachment time occurred at an optimal excitation frequency of $F^+_{opt} \approx 1.5$, which was independent of amplitude and flap inclination. The control over the process was achieved by enhancing large spanwise vortices in the flow. Spatial amplification of consecutive vortices induces mean transport of fluid away from the flap surface which causes the main stream to reattach [17].

Flow separation control techniques using an higher order of magnitude of the dimensionless frequency are supposed to work with a different actuation mechanism, so they are classified as a different kind of techniques.

2.3 Active flow separation control

Active Separation Control Techniques have gained a big interest in the last decade since their big potential: they are able to achieve and to enhance the results gotten by Passive Techniques without the expenses in terms of energy and induced drag one should pay using those techniques. On the other hand an active flow control technique might require mechanical elements which would increase the complexity of the aerodynamics device too much. Dealing with this two aspects of the active flow separation control, researchers nowadays are pushing the envelope in the direction of techniques able to achieve an active flow control trying to reduce at the minimum the complexity of the system.

Such a device could be the Dielectric Barrier Discharge Plasma Actuator. Several are the aspects that make such a device very fascinating and appealing: it does not require mechanical elements, it does have a very simple geometry and its size is such that it does not affect much the controlled aerodynamics element, it does have a low energy consumption and a very fast reactivity with respect to the input.

There are two main different kinds of DBD plasma actuators: AC-DBD plasma actuator and NS-DBD plasma actuator. They have exactly the same geometry and the construction procedure is very similar but they differ from each other by the physical mechanism by which the flow control is achieved.

Passive	**Active**
VGs	Wall Heating/Cooling
Surface Shaping	Suction/Blowing
Winglets	Flaps

2.4 AC-DBD Plasma Actuators

The typical layout of a Dielectric Barrier Discharge (DBD) Plasma Actuator is basically composed by two electrodes separated by a layer of dielectric material. In the Fig.2.2 an example is given:

Between the two electrode an AC voltage signal is applied, which must be sufficiently high in order to breakdown through the air and sufficiently low in order not to breakdown through the dielectric layer. With such a voltage value it will create a stream of electrons propagating from an electrode towards the other one forming the so called “cold plasma” region. This is a self limiting process because the charged particle accumulated on the dielectric surface will create an electrical field opposed to the discharge itself, and in order to overcome this phenomenon a quite high voltage between the electrodes need to be applied. Within the discharge period, and within the plasma region, many chains of chemical reactions will take place. Not getting into the details the electrons of the plasma stream, hitting the air particles

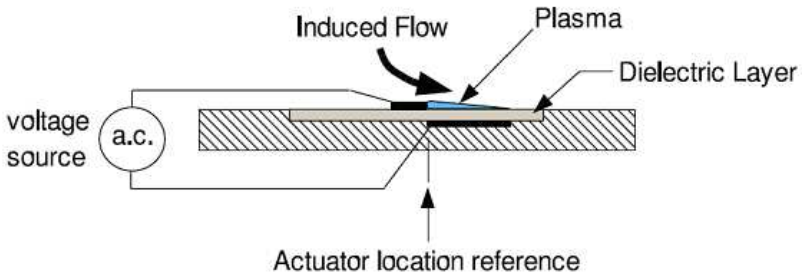

Fig. 2.2: Typical AC-DBD Plasma Actuator geometry [19]

between the electrodes of DBD plasma actuator, create a great number of ions by species oxidation. The peculiar waveform of the AC signal, that continuously changes polarity, drives these charged particles forward and backward between the electrodes of the actuator generating an ion flow. Such ion flow is able to introduce into the flow field a limited amount of momentum in the near wall region [19]. For these actuators the mechanism of flow control is through a generated body-force vector field that couples with the momentum in the external flow. The body force can be derived from first principles, and the effect of plasma actuators can be easily incorporated into flow solvers so that their placement and operation can be optimized. It has been shown that such an actuator is able to produce a vortex over the exposed electrode which could inject into the near wall region a momentum of the order of 3.8 mN. The rotating verse of the vortex is depending on the disposition of the anode and the cathode with respect each other [20] [21].

This kind of DBD plasma actuator have been subjected to numerous studies related to boundary layer control and separation flow control.

An experimental approach to quantify the effect of cold plasma actuators on a laminar flat plate boundary layer in order to evaluate the effect on laminar to turbulent transition was carried out [22]. The paper showed the experimental results obtained with DBD actuator: the characteristics ionic wind generated and the velocity profiles modified by this ionic wind. Moreover complementary information was given by hot wire measurement on the velocity fluctuations inside the laminar boundary layer.

An other experimental study has been undertaken to reduce skin-friction drag by applying a spanwise oscillation in the near-wall region of a turbulent boundary layer using RF glow- discharge surface plasma at Re = 380 [23]. The oscillatory plasma forcing was created using two opposing sets of asymmetric plasma actuators. By alternately activating the electrodes, skin-friction drag was reduced by up to 45% in the downstream of the actuators. The plasma action creates a tangential force very close to the wall surface, which creates alternating, co-rotating streamwise vortices in the inner region of the boundary layer. A 40% reduction in mean streamwise velocity and a 30% reduction in turbulent intensity were observed. This was ac-

companied by over 50% reduction in sweep duration and a 30% reduction in sweep intensity.

In others studies the amount of momentum transferred to the air using AC-DBD plasma actuator has been investigated [24]. It was found that the momentum added by a plasma actuator is fully contained within the boundary layer of an induced flow and is on the order of milli-Newtons. As a result, the actuator lacks the ability to use "brute force" methods to alter the flow field around an object, and must rely upon instabilities in the flow to bring about changes. To further investigate the effects of the plasma actuator on the boundary layer, the actuator has been placed on a flat surface with both a laminar and a turbulent boundary layer, and its effects on the flow upstream, immediately downstream, and far downstream were measured. Boundary layer traverses were performed with a boundary layer pitot probe for free stream velocities of approximately 4 and 6.5 m/s. The results show that regardless of the orientation of the plasma actuator, the actuator will trip a laminar boundary layer, providing the ability to electronically control it. It was also found that the actuator effect on a turbulent boundary layer is limited to a localized region immediately downstream of the plasma actuator.

An investigation about control of leading-edge flow separation that occurs over a NACA six digit airfoil at high angles of attack showed reattachment for angles of attack that were 8 degrees past the stall angle. This was accompanied by a full pressure recovery and up to a 400% increase in the lift-to-drag ratio. The airfoil was operated over a range of free stream speeds from 10 to 30 m/s, giving chord Reynolds numbers from 77 $\times 10^3$ to 333 $\times 10^3$ [25].

An other study about the applicability of Single Dialectic Barrier Discharge (SDBD) plasma actuators for use as active flow control devices, capable of enhancing the performance of airfoils, was carried out. Measurements were carried out on two thick airfoils with simple flaps, With a chord Reynolds numbers tested between $0.8\text{x}10^5$ and $3\text{x}10^5$. The input momentum was shown to be very weak and not sufficient to prevent separation at Reynolds numbers greater than 10^5. The SDBD plasma actuators used in this study may only provide sufficient momentum to be effective at very low Reynolds numbers. Under special circumstances the passive presence of the actuator on the surface may trip the boundary layer making it more resistant to separation, but in those cases a proper roughness strip or vortex generators may delay separation more effectively [26].

The peculiar results in common to all these studies is that the AC-DBD plasma actuator, even if able to affect the flow at low velocity regimes, decreases its effectiveness with increasing the Reynolds number. This because, fixing the physical gas propriety and typical length of the flow motion, an increase of the Reynolds number translates in an increase free stream velocity; when such velocity becomes larger and larger with respect to the momentum inputted in by the AC-DBD actuator, its relative effect becomes smaller and smaller. Recent parametric studies about optimization of the AC-DBD plasma actuator have been carried out aimed to maximize the body force created by the actuation mechanism, and so positively

affect the induced velocities introduced near the wall.

Several studies have shown that a surface dielectric barrier discharge (DBD) may be used as an electrohydrodynamic (EHD) actuator in order to control airflows. A parametric study has been performed in order to increase the velocity of the ionic wind induced by such actuators [27]. The results show that an optimization of geometrical and electrical parameters allows to obtain a time-averaged ionic wind velocity up to 8 m/s at 0.5 mm from the wall.

The momentum-transfer performance of a plasma actuator was investigated experimentally for the effects of ambient-gas pressure, ambient-gas species, and electrode configuration [28]. For measurement of the momentum-transfer performance, the force exerted by the actuator, in addition to the induced velocity, was measured; the consistency between both measurement methods was demonstrated. Results showed that the ambient-gas pressure under which a plasma actuator operates has a considerable effect on the momentum-transfer performance. In fact, the performance does not decrease in a linear manner with decreasing ambient-gas pressure; rather, it initially increases and then decreases. The chemical species of the ambient gas also has a considerable effect on the momentum-transfer performance. The momentum transfer in air is greater than that in nitrogen gas at pressures of less than 1 atm, which suggests a considerable contribution of oxygen molecules in the air. The momentum-transfer performance in carbon dioxide gas is slightly greater than that in nitrogen gas for pressures of less than 1 atm, although they are comparable at 1-atm pressure. Furthermore, the electrode configuration was found to strongly affect the momentum-transfer performance of the plasma actuator.

In other studies [29] complementary and coherent electrical, optical and aerodynamic measurements as a function of various parameters and geometries were performed. They measured the influence of the frequency and applied voltage of the discharge on the dissipated power. Experimental data yielded an empirical formula to calculate dissipated power and the energy lost in the dielectric was estimated. The plasma temperatures were also evaluated by spectroscopy emission measurements of N2 molecular bands. The velocity of the airflow induced by the DBD discharge in initially still air was measured as a function of the power dissipated in the discharge for different thicknesses and types of dielectric.

Several different models, often with conflicting explanations, have been offered to explain the process of this momentum coupling. The DBD is known to proceed in two stages during the discharge cycle, one on the positive-going portion of the applied AC high-voltage waveform and the other on the negative-going portion. By using the actuator to drive a second-order mechanical system, [30] it has been shown that the great majority (97%) of the momentum coupling occurs during the negative-going portion of the discharge cycle and this behavior has been related to dramatic differences in the structure of the discharge revealed with high-speed photography.

Others experimental studies [31] present measurements of how variations in the dis-

charge geometry of surface-mounted dielectric barrier discharges (DBDs) affect the force transferred to atmospheric pressure air. This studies include both single barrier plasma actuators (one electrode insulated) and double barrier plasma actuators (both electrodes insulated) operated in quiescent air. Stagnation probe measurements of the induced air flow and direct force measurements using an electronic balance show that, for both actuator types, parallel time-averaged forces increase as the high voltage electrode diameter decreases. For single barrier actuators, this increase is exponential rather than linear.

Some other paper [32] presents the results of a parametric experimental investigation aimed at optimizing the body force produced by single dielectric barrier discharge plasma actuators used for aerodynamic flow control. A primary goal of the study was the improvement of actuator authority for flow control applications at higher Reynolds number than previously possible. The study examined the effects of dielectric material and thickness, applied voltage amplitude and frequency, voltage waveform, exposed electrode geometry, covered electrode width, and multiple actuator arrays. The metric used to evaluate the performance of the actuator in each case was the measured actuator-induced thrust which was proportional to the total body force. In this paper was demonstrated that actuators constructed with thick dielectric material of low dielectric constant produce a body force that is an order of magnitude larger than that obtained by the Kapton-based actuators used in many previous plasma flow control studies. These actuators allow operation at much higher applied voltages without the formation of discrete streamers which lead to body force saturation.

So limitations for this actuator, in order to improve its effect, arise from several factors: dielectric thickness, dielectric properties of the barrier material, breakdown voltage of air and geometric arrangement of the actuator itself.

More effectively the AC-DBD plasma actuator have been employed in order to affect the secondary structure of the global flow dynamics. An example of such application is the delay of laminar to turbulent transition by means of Tollmien-Schlichting (TS) wave cancellation. The T-S wave at their linear amplification stage have an energy content on the order of 0.01% of the free stream velocity [33]. Similar techniques have been investigated by means of vibrating strings or membrane for example investigations on active attenuation of naturally occurring TS instabilities on an unswept wing [34] has been carried out. TS disturbances are canceled in their linear stage by superimposition with artificially generated counter waves in order to shift the laminar–turbulent transition downstream. In this method, the need for energy input is considerably lower than the stabilization by manipulation of the local mean velocity profile (e.g. boundary layer suction). An optimum TS wave cancellation is achieved by a fast digital signal processor performing an adaptive control algorithm. As a follow up of these experiments, recent investigations focus on the application of multi-channel control systems. This approach is essential to attenuate three-dimensionally dominated boundary layer instabilities by spanwise arranged sensor–actuator systems. Furthermore, the employment of multiple sen-

sor–actuator systems allows a streamwise repeated damping to extend the delay of laminar–turbulent transition considerably.

TS wave cancellation as been successfully achieved by AC-DBD plasma actuator. Experimental studies [35] shown that artificially excited TS waves were canceled using plasma actuators operated in pulsed mode. In order to achieve this a vibrating surface driven by an electromagnetic turbulator was flush mounted in a flat plate to excite the TS waves. These were amplified by an adverse pressure gradient induced by an insert on the upper wall of the test section. A control plasma actuator positioned downstream of the excitation actuator attenuates the waves by imparting an unsteady force into the boundary layer to counteract the oscillation. As a result the amplitude of the velocity fluctuations at the excitation frequency was reduced significantly depending on the distance from the wall. Also a parameter study was performed to identify the influence of several operation parameters of the control actuator. In the same conditions a different experimental study [36] shown that plasma actuator is able to attenuate the waves by imparting a steady or unsteady force into the boundary layer. In the case with steady actuation the two actuators change the velocity profile of the laminar boundary layer, which then attenuates the waves by itself. In the case of pulsed actuation the actuator creates an unsteady body force to counteract directly the oscillation. As a result the amplitude of the velocity fluctuations at the excitation frequency is reduced significantly in both cases.

Also investigations about manipulating unsteady structure such as shedding vortex using this kind of plasma actuator have been carried out with interesting results. For example a plasma actuator was used to control leading-edge flow separation and dynamic stall vortex on a periodically oscillated NACA 0015 airfoil [37]. The effectiveness of the actuator was documented through phase-conditioned surface pressure measurements and smoke flow visualization records. The airfoil was driven in a periodic cycle corresponding to $\alpha = 15$ deg plus 10 deg sinwt. Three cases of control with the plasma actuator were investigated: open-loop control with steady plasma actuation, open-loop control with unsteady plasma actuation, and closed-loop control with steady plasma actuation. For closed-loop control, the actuator was activated in selected portions of the oscillatory cycle based on angle-of-attack feedback. All of the cases investigated exhibited an increase in cycle-integrated lift with improvements in the lift-cycle hysteresis. In two cases, the pitch-moment stall angle was delayed and in one of these, the adverse negative moment peak was significantly reduced.

DBD plasma actuators have been used to control the flow around a circular cylinder at Re = $1.5x10^4$ [38]. It was shown that the vortex shedding was suppressed when the surface plasma placed near the natural separation point was activated in a pulsed mode at non-dimensional frequency above 0.6 with a force coefficient, Cp, greater than 0.05%. Plasma actuator performance on flow control was summarized by mapping the changes in drag and lift fluctuations as a function of the forcing frequency and the force coefficient. They showed that more than 70% reduction

in lift fluctuations was obtained with up to 32% drag reduction at fp+ = 2.0 and Cp = 0.32%. In this conditions narrowing of the wake was observed as the plasma promoted shear layer roll-ups at the forcing frequency. This, however, did not affect the shear layer on the opposite side of the wake. At non-dimensional forcing frequencies less than 0.6, the vortex shedding locked onto a multiple of the plasma frequency to amplify the wake oscillations. This caused more than 85% increase in lift fluctuations with 8% drag increase at fp+ = 0.2 and Cp = 0.01% . The efficiency of flow control using DBD plasma was found to be 1%–2% for drag reduction while around 6% for drag increase.

Unfortunately, even if the AC-DBD plasma actuator looks very promising for controlling the boundary layer, the momentum it is able to transfer into the flow is too small for controlling the separation for an aerodynamics application such as airplane flight. So a peculiarity of the AC-DBD plasma actuator is its quite low flow control authority. Recent experimental works demonstrated that this actuator could produce a thrust force of 0.2-0.3 mN/W [39] [40]. It has been shown that the induced flow velocity by such an actuator is about 5m/s [41], till up to 8 m/s [42]. Lastly researchers have been able to achieve, by the optimization of the discharge waveform, better results getting a value of the inputted velocity up to 11m/s [20]. A reason for such a behavior could be found looking at the restrictions of the physical mechanism of creating ionic wind. It has been observed [20] [21] that the ionic wind is not only created by the discharge but it is also driven by the discharge: this translates in the fact that, while discharging, the induced electrical field drives the ions from an electrode towards the other one, for reasons of clarity the electrodes will be named electrode one (where the discharge stars from), and electrode two. However, the typical shape of the AC waveform induces a periodic change in the sign of the induced electrical field, this allows the division of the discharge period in two parts: the first part will be defined from the beginning of the discharge till the time instant when the electrical field change its sign, and similarly, the second part will last as long as the induced electrical field with the sign changed will last. So in the first part of the discharge the ions are driven from electrode one towards electrode two while during the second part of the discharge the ions will be driven backwards. The effect of the AC-DBD actuator, due to the first part of the discharge, is decreased during the second part of the discharge by this self-limiting mechanism.

Thus optimization techniques based on discharge waveform shaping are sought [21]. So, in order to increase control authority of the DBD plasma actuators researchers have pushed the envelope looking for new methods for applying DBD plasma technology. The shape of the discharge input has been felt to be a key parameter for such an aim.

Summarizing It could be stated that the BDB plasma actuator is able to control the BL to some extent. Nevertheless this kind of actuator presents several limitations:

- The mechanism of actuation is self limiting

- The body force produced is often small with respect to the flow momentum under control
- High Frequency required for wave cancellation even for small free stream velocity
- It is effective only at low Reynolds numbers
- It is more effecting in enhancing drag instead of reducing it.

All these characteristics of the DBD plasma actuator limit its applicability. However considering its low energy consumption and cheap and easy constructiveness it is still very appealing as new technology. This is why the researchers continued to test it with different discharge modes looking for new solution of applicability.

2.5 NS-DBD Plasma Actuators

2.5.1 State of Art

The possibility to control shock waves (SW) by plasma applications, widely documented by Bletzinger looking also at its possible interactions with aerodynamics [43], has been demonstrated by several experimental investigations [44] [45] [46] [49] [50].

In [43] is presented a review of the studies about plasmas and high speed flows and shocks. Energy addition to the flow results in an increase in the local sound speed that leads to expected modifications of the flow and changes to the pressure distribution around a vehicle due to the decrease in local Mach number. There have been a large number of experimental studies on the influence of a weakly ionized plasma on relatively low Mach number shocks and inherently also on the influence of the shock on the plasma. Experiments with dielectric barrier discharges and focused microwave plasmas proved that such devices can produce very localized heating. The latter appears more attractive for energy efficiency in flow control. Tailored localized ionization and thermal effects are also of interest for high speed inlet shock control and for producing reliable ignition for short residence time combustors.

For example an experimental study data on the non-equilibrium plasma - gas flow interaction for hypersonic flows and the gas parameters during shock wave - non-equilibrium plasma interaction were obtained [48] [47]. Basic factors that determine the interaction process in such a system and the effect of charged and excited particles on the interaction dynamics were revealed. An experimental data for the gas discharge influence on the flow pattern around the model in the wind channel with Mach number M $\sim$ 8 were shown. The measurements of the drag force for different gas discharge parameters were performed and the conclusion was made that the gas discharge affects the flow mainly by thermal heating in the investigated range of parameters. In this work calculations support the conclusion about the thermal nature of the shock wave-plasma interaction.

In a different experimental work [49] the summary of combined experimental and computational investigations is presented for the plasma injection from a hypersonic blunt body for drag reduction. The systematic pursuit addresses all speculated mechanisms that can generate favorable magneto-aerodynamic interactions: the counterflow jet shock aerodynamic interaction, the non-equilibrium thermodynamic and chemical phenomenon, and the electromagnetic-aerodynamic interaction. The computational study was carried out by solving both the three-dimensional and the axial-symmetric, mass-averaged, Navier-Stokes equations for counterflow jet interaction. The experimental investigation of the plasma injection was conducted in a nominal Mach 6 open jet, blow-down tunnel. The weakly ionized, counterflow jet generated by a plasma torch has a vibrational temperature of 4400 K, an electron temperature around 20,000 K, and electron number density greater than $3 \times 1012/cm^3$

All these works opened the way to researches aimed to find new techniques for flow controlling based on thermal mechanisms. Opaits, in the 2005 [51] proposed to use nanosecond (NS) discharge for DBD plasma actuators. With such a discharge it is possible to increase by several times the value of the induced electrical field with respect to what the AC-DBD plasma actuator is able to do, which seems to be an evident advantage of using this kind of discharge. The value of E/n (where E is the electrical field and n is the concentration of neutral particles) can then exceed the breakdown threshold for this kind of discharge. Beside, also considering its low energy consumption, the possibility to operate within a wide range of pressures, gas composition and velocities, and the capacity to work also at high humidity conditions, it is easy to understand why such proposed approach resulted to be very successful.

The first investigation showing the possibility of boundary layer separation control is due to Opaits [51], in this work the influence of barrier discharge on the flow pattern for the NACA-0015 profile within the velocity range 20 - 75 m/s was investigated. The pressure distribution near the profile was obtained by system of pressure gauges. Without discharge the stall angle was equal to 15 degrees. When the additional momentum was produced by the actuator it was obtained flow without separation up to angle of attack $\alpha = 21$ degrees. It was shown that gas acceleration by discharge can be explained by interaction between non-compensated charge in the streamer head region and strong electric field.

A further investigation on this subject [52] showed very interesting results. In this research the influence of pulsed sliding discharge on the flow separation has been investigated. The high efficiency of pulsed discharge was shown within the velocity range from 20 to 110 m/s. The dynamics of discharge propagation with nanosecond time resolution was obtained. The influence of electrodes geometry was investigated and it was found that discharge affects flow separation while the electrodes were placed in parallel to the gas flow so the streamers propagated perpendicular to the flow. High efficiency was shown for a velocity up to 110 m/s and the main plasma effect on the flow was thought to be the turbulization of the boundary layer. The optimal frequency of the pulsed nanosecond discharge was found to be $f_{opt} = \frac{U_0}{L}$, where U_0 is the free stream velocity and L is the distance from the leading edge to the separation point. This result has been confirmed by Patel [53].

Afterwards, many other experimental works have demonstrated the applicability of NS-DBD plasma actuator for flow control and flow separation control purposes. For example in an experimental work [54] it has been shown high efficiency of the nanosecond pulsed SDBD to control the boundary layer separation, lift and drag force coefficients, and acoustic noise reduction in the Mach number range from 0.05 to 0.85. In this paper the author presents a detailed explanation of the physical mechanism of the pulsed SDBD effect on the flow. Actuator-induced gas velocities show near-zero values for nanosecond pulses. The measurements performed show overheating in the discharge region at fast ($\tau \simeq 1\mu$s) thermalization of the plasma inputed energy. The mean values of such heating of the plasma layer

can reach 70, 200, and even 400 K for 7-, 12-, and 50-ns pulse durations, respectively. The emerging shock wave together with the secondary vortex flows disturbs the main flow. The resulting pulsed-periodic disturbance causes an efficient transversal momentum transfer into the boundary layer and further flow attachment to the airfoil surface. Thus, for periodic pulsed NS-DBD, the main mechanism of impact is the energy transfer and heating of the near-surface gas layer. The following pulse-periodic vortex movement stimulates redistribution of the main flow momentum.

In a different research [55] separation control experiments on a rectangular wing were carried out using DBD plasma at subsonic speed for chord Reynolds numbers between 0.35 x 10^6 and 0.875 x 10^6. Surface pressure measurements and flow visualization shown that global flow separation on the wing can be mitigated or eliminated with the plasma actuators. The data were obtained for a wide range of angle of attack, flow speed, plasma excitation frequency and power. New applications of several kinds of voltage pulses for plasma excitation are discussed including microsecond and nanosecond pulses. It was found that control efficiency strong depends on discharge frequency.

Common result of all these investigations is that the control efficiency is strongly dependent on the discharge frequency. For further technological development it is very important to understand the physical actuation mechanism of the NS-DBD actuator in order to be able to control and optimize it, therefore to be able to design it for industrial applications. A big debate about such an issue has been going on during the last six years. The most quoted theory relies on thermal mechanism.

Roupassov [56] explained that the plasma governs the flow through two main mechanisms, either by energy transfer or momentum. The mechanism is based on the discharge energy transfer, which is a quite complicate multi-step process [57]. The electrons, during the discharge, gain energy from the applied electrical field, and depending on that value the mean electron energy can reach several electron volts. Based on the value of the mean electron energy depends the rate of the energy transfer between electrons and molecules. These conditions provide active excitation of the internal degrees of freedom of molecules as well as their dissociation and ionization by electron impact. The energy release during molecular dissociation and ionization, by electron impact, is a very fast process: particles decompose with high translational energy and the rate of thermalization, in these conditions, usually is on the order to the nanosecond. Such a mechanism is depending on the initial voltage applied to the electrodes of the DBD plasma actuator. In the Fig.2.3 [56] a visualization flow is give as an example of what a NS-DBD Plasma Actuator is capable to do.

The same paper shows also the forming SW with respect to the one obtained by CFD calculations in Fig.2.4.

Another mechanism explanation relies on the hypothesis that the flow velocity can be changed during the interaction of the electrical field and uncompensated spatial plasma charge. It could be explain by two different mechanisms, steady and

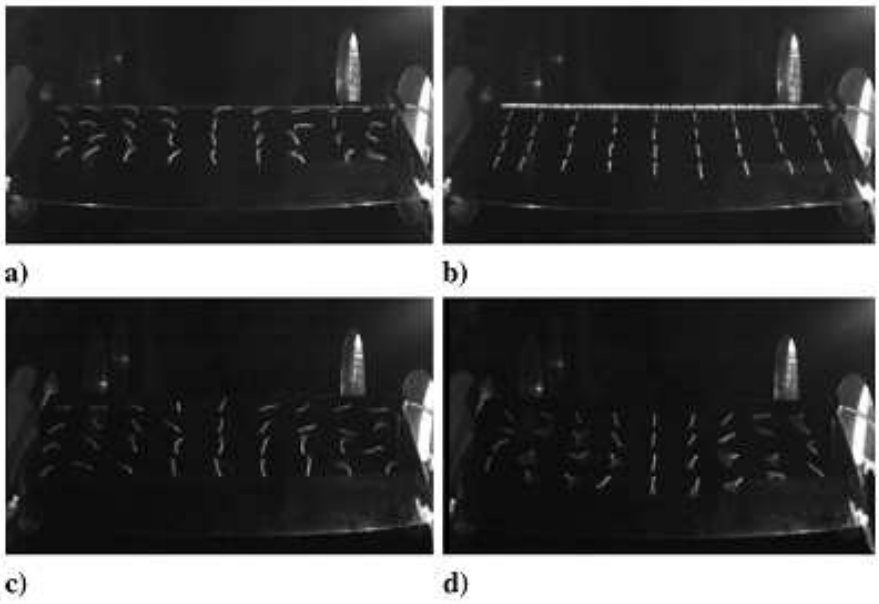

Fig. 2.3: Tuft flow visualization[56]. V = 12.5 m/s,α = 9 deg. a) Initial detached flow (discharge is off); b) attached flow (discharge is on). V = 11.2 m/s, α = 17 deg. c) Initial detached flow (discharge is off); d) attached flow (discharge is on).

unsteady: in both the cases the uncompensated spatial charge wave front results accelerated by the electrical field in the region of the discharge.

However NS-DBD plasma actuator has been successfully tested for separation flow control at high Reynolds and Mach numbers only in few investigation works [56] [58] [59] [60].

In [58] the efficacy of DBD plasmas driven by repetitive NS pulses for flow separation control was investigated experimentally on an airfoil leading edge up to Re=1x10^6 (62 m/s). The NS pulse driven DBD plasma actuator transfers very little momentum to the neutral air, but generates compression waves similar to localized arc filament plasma actuators. Experimental results indicated that NS-DBD plasma performs as an active trip at pre-stall angles of attack and provides high amplitude perturbations that manipulate flow instabilities and generate coherent spanwise vortices at post-stall angles. These coherent structures entrain free stream momentum thereby reattaching the normally separated flow to the suction surface of the airfoil. In this paper is shown a very clear schlieren image of the SW reported here in Fig.2.5.

Moreover in this paper also some interesting data about C_L and momentum transfer into the BL are give, as reported in the Fig.s 2.6 and 2.7

In a different [60] work is presented the ongoing development and use of DBD plasma actuators driven by repetitive nanosecond pulses for high Reynolds number aerodynamic flow control. Leading edge separation control on an 8-inch chord NACA 0015 airfoil was demonstrated at various post-stall angles of attack for Reynolds num-

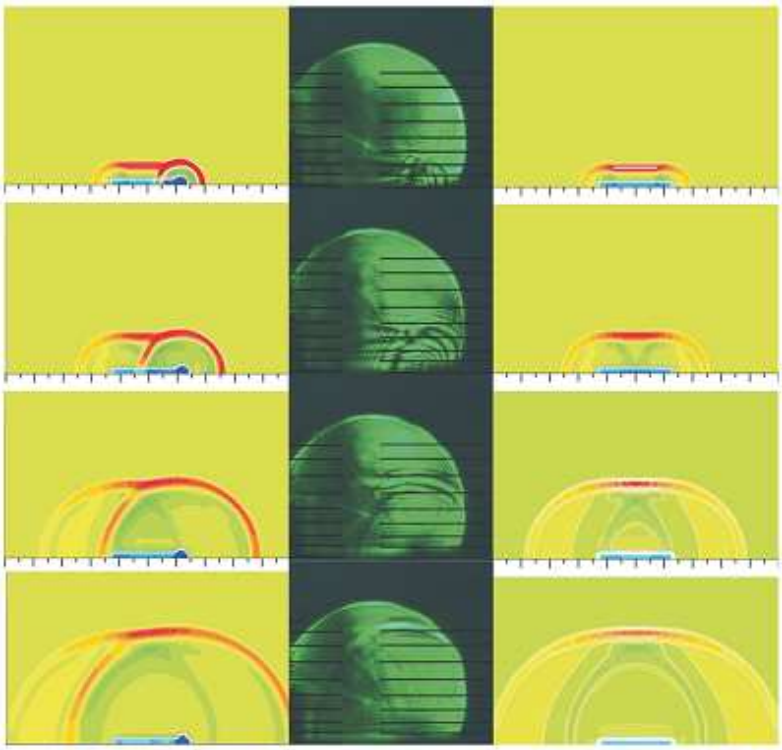

Fig. 2.4: Dynamics of flow development near surface. From top to bottom: 4, 8, 16, and 25 μs after the discharge. Single scale division both in horizontal and vertical directions corresponds to 1 mm. Left column: numerical modeling; discharge with "hot spot" near the edge of the exposed electrode. Right column: numerical modeling; homogeneous energy distribution. Center column: experimental shadow images of shock waves formation. Pulse duration is 50 ns.[56]

bers and Mach numbers up to 1.15x10^6 and 0.26 respectively (free stream velocity up to 93 m/s). The NS-DBD can extend the stall angle at low Re by functioning as an active trip. At post-stall angle, the device generates coherent spanwise vortices that transfer momentum from the free stream to the separated region, thus reattaching the flow. An example is give with smoke flow visualization technique in Fig.2.8

Another experimental study about flow separation control with a nanosecond pulse plasma actuator proved the scalability of the actuator itself [59] . In this study the discharge used had a pulse width of 12 ns and rising time of 3 ns with voltage up to 12 kV and repetition frequency was adjustable up to 10 kHz. Different geometries of the actuator were tested at a Reynolds number of 3.3 million. In stall conditions the significant lift increase up to 20% accompanied by drag reduction up to 300% was observed and the critical angle of attack shifted up to 5–7 degrees. The relation of the optimal discharge frequency to the chord length and flow velocity was proven. The dependence of the effect on the position of the actuator on the wing was studied, showing that the most effective position of the actuator is on the lead-

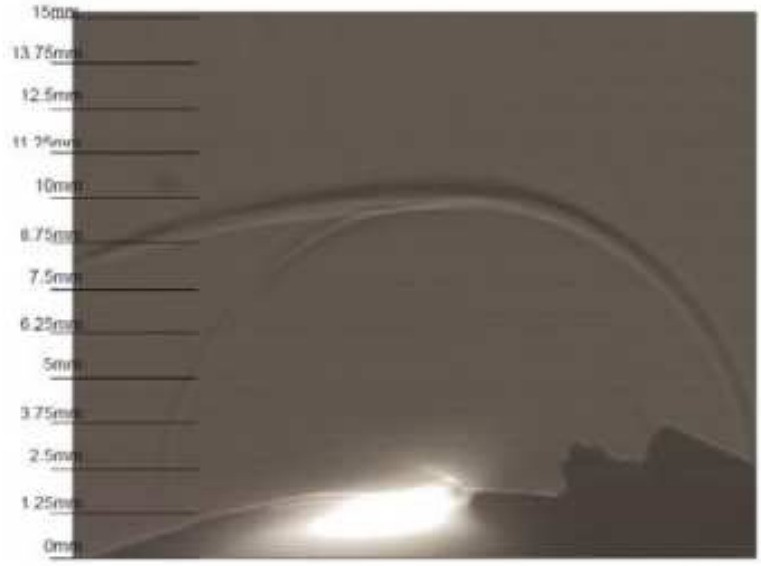

Fig. 2.5: Phase-averaged schlieren image of compression waves generated by NS-DBD plasma actuator viewed along the major axis of the discharge a 30 cm DBD load.[58]

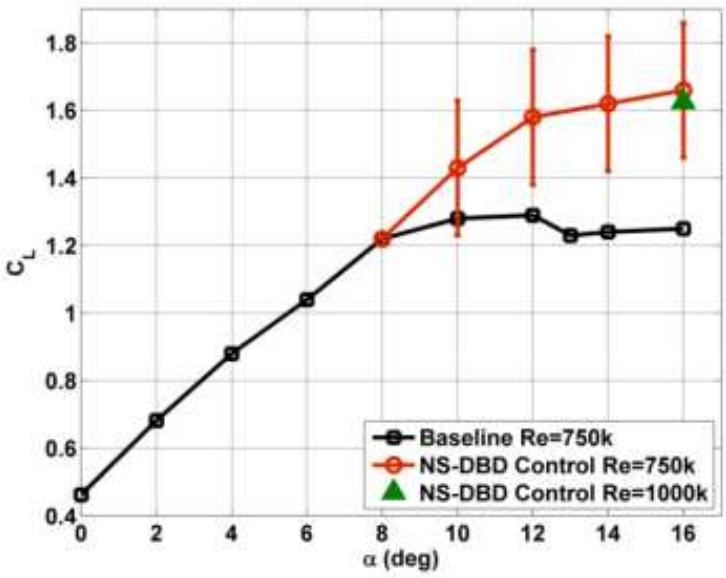

Fig. 2.6: Effect of active control with NS-DBD plasma actuation on C_L for the OSU airfoil.[58]

ing edge in case of leading edge separation. In order to study the mechanism of the nanosecond plasma actuation experiments using schlieren imaging were carried out. It shown the shock wave propagation and formation of large-scale vortex structure in the separation zone, which led to separation elimination. PIV diagnostics technique was used to investigate velocity field and quantitative properties of vortex formation. In flat-plate still air experiments small-scale actuator effects were inves-

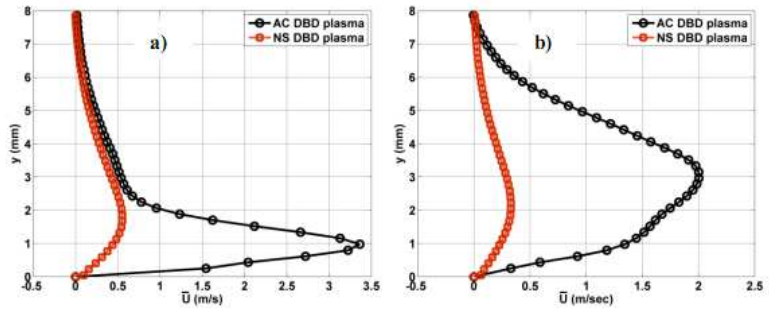

Fig. 2.7: Mean velocity profiles for NS and AC-DBD plasma actuators operating in quiescent air with 2 kHz carrier frequency using 100% (a) and 50% (b) duty cycle at 90 Hz measured 20 mm downstream on a 30 cm DBD load.[58]

(a) Before Actuation (b) After Actuation

Fig. 2.8: Smoke flow visualization at Re = 1.15x10^6 and $\alpha = 18°$ with no actuation (a) with NS-DBD plasma actuation at $F^+ = 2.75$(b).[60]

tigated. Measured speed of flow generated by actuator was found to be of order of 0.1 m/s and a span-wise non- uniformity was observed. The experimental work is supported by numerical simulations of the phenomena. The formation of vortex similar to that observed in experiments was simulated in the case of laminar leading edge separation. Model simulations of free shear layer shown intensification of shear layer instabilities due to shock wave to shear layer interaction. In the Fig.2.9 is given the C_L and C_D obtained in this work[59],at a Reynolds number about one million, and in the Fig.s 2.10 and 2.11 the result the CFD calculation done in order to support the vortex formation mechanism is also shown.

The scope of this experimental work is to investigate the features and the effects of the NS-DBD plasma actuator in details and to propose a possible physical mechanism of actuation.

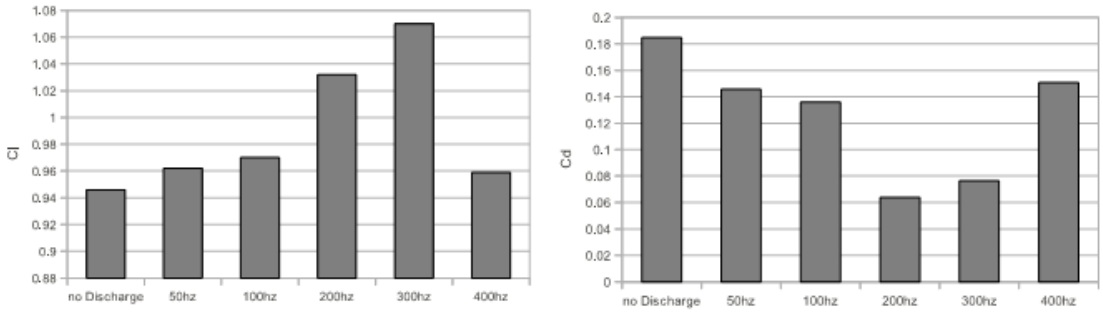

Fig. 2.9: Lift and drag coefficient at different discharge frequencies. V = 20 m/s, α = 15°.[59]

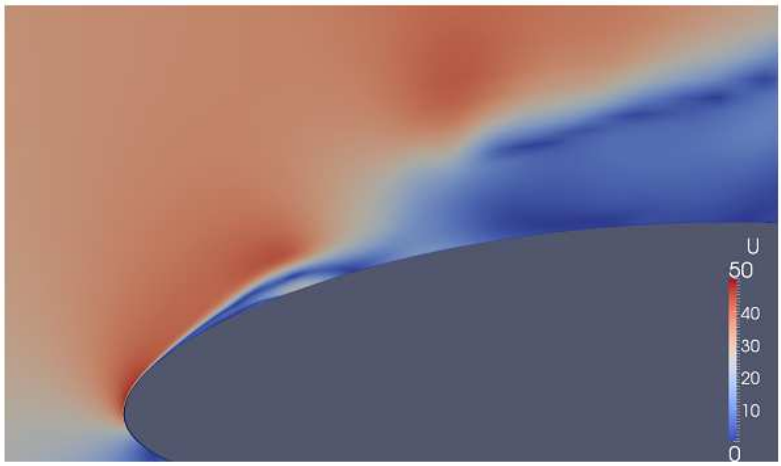

Fig. 2.10: Simulation of the laminar separation with actuation: velocity field after the discharge. Magnitude of the velocity is shown by the color.[59]

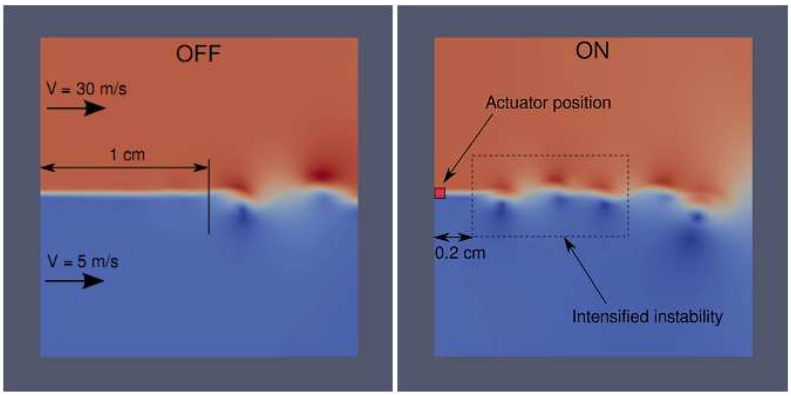

Fig. 2.11: Velocity field without and with actuation in shear layer simulation. Thickness of the shear layer at the inlet is 0.5 mm.[59]

2.5.2 Phenomenology

This paragraph is aimed to help the reader either to follow the discussion coming in the next chapters either to understand what the author figured out about the phenomenology of the NS-DBD Plasma actuator. Such a device is basically composed of two electrodes, usually made out of copper, separated by a dielectric material, usually kapton tape. An high voltage nanosecond pulsed discharge is applied to the electrodes. In its symmetrical fashion is given in Fig.2.12 hereafter, with typical dimensions.

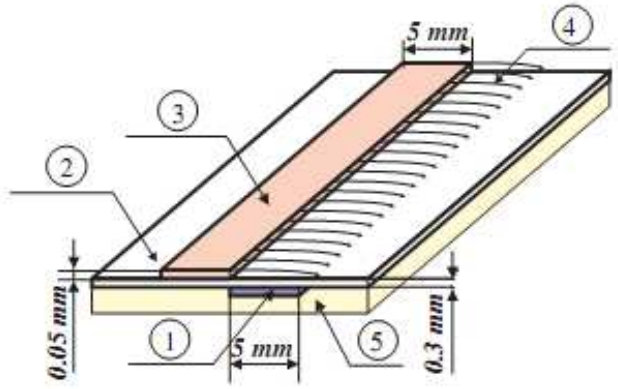

Fig. 2.12: Scheme of discharge gap with characteristics dimensions. 1: high-voltage electrode; 2: dielectric layer; 3: ground electrode; 4: zone of discharge propagation; 5: model surface. [56]

When the wave input is given a barrier discharge happens between the electrodes: electrons, distributed in channels, leave the ground electrode (the one exposed to the flow), traveling along the dielectric surface, trying to reach the high voltage electrode. When the electrical field becomes too weak, few millimeters far from the exposed electrode, the electrons move backwards. The dielectric layer, practically, does not allow the discharge to happen completely, so far, for "barrier" kind of discharge, there is no spark. Instead of it a light blue glow is visible during the discharge, if the discharge frequency is high enough. For this kind of discharge also peculiar is the low energy consumption, since the dielectric layer does not allow the energy to flow away from the font.

Thus electrons traveling during the discharge hit up the air particles in a small volume just above the covered electrode. The mean energy of the electrons is such that when they hit the molecules they are able to dissociate them in sub particles, exciting their vertical translational degree of freedom. The discharge lasts few tens of nanoseconds. The thermalization mechanism takes about one microsecond. So in a very small fraction of time the hit volume increases its temperature of about ten times [56], though the temperature increase depends upon the discharge characteristics. In such a small fraction of time the gas within the hit volume,

increasing its heat, does not have time to expand. Thus, the pressure within the hit volume rises as quick as the heat does. Only after few tens of microseconds the gas starts expanding adiabatically. In this way, a shock wave, with a velocity a bit higher than the speed of sound, will be generated. In a condition of leading edge separation, with the actuator mounted close to the separation point (separation line in a bi-dimensional case), the shock wave will travel as far as its energy content will allow it to do, in all the directions within the field of motion. Thus, moving downstream the separation point, it will travel into two different domains of the field of motion, because of the presence of the shear layer, a gas dynamics discontinuity [63], that divides the region of the free stream flow from the recirculation flow of the separated region. In this scenario the shock wave will be moving in two means with two different velocities, this will result in the fact that the shock wave will have two different velocities itself depending on which region it is traveling in, and so in the shear layer a pressure gradient rises up due to this particular phenomenon [59]. This will produce a disturbance that, somehow, drives the shear layer to the breakdown.

For a deeper understanding of the just mentioned phenomenology, a graphical explanation is felt to be necessary. In the following Fig.2.13 a schematic sketch of the plasma actuator (side view) is shown: it is shown how the two electrodes are displaced with respect to each other and how they are separated by the dielectric layer.

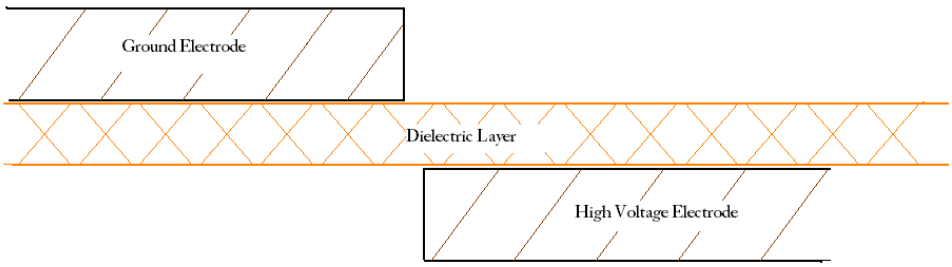

Fig. 2.13: Sketch - Actuator Side-view, generic layout. In the sketch the dimensions are exaggerated for clearness reasons.

Now, imagining the discharge: the natural behavior of the electrons flow is to follow the shortest possible path but breaking through the air it will be driven towards the regions where there will be the lowest dielectric resistance felt by the electrons themselves. Thus one might think that the discharge happen somehow similarly to that one shown in the Fig.2.14 : electrons leaving the exposed electrode and moving as close as possible to the dielectric surface, where the electrical field is stronger.

Within few tens of nanosecond the discharge is over and the temperature in the hit region, where the electrons have flowed through, start rising. This is sketched in the Fig.2.15.

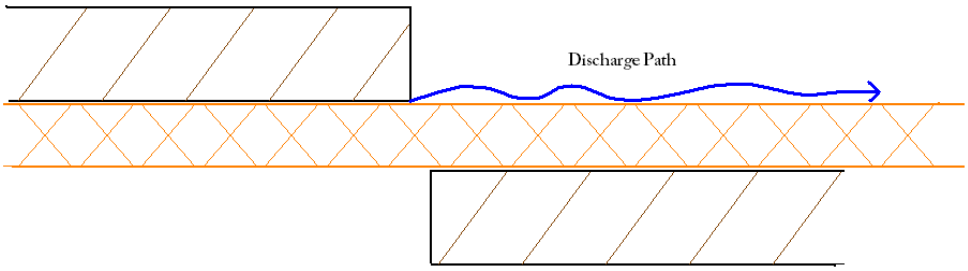

Fig. 2.14: Sketch - One of the several possible discharge path

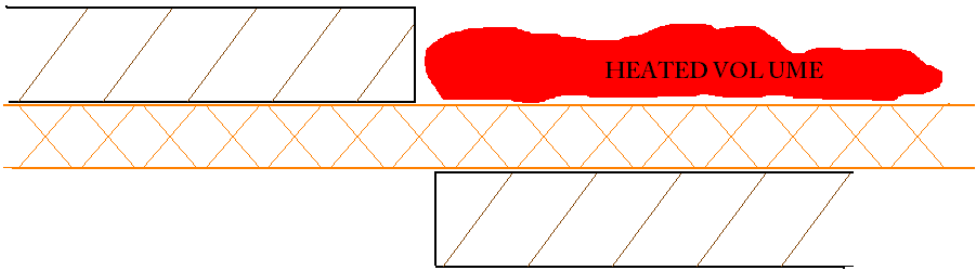

Fig. 2.15: Sketch - Gas volume heated up by the discharge

The temperature rising takes about one microsecond [56]. With the temperature, also the pressure within the hot volume rises producing after few microseconds a very fast adiabatic expansion of the gas within the volume. Such an expansion moves in all the directions, and the vertical size of the bi-dimensional volume shown in the Fig.2.15 is much smaller than the horizontal one since the geometry of the discharge. So it might be assumed that the expansion will be about the vertical direction mainly: the flow expands upward and downward. As shown in Fig.2.16 the expansion produces a shock wave.

For now the discussion will be focused on the upper part of the SW. Later in this paragraph the lower part of the expansion will be discussed as well.

If now one considers the actuator placed on the very leading edge of an airfoil, in a still air condition, it could be seen how a shock wave produced by the actuator travels towards the far field. A sketch of such a situation is presented in Fig.2.17.

If now one places the same airfoil with the same plasma actuator in a leading edge flow separation condition it might be easy to see the different velocities at which the shock wave travels. Such velocities depend on the velocity of the mean it is traveling through. Again a sketch of this situation is shown hereafter in Fig.2.18.

The shock wave will produce a pressure gradient throughout the shear layer. Such

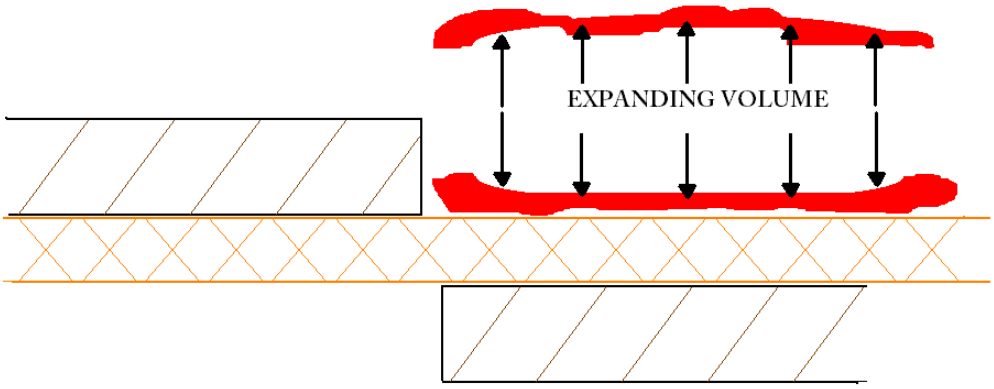

Fig. 2.16: Sketch - volume heated up expanding, forming a SW

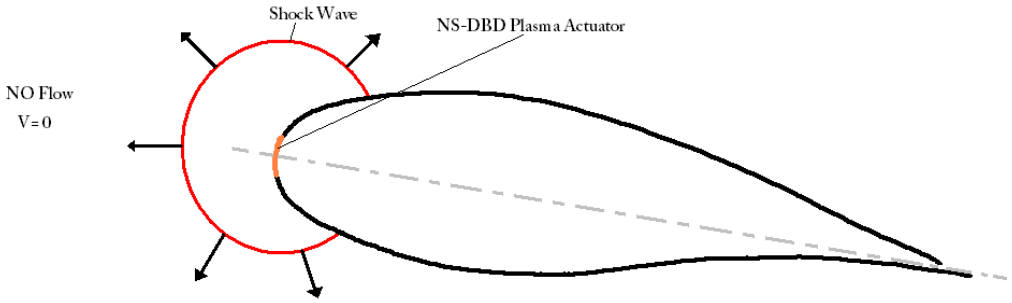

Fig. 2.17: Sketch - SW on an airfoil with no flow. The SW expands in all the directions.

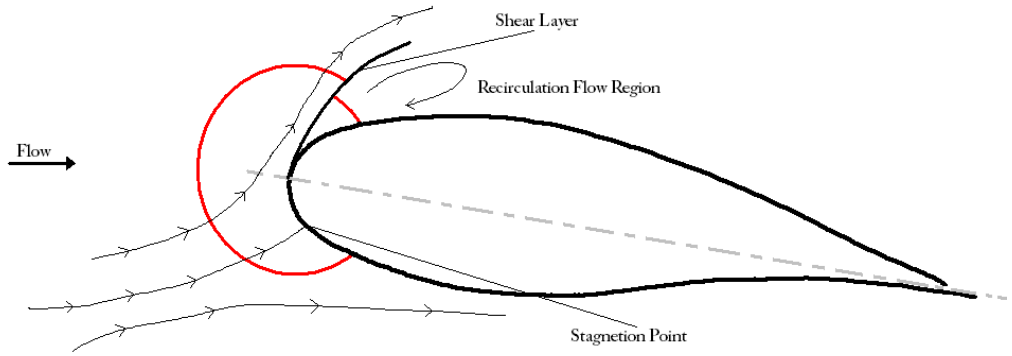

Fig. 2.18: Sketch - SW on an airfoil interacting with a leading edge separated flow. Since the presence of the Shear Layer the SW will move in two media with different velocities, so the SW will move with two different velocities as well.

a phenomenon has been proved also by simulations [59].

Zooming in, now, on the shear layer it might be possible to figure out how the SW

distributes itself through it and how it could interact with the particles inside it. In Fig.2.19 is given a sketched representation of how the SW is distributed into the SL with a representation of the velocities of the pre and post shock regions [63].

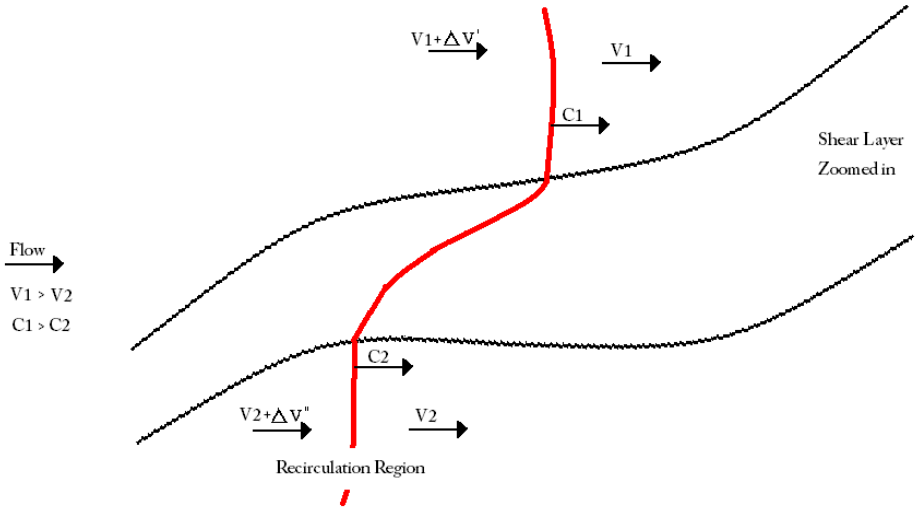

Fig. 2.19: Sketch - Zoom in on the SW into the SL with representation of the velocities of both the pre and the post shock regions, in both the domains separated by the SL

The gradient of pressure will produce a disturbance into the shear layer.

Since the upper part of the shear layer velocity profile will meet the pressure disturbance, produced by the shock wave, before the lower part it will be affected first, Fig.2.20

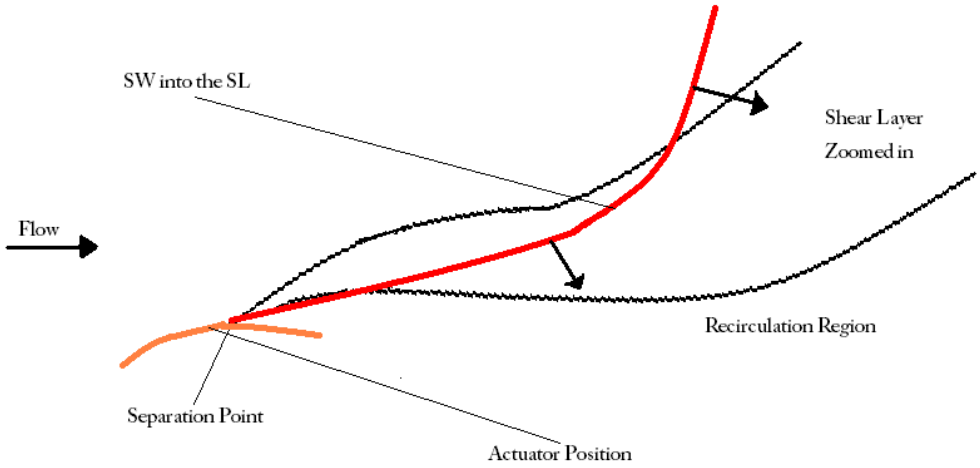

Fig. 2.20: Sketch - Very first interaction of the SW traveling throughout the SL

Now, for the conservation of momentum, since the upper part of the shear layer get pushed in a direction, the lower part will be pushed in the opposite direction. The latter phenomenon is illustrated in Fig.2.21.

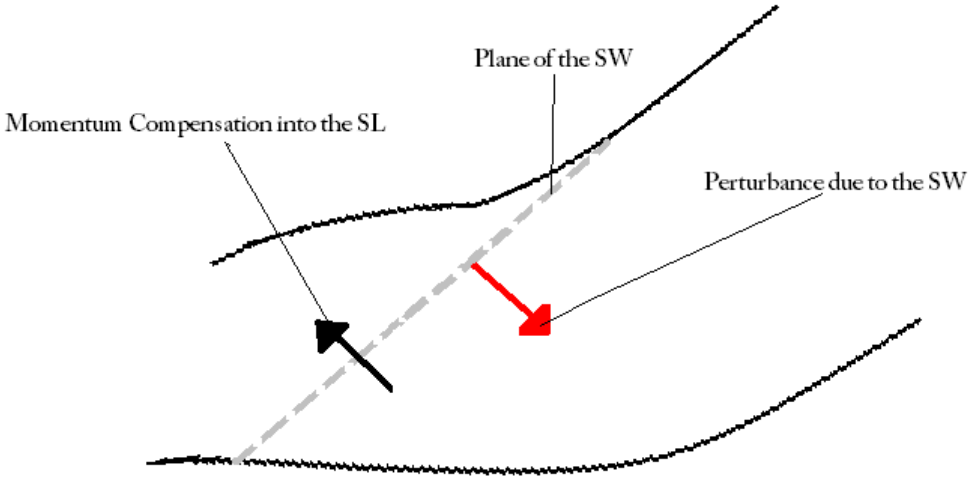

Fig. 2.21: Sketch - Disturbance formation due to momentum conservation into the SL

The pressure disturbance into the SL produced by the SW might be schematized as it is shown in Fig.2.22. Such a schematization is done in order to make the understanding process easier.

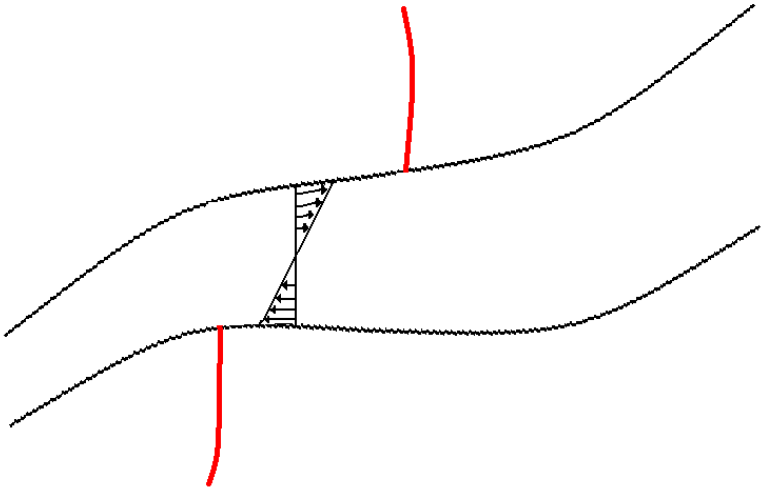

Fig. 2.22: Sketch - velocity profile due to the perturbation in the shear layer

Now, in order to figure out how the pressure disturbance, introduced into the shear layer, works it might be wise to start with a more easy situation: considering a

laminar flow separation. Thus a laminar shear layer could be thought and a sketch with the relative velocity profile is given in Fig.2.23.

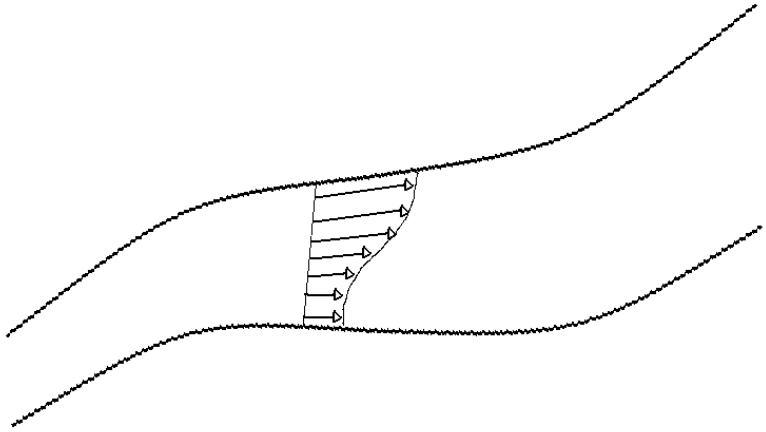

Fig. 2.23: Sketch - Velocity profile in a laminar SL

Now, dividing the shear layer in small portions ∂s, one might ask oneself what would happen if in the free shear layer, as represented in Fig.2.23, the discussed pressure disturbance was applied.

As it could be understood from Fig.2.24, where the dimensions have been exaggerated for a better visualization of the phenomenon, the two velocity profiles will add to each other. The relative effect of the disturbance is higher in the lower region of the shear layer where the momentum of the flow is lower.

The momentum transferred by the pressure disturbance, since the continuum of the mean, is convected in the whole shear layer domain. So the half upper part of the disturbance transmits a momentum in the downstream direction while the half lower part does the same in the upstream direction.

Thus the induced pressure disturbance will mainly affect the flow in the lower part of the SL because the relative momentum of the flow in that region, being smaller than the one of the upper part, is more likely affected by the momentum introduced by the pressure disturbance.

So, It will be traveling upstream affecting the velocity profile of the previous (in upstream direction) ∂s of the shear layer.

For better explaining how the disturbance behaves, as illustrated in Fig.2.25, a SW, and then the pressure disturbance it produces, is introduced into a laminar shear

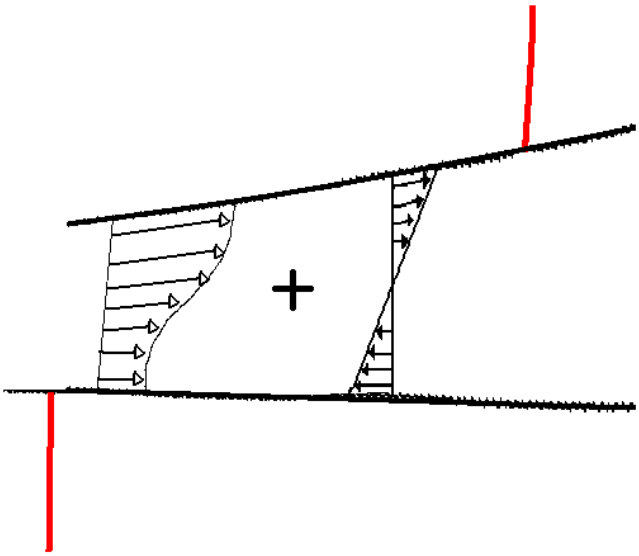

Fig. 2.24: Sketch - Addition of velocity profiles into the laminar SL

layer, divided in ∂s, at the location ∂s_1, by a NS-DBD plasma actuator placed at the leading edge of an airfoil, in a condition of leading edge separated flow, at the time instant t_1:

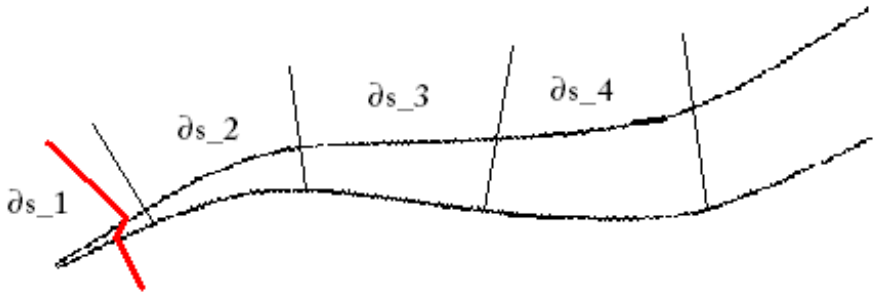

Fig. 2.25: Sketch- SL divided in ∂s with SW in the region 1

The disturbance will change the velocity profile in the region ∂s_1. Zooming in one might see schematically, as in Fig.2.26:

the velocity at the lower part of the profile gets reduced while the upper part is weakly increased, Fig.2.27. Forwarding in time, at a time instant $t_2 > t_1$, the shock

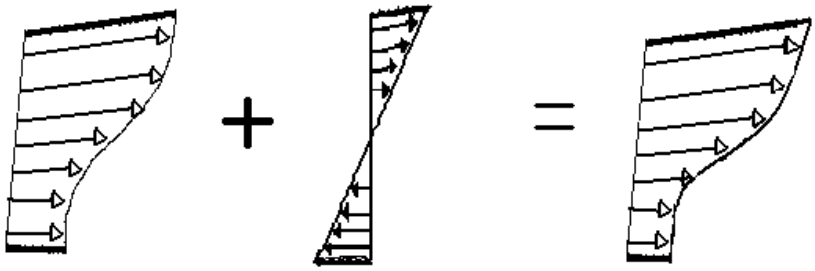

Fig. 2.26: Sketch - Interaction of velocity profiles into SL in ∂s_1 at time t_1

wave will be moving downstream getting into the region ∂s_2. Again the pressure disturbance will affect the flow field, changing it as well as it does it into ∂s_1 region. So Fig.2.27 illustrate also the velocity profile, in region ∂s_2 at time t_2.

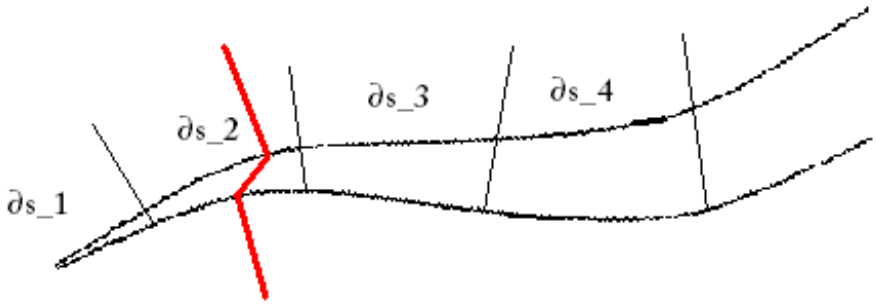

Fig. 2.27: Sketch - SL divided in ∂s with SW in the region 2

However, the disturbance produced at the time t_2 will move further backwards, in the upstream direction, getting in the region ∂s_1, again affecting the flow also there, so the new situation in region ∂s_1 might be represented as in Fig.2.28.

Forwarding in time the relative effect of the disturbance will affect the upper part of the profile less and less. On the other hand the opposite happen regarding the lower part of the velocity profile which will be affected more and more since the relative difference in the momentum content of the two velocity profile, in that region, increases. This phenomenon will be repeated at any time instant. At a time instant $t_3 > t_2$, the shock wave will be located in region ∂s_3.

The velocity profile in region ∂s_1, having been already affected by the former disturbances, now might become as in Fig.2.30.

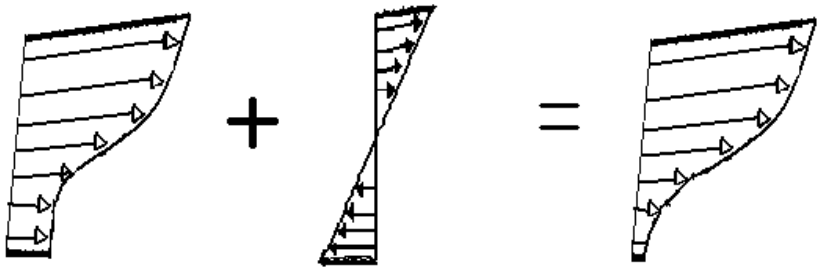

Fig. 2.28: Sketch - Interaction of velocity profiles into SL in ∂s_2 at time t_2

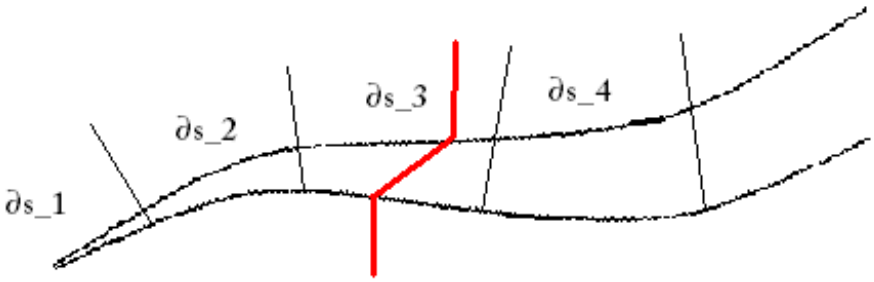

Fig. 2.29: Sketch - SL divided in ∂s with SW in the region 3

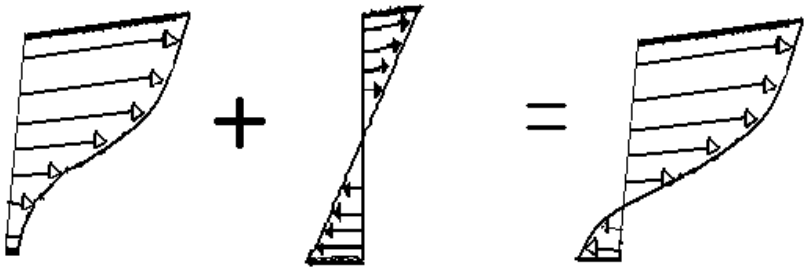

Fig. 2.30: Sketch - Interaction of velocity profiles into SL in ∂s_3 at time t_3

Such a velocity profile produces a vortex, shown in Fig.2.31, which is able to breakdown the shear layer, allowing the free stream flow to pass through.

The vortex as well is convected downstream in the far field.

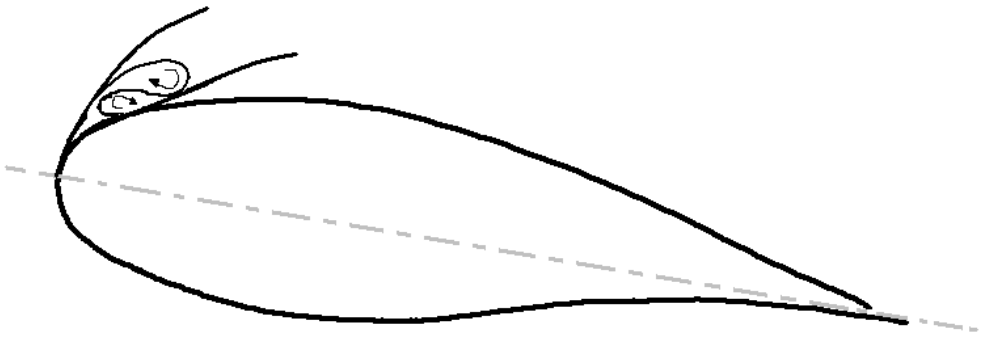

Fig. 2.31: Sketch - Vortex generated by the pressure disturbance traveling into the SL

Another effect produced by the NS-DBD plasma actuator is the downwards expanding gas which will be also investigated here. Since the discharge is thought to happen very close to the dielectric surface, it might not be able to produce an appreciable effect, but if it does, it could transmit momentum to the flow in the downwards-vertical direction, very close to the wall.

This phenomenon will be now analyzed in more details. Again is felt necessary for understanding a graphical sketching of the phenomenon.

For simplicity a boundary layer, developing till the separation point, on a flat plate is considered, as sketched in Fig.2.32.

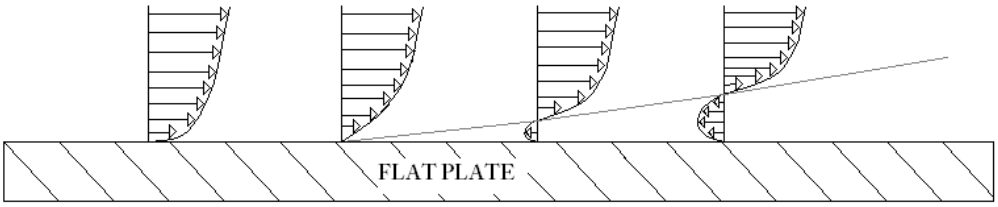

Fig. 2.32: Sketch - Boundary Layer on a flat plate

Two possible scenarios are foreseen depending on the position of the actuator with respect to the position of the separation point. Placing the actuator exactly at the point of separation is an hard task, therefore it will be analyzed the case where the actuator is placed just before the separation point, and the case where the actuator is placed just after the separation point. So it could be figured out, in the first scenario, a situation as shown in Fig.2.33.

The two adding velocity profiles, in Fig.2.33, are overlapped in the reality, but for explicative reasons they have been sketched separated, showing a possible interac-

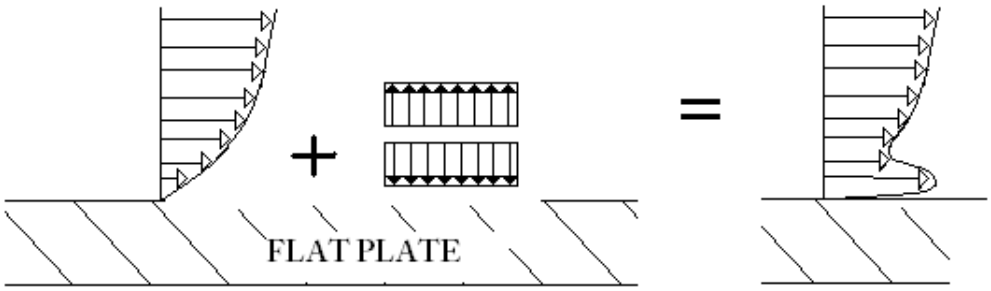

Fig. 2.33: Sketch - Case 1: effect on a flat plate BL of the lower part of the expansion of the heated gas volume. In the sketch, for a reason of completeness also the upwards pushing part of the expansion is shown, but it is not taken into consideration for this discussion so it will never be drawn again.

tion between each other. In the same manner a sketch of the second scenario is proposed in Fig.2.34.

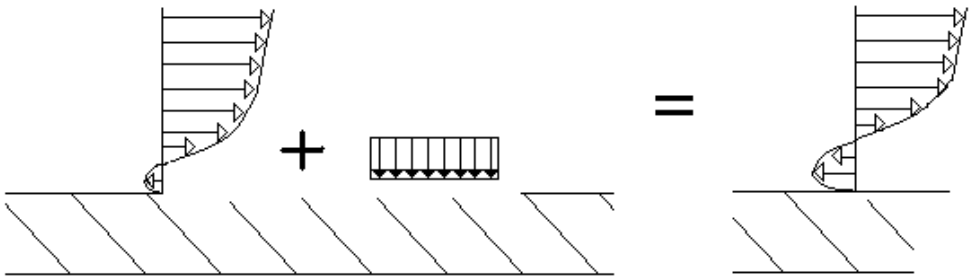

Fig. 2.34: Sketch - Case 2: effect on a flat plate BL of the lower part of the expansion of the heated gas volume.

It could be see that in the former case the flow, interacting with the disturbance, gets some momentum transferred , which may help the flow to stay attached on the flat plate a bit longer. In the latter case the interference of the disturbance with the flow actually may advance the separation point upstream. This scenario brought to the light an issue about the location of the actuator with respect to the separation location.

Since the actuator seems also capable to advance separation special attention need to be taken placing it. This phenomenon also will be investigated further.

The expansion of the hot volume in the downwards direction might also provoke a second order effect: the local vibration of the actuator itself. This phenomenon will not be investigated but discussion will be carried out about it, as well as for all the other phenomena.

Another effect of NS-DBD plasma actuator more commonly considered a side effect must be remembered here:: during the nanosecond discharge the NS-DBD plasma actuator does produce Electromagnetic (EM) noise. Due to this side effect testing this kind of actuator is a very difficult and challenging task. Such noise, generated by the fast changing in time of the electromagnetic field, travels in all directions in the space around the source. The peculiarity of the EM noise is that it interacts with all the electronics it meets on its way, making them go crazy, or freezing them or, in a rare cases, breaking those electronics down.

This puts some limitations in testing the actuator as well as, of course, in using it for any industrial application. This is a very delicate issue since it might affect the interest of potential investors for a further research limiting, if not even erasing, any chance of future applications of the NS-DBD actuator.

Also this issue will be discussed eventually in this work.

2.6 Position in the State of the field

After having carried out a literature review about DBD plasma actuators placing this work into the state of the field is necessary.

This is a purely experimental investigation which have been externally supported with CFD calculations carried out from the PhD Student Ilya Popov at Delft University of Technology.

The type of actuator studied within this work is only the nanosecond kind, so no data comparison about the AC and the NS-DBD kind of actuator has been presented.

Experimentally, in order to prove the possible utilization of the NS-DBD actuator for industrial application, the Reynolds number achieved with a successful active flow control has been doubled with respect to the highest Reynold number findable in the most recent literature.

The kinds of airfoil used for the investigation are basically three: NACA0015 for having reference data available from the literature, a NLF model for studying the mechanism at low turbulence level, and a 5-digit NACA commonly used in the wind energy field, for studying some interesting industrial application configurations.

From this research it was learned that the location on the actuator is a very sensible issue which requires a lot of attention and that the optimal frequency of discharge is not linear anymore for high angles of attack.

This research can be seen as a first step towards a research about a combination of AC and NS DBD plasma actuator, for studying, designing and developing strategies of active flow controls aimed to get the DBD plasma actuator at an "industrial applications" stage.

2.7 Research Goals

The aim of this work is to investigate the above mentioned phenomena, in order to look for evidences and eventually proposing the physical mechanism of actuation. Moreover the structural impact of the actuator on different kind of airfoils will be also investigated, and it will be also tested in severe conditions like high humidity flow or presence of ice.

Furthermore a study, and a discussion, about the scalability of the device will be carried out. Eventually a discussion about possible industrial application for the actuator will be done.

Summarizing, starting from what is known about the NS-DBD plasma actuator, and from what is thought to be the phenomenology involved, the aim of this experimental work is to closely observe the actuation, trying to provide any evidence of the phenomena discussed in the section Phenomenology(2.5.2), for figuring out the physical mechanism of the actuation.

Special attention will be given to the side effects produced by the actuator itself. Furthermore the scalability upwards will be investigated and eventually industrial applications will be proposed and discussed.

Chapter 3

Experimental Setup

In this work flow separation control on airfoils with the nanosecond pulsed plasma discharge is studied. There are two major kinds of discharge which are used for the separation control — AC discharge and nanosecond pulsed plasma discharge. The AC discharge is the most well-known one, and its effect is the result of a momentum increase due to ionic wind created by the discharge. But this ionic wind is quite slow (velocities up to several meters per second [20] [41] [42]) and thus the range flow speeds at which this type of actuators is effective is limited. The mechanism of flow control by nanosecond pulsed plasma discharge is different. It is supposed that the vorticity is created by the shock wave, which is produced from the layer of the hot gas. This hot gas is generated during the fast thermalization process, in which more then the 60% of the discharged energy is converted to heat in less then 1 μs [56].

The current work continues studying the performances of nanosecond pulsed plasma actuator. A series of wind tunnel experiments was carried out with different actuator layouts under different conditions at flow speed up to 80 m/s.

3.1 Setup

In the experiments a linear actuator was used in four different wind tunnels at a speed up to 10 till 80 m/s. It was made of layers of kapton and copper foils. Generic actuator layout is presented in figure 3.1.

The actuator consisted of a base layer of insulator (1) attached onto the surface of the airfoil, a covered electrode (2), an inter-electrode layer of insulation (3) and an exposed electrode (4). The thickness of the inter-electrode insulation was about 0.15–0.20 mm. Another adjustable parameter was the inter-electrode gap (d). In

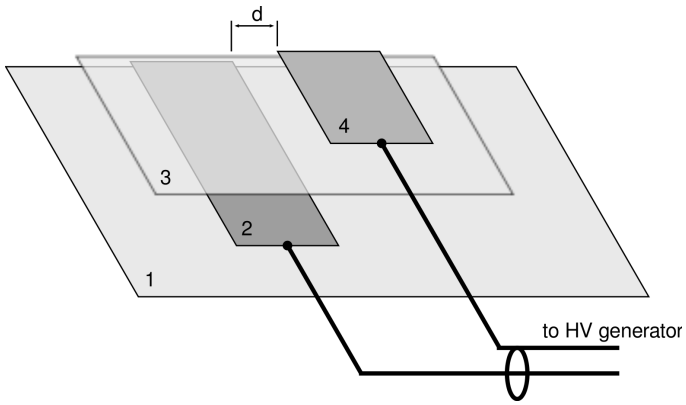

Fig. 3.1: Actuator layout. 1 — base insulation layer, 2 — covered electrode, 3 — inter-electrode insulation layer, 4 — exposed electrode, d — gap width.[59]

the latter series of experiments a dielectric airfoil was used thus the base layer of insulator (1) was not needed anymore.

The sets-up actually were different for the four wind tunnels but basically it can be generalized: the length of the actuators tested is from 20 cm for structural tests to 120 cm in the LTT.

High voltage electric pulses were fed to the actuator by a coaxial cable. One of the electrodes was connected to the ground, and another was a high-voltage one. In the majority of the cases, exposed electrode was ground, and the high-voltage electrode was the covered one.

High voltage nanosecond pulses were provided by a nanosecond pulse solid-state generator, which was capable of producing pulses up to 10 kV of magnitude with rising time of 3 ns and length of 15 ns at repetition frequencies up to 10 kHz. This pulse generator was controlled by a arbitrary function generator, and the shape of the pulses was monitored by an oscilloscope by a back current shunt technique. Moreover, by the shunt, it has been calculated also the energy input into the flow given by the discharge. The energy calculation is based on the difference between the time integral of the pulse inputted and the pulse reflected back into the power generator through the HV cable.

All the experiments were performed in low speed wind-tunnels of Delft University of Technology; the speed of the flow was always kept between 10 and 80 m/s (Reynolds number $4x10^5$ and 3.2 millions respectively), and a Data Acquisition System(DAS)(different for each tunnel) was always controlled by a computer.

With DAS are meant all the interfaces between the computer and the acquisition equipments such as pressure transducers as well as thermo-couples as well as extensometers from the balance and so on.

3.2 Facilities

The tests have been carried out at the facilities of the University of Technology of Delft, in particular at four wind tunnels, all of them low speed: the V-Tunnel, the LTT(low turbulence tunnel), the M-Tunnel and the W-Tunnel.

3.2.1 V-Tunnel

The vertical low turbulence wind tunnel is a tunnel with an open test section and a vertical inflow from below. The inflow is through a circular exit with a diameter of 0.6m diameter. Due to the high contraction ratio of the settling chamber the quality of the airflow is very high in terms of the turbulence level that is smaller than 0.1%.

Next to this the tunnel is relatively silent, which enables performing aeroacoustic experiments. The maximum achievable velocity is 45m/s. The V-tunnel is one of the low speed wind tunnel of TUDelft.

The tests have been carried out in this tunnel and the actuator has been tested at 10, 20, 30 and 40 m/s.

A balance able to measure horizontal stresses was installed on the wind tunnel; the balance was, in turn, linked by a coaxial cable to a data acquisition device(DAD) that converted the signal in a readable value expressed in Newton.

Additionally a pitot probe was also installed on the wind tunnel; the probe was connected by two pipes to a reader able to give the differences between the total pressure and the static one, so by such a device it has been possible to read the effective dynamic pressure of the flow by this value to calculate the effective velocity of the flow.

3.2.2 Low Turbulence Tunnel (LTT)

The Low-Speed Low-Turbulence Wind Tunnel(LTT) is owned by the Faculty of Aerospace Engineering of Delft University. It is an atmospheric tunnel of the closed-throat single-return type, with a contraction ratio of 17.8.

The six-bladed fan is driven by a 525 kW DC motor, giving a maximum test section velocity of about 120 m/s. The maximum Reynolds number for two-dimensional testing is about 4.8 million based on a chord model of 0.6 metres. The free-stream turbulence level in the test section varies from 0.015% at 20 m/s to 0.07% at 75 m/s. The interchangeable octagonal test sections are 1.80 m wide, 1.25 m high and 2.60 meters long.

Mechanically actuated turntables flush with the test-section top and bottom wall provide positioning and attachment for a two-dimensional model. The standard

wind tunnel testing equipment consists of an electronically read 200 tubes multi-manometer with fiber optic cells, a 6-component balance, a 192 ports electronic pressure scanner system and hot wire anemometry and PIV systems. For flow visualization purposes an infra-red camera system is available. Data are recorded using an electronic data acquisition system and are on line reduced using the HP 9000-712 laboratory computer.

3.2.3 M-Tunnel

The M-tunnel is a model tunnel of the Low turbulence tunnel facility and is rather unique, since it can be used as both an open jet or a closed wind tunnel. Depending on whether it is used as an open tunnel or closed tunnel, the maximum velocity is 35 m/s or 50 m/s respectively. The test section of the tunnel is 0.4 m x 0.4 m square and due to the large contraction ratio the turbulence level of the flow in the test section is low.

3.2.4 W-Tunnel

The W-tunnel is an open jet wind tunnel with a square 0.4 m x 0.4 m exit. The maximum velocity is about 35 m/s and can be regulated by setting the revolutions per minute of the centrifugal fan. Depending on the flow velocity, the minimum achievable turbulence level can be in the order of 0.5%.

The tunnel setup is very simple: after the plenum and the centrifugal fan the flow passes through a diffuser. The flow than enters the settling chamber, after which it enters the contraction, a small tunnel nozzle and the tunnel exit. In case particles are added to the flow an external ventilation system can be used to filter the added particles out of the air.

3.3 Instrumentation

The instrumentation used in order to test the actuator was composed of nanosecond pulse solid-state generator, which was capable of producing pulses up to 12 kV of magnitude (nominal value) with rising time of 3 ns and length of 15 ns at repetition frequencies up to 10 kHz linked to the actuator by a coaxial cable with an impedance of 100 Ohms; an oscilloscope Tektronix TDS 3054C used for monitoring the pulse input and a function generator Tektronix AFG 3252 used for building the input pulse and for trigger the test.

The power generator was monitored by the oscilloscope and controlled by the function generator.

Hereafter, in the Fig.3.2, we can see a block scheme of the configuration of the set-up.

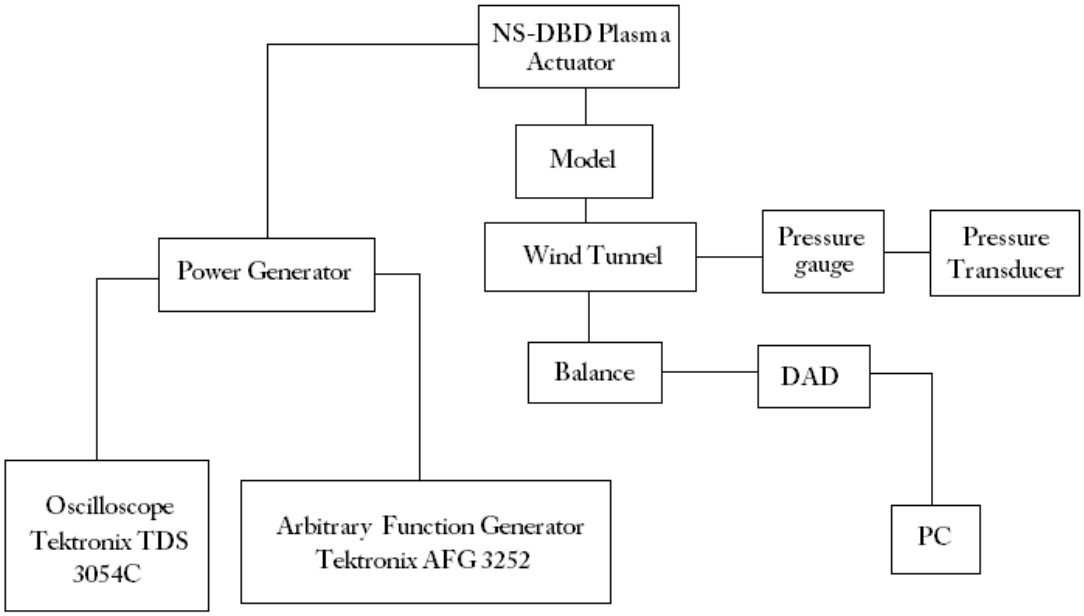

Fig. 3.2: Generic Block Scheme of a set-up

Moreover photos of the Power Generator, Oscilloscope and the Arbitrary Function Generator are presented in the Fig.s 3.3 and 3.4

3.4 Actuator

3.4.1 Geometry of the actuator

The geometry of the actuator is quite easy to realize; it is composed basically of two electrodes: a ground electrode and an high voltage electrode.

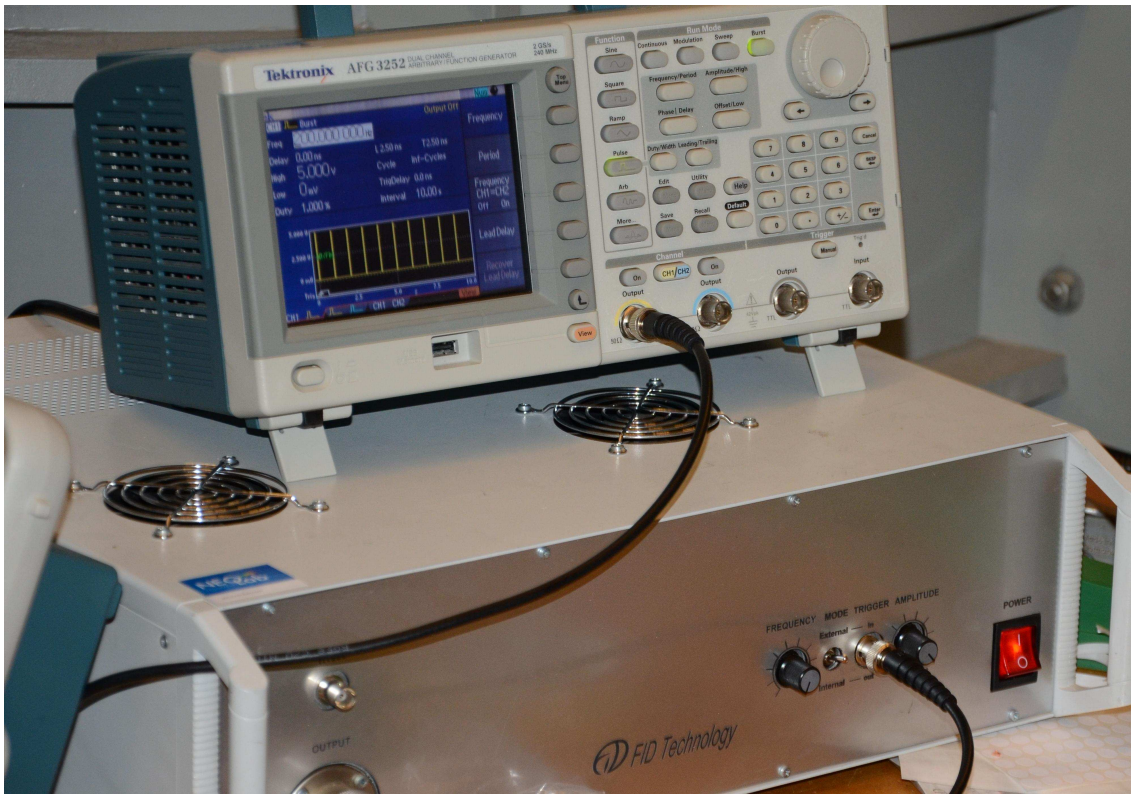

Fig. 3.3: On the botton the FID solid state power generator , on the top the Arbitrary Fanction Generator Tektronix AFG 3252

These two electrodes are never overlapped, this means that there is always some space between them and they are electrically separated by a layer of a dielectric material. The dielectric was made out of three layers of kapton tape, but the number of layers must be basically design on the applied voltage. Copper foil has been used for the electrodes. Both these things are easily findable in commerce.

Generic actuator layout is presented in Fig.3.1. The actuator consisted of a base layer of insulator (1) attached onto the surface of the airfoil, a covered electrode (2), an inter-electrode layer of insulation (3) and an exposed electrode (4). The thickness of the inter-electrode insulation was about 0.15–0.20 mm. Another adjustable parameter was the inter-electrode gap (d).

Geometrical parameters have been investigated such as the thickness of the dielectric layer, the horizontal distance between the two electrodes(gap), the width of the electrodes and the position of the actuator with respect to the leading edge of the wing.

	Thickness Dielec.	**Gap**	**Width Electrode**	**Pos. wrt LE**
range	0.1 mm - 0.3 mm	0.3 mm - 3 mm	5 mm - 10 mm	-5 cm - +5 cm

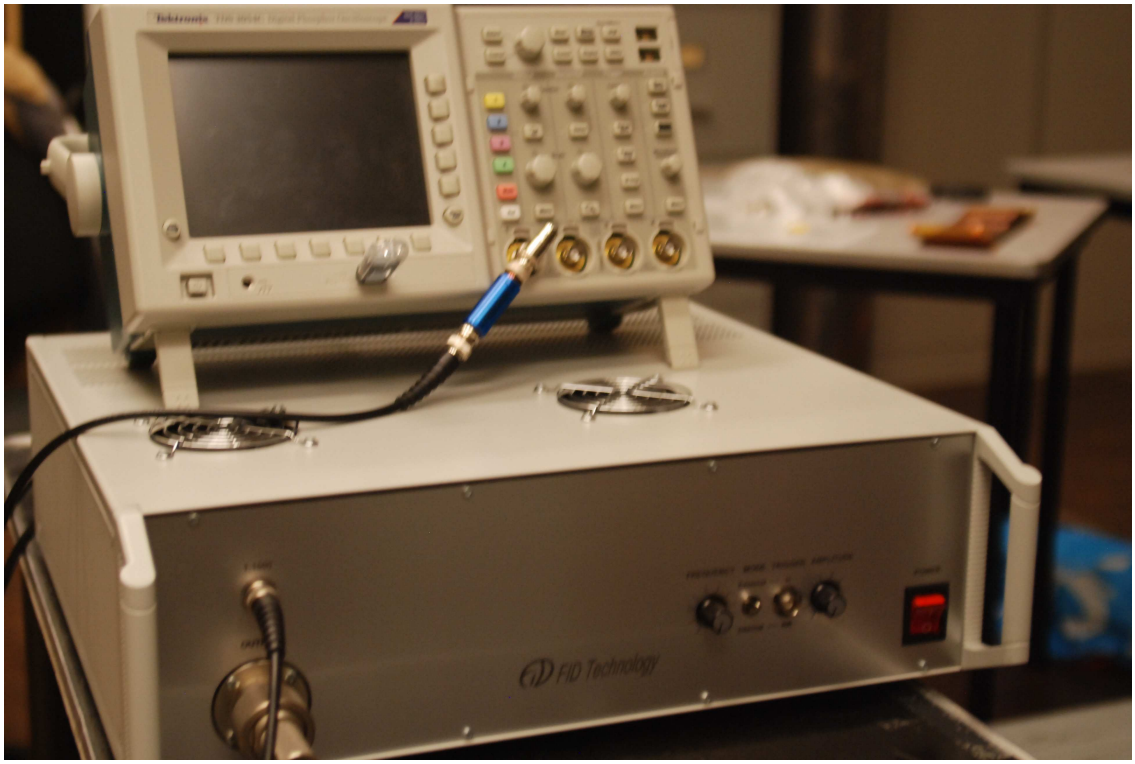

Fig. 3.4: On the botton the FID solid state power generator, on the top the Oscilloscope Tektronix TDS 3054C

3.4.2 Nomenclature

A universal way to name the actuator used will be used. The structure of the name will be composed in this way:

$$\mathbf{act\_\pm X_1/\pm X_2\_\pm Y_1/\pm Y_2\_Z}$$

where the distance will be indicated with the X coordinate in millimetres, from the leading edge of the profile till the front edge of the first electrode (regardless whether it was the ground electrode or HV electrode), as it is shown in Fig.3.5. The symbol plus or minus will indicate the direction of the measurement, so by that it will actually be defined if the electrode is on the upper part or on the lower part of the model.

The distance between the first electrode and the second one, that is practically the size of the gap between the two electrodes. will be indicated with the Y coordinate. Again the symbol plus or menus will state the exact position of the gap with respect to the position of the first electrode mentioned above. Thus the second electrode will be placed at the end of the gap. In this way the actuator is geometrically positioned on the model. The last coordinate, the Z, will indicate the thickness of

the dielectric layer in millimeters as well. The copper electrods have always the same thickness.

In the Fig.3.5, here below, the electrodes are painted in gray and the coordinates X_1 and Y_1 are shown. In the figure the dimensions are exaggerated for clarity reasons.

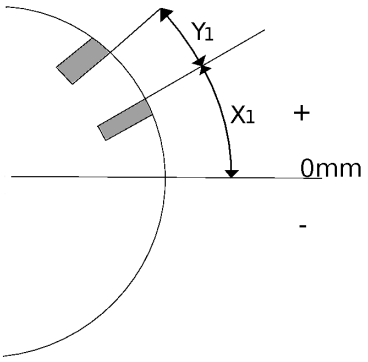

Fig. 3.5: Nomenclature scheme for defining univocally any actuator tested

In the case the coordinates X_2 and Y_2 will not appear it means that the actuator will only have one gap and only two electrode, which geometry is actually the most common one.

3.5 Models

The model used carrying out this experimental research have been a NACA 0015, a NLF-mod22 and a NACA 63-618. Such models have been tested in the V-tunnel, LTT and M/W-tunnel respectively.

The first one, the NACA 0015 has been selected at the first stage of the research itself. Being a very known airfoil a big amount of reference data are available in the literature. A picture of this model, in the V-tunnel test set-up, are presented in the Fig.s 4.1 and 4.2.

The NLF, or Natural Laminar Flow, airfoil has been selected for the test campaign in the LTT because it was furnished with pressure taps all over the upper and lower side of the profile. Moreover because of it characteristic stall behavior it was a good benchmark for future investigations. A picture of this model is given in Fig.4.14.

The last model used, the five digit NACA 63-618 was made on the purpose of being tested with NS-DBD Plasma Actuator. This is way the model is made out of dielectric material. Such a model has been selected for its characteristic trailing edge separation, this means that the separation of the flow along the upper surface of the airfoil happens smoothly which thing might imply that small changes in

the pressure distribution on the model might be enough for appreciating small reattached portions of the flow on the airfoil itself. Pictures of the model with different actuator configurations are presented in the Fig.4.45.

Chapter 4

Experimental Results

The scope of this chapter is to show the results of an experimental study of flow separation control with a nanosecond pulsed plasma actuator. Such investigation has been performed in four wind-tunnels of TUDelft.

The first series of experiments was carried out with a NACA-0015 airfoil with the chord of 20 cm. A linear actuator of different geometries was attached to the airfoil at different positions. The discharge used had a pulse width of 20 ns and rising time of 2 ns, and the voltage up to 12 kV. Repetition frequency was adjustable. The relation of the optimal discharge frequency to the chord length and flow velocity was proven. Different geometries of the actuator had been tested, including different insulator thicknesses, gap sizes and three and four electrode configurations; moreover for the latter testes also a configuration with a parallel of three actuator had been studied. Also the dependence of the effect of the actuator with respect to the position of it on the wing has been studied.

It appeared that the only effective position of the actuator is on the leading edge, but also a dependence on the shift of the actuator relative to the centerline of the profile by several millimeters was found. However it has been proved that a multi-actuator system is able to reattach the flow up to conditions which a single actuator could not reach. At the V-Tunnel separation elimination was shown at the velocities up to 40 m/s with a lift increase, in term of C_L, up to 20% and an increase of the stall angle of several degrees has been observed.

A second series of experiments was carried out at the LTT on the laminar airfoil NLF-MOD22A with a chord of 60 cm. In these experiments the pressure distributions on the surface of the airfoil and in the wake were obtained. At a flow speed of 30 m/s a notable increase of lift coefficient was found combined with a decrease of of drag coefficient (based on wake measurements). With this airfoil it was found to be harder to achieve separation elimination and the effect was found to be sensitive

to the actuator geometry and position. The experiments are supported by numerical simulation of the interaction of the shock wave produced by the discharge with the boundary layer (Simulation done by Ilya Popov).

A third series of experiments was carried out, at the M-Tunnel, on a NACA 63-618, a NACA 5-digit airfoil, typical wind turbine airfoil, with a chord of 20 cm. In these experiments the lift and the drag were measured with a velocity up to 10, 20 and 30 m/s, by using a balance of forces, for only one geometry of the actuator positioned on the leading edge of the airfoil. For this series of tests a special test section was applied to the open-jet wind-tunnel so the results do not need to be corrected for the open-jet effect of the wind tunnel. Separation elimination was shown again, and with this configuration the separation angle of attack was shifted more with respect to the first series of experiments. Again a lift increasing up to the 20% was shown.

A fourth series of experiments, Schlieren tests, was carried out with the same profile at the W-tunnel in order to find out the mechanism of the actuation. The parameters tested were: geometries, velocities of the flow, frequencies, angle of attach, number of pulse for each burst, and frequency of the pulses for each burst. It appeared that the use of a burst mode discharge increases the efficiency of the actuator, and it depends on the period of the pulses for each burst. Nevertheless it was found out that the energy input in the flow, in the case of a parallel actuator system is lower with respect to the case of a single actuator,

Again at the W-Tunnel a PIV campaign has been carried out on both the 5-digit NACA model, already used for the Schlieren tests, in a flow with a velocity up to 30 m/s, and on a flat plate in a still air box. A magnification of about three has been selected for the tests in order to investigate the discharge region very closely, looking for evidences of the actuation physical Mechanism. Very interesting results were acquired for the PIV test section.

Moreover a series of aerodynamics tests have been carried out in order to investigate geometry parameters of actuators such as the distance between the electrodes or the positioning of the actuator itself with respect to the leading edge; a series of structural tests have been carried out as well in order to get information about the thermal and the structural impact of the actuator on a wing.

The actuator has been tested in severe conditions, and its effectiveness has been shown in high humidity condition. Still air test has been performed in order to observe if the presence of ice in the discharge region could affect the actuator functioning/working. In this section, the most significant results obtained will be presented.

4.1 Tests @ V-Tunnel

In the V-tunnel several series of tests have been carried out: at 10, 20,30 and 40 m/s, with alpha(angle of attack) between 0 and 30 degrees.

The model used for the tests was a NACA-0015 that is a symmetrical airfoil, with a percentage thickness of the 15% of the chord; the chord was about 20 cm and the span of the model was 75 cm.

It is needed to be pointed out that because of the downwash effect the angle of attack tested in this wind tunnel needs to be correct(for corrections see Appendix A).

In the Fig.s4.1 and 4.2 is shown the set-up used in the V-tunnel test campaign.

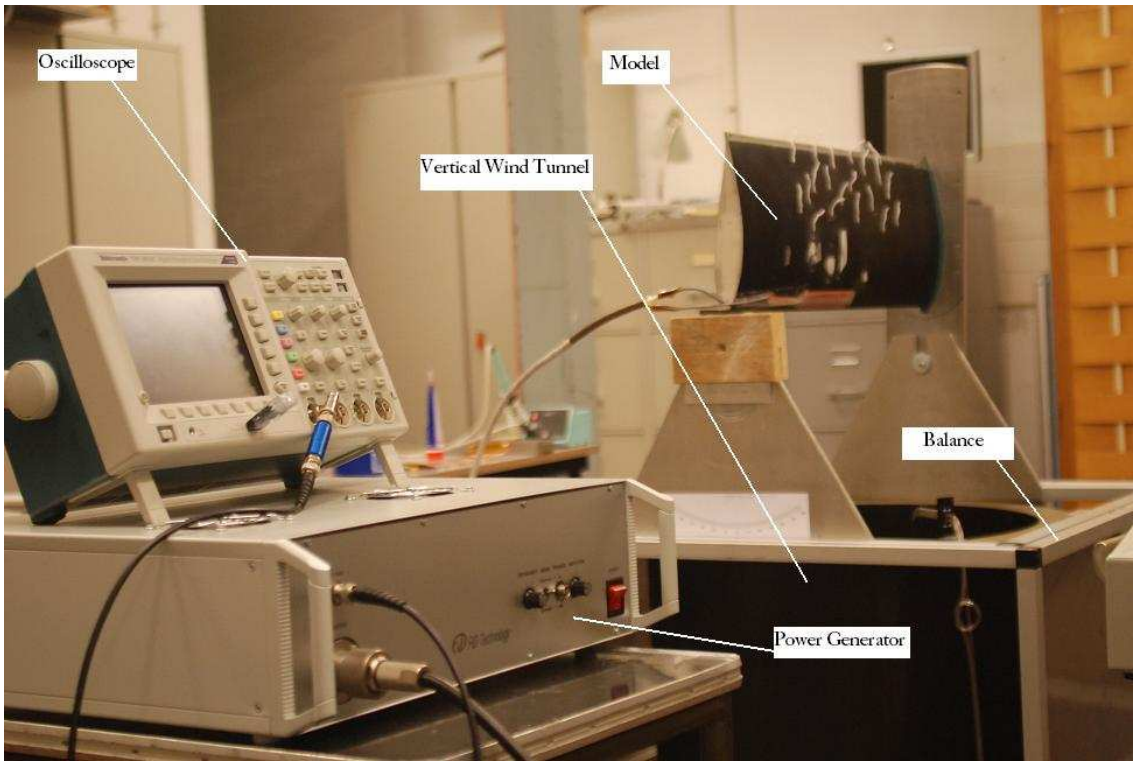

Fig. 4.1: Set-up of the Vertical Wind-Tunnel test campaign

In particolar in the Fig.4.2 is appreciable the blue glow due to the electrical discharge. Such a glow is visible at naked eye only if the frequency of the discharge is high enough.

4.1.1 Description

The actuator used for these series of tests was roughly 70 centimeter long; each electrode was ten millimeter wide and 0.17 millimeter thick.

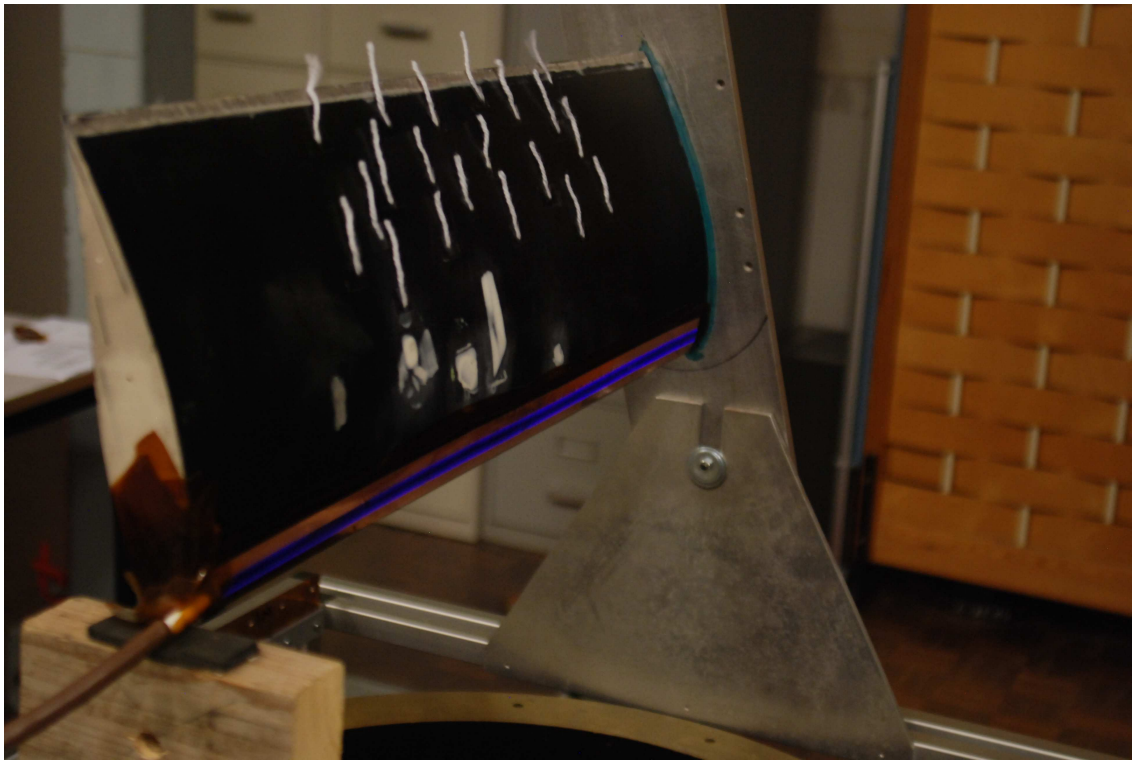

Fig. 4.2: In the picture is visible the blue glow due to the discharge into the NS-DBD Plasma Actuator

The test itself consisted in letting the tunnel run, actuating the discharge, and acquiring measurements by Data Acquisition System (DAS).

The DAS was controlled by a computer which was able to have a direct reading of the lift acting on the wing, and averaging it on a number of ten measurements, so, once a velocity was fixed , for each angle of attach, an average on ten measurements gave us the value of the calculated C_L.

Each series of tests was aimed to produce a lift polar (C_L vs α) and by a direct comparison of the obtained curves, the conditions and the actuator geometries for further testing were decided.

Several kinds of actuators have been investigated: two electrodes, three electrodes (symmetrical and not symmetrical), four electrodes(or double actuator).

Actually the three and four electrodes actuators have not given good results: one of the most probable reason is that for those actuators the energy density distributed over the discharge region was too low for getting any effect.

4.1.2 Results @ V-Tunnel

The first series of tests carried out at the V-tunnel was with a flow velocity up to 10 m/s. In Fig.4.3 the calculated polars (C_L vs α) can be seen.

The actuator chosen was: act_+20_+0.5_0.2: this means that the front edge of the first electrode is met along the surface of the wing 20 millimeter far from the leading edge of the model, on the upper part of the airfoil, since the sign is plus; the gap between electrodes is roughly 0.5 millimeter in the same direction starting from the edge of the first electrode and the thickness of the dielectric layer is roughly 0.2 millimeter. In this case (and almost in all the cases) the first electrode that has been met along the surface form the leading edge is the High Voltage (HV) electrode and it is covered by the dielectric layer, so the Ground (Gd) electrode is the one exposed to the flow.

Two cases are shown: Actuator ON and Actuator OFF.

Before proceeding with showing results it must be state that, since the configuration of the vertical wind tunnel the maximum lift achievable in this wind tunnel is always lower than the theoretical one. So for the data acquired in this test campaign extra correction might be required, but since this test campaign was aimed to observe the phenomenon of the actuation and to get an idea about what it could be able to achieve a relative comparison of data between configurations with actuator ON and OFF are enough.

Thus there is no need of extra corrections for this data since the interest in this case is not toward the absolute value of the lift reachable but only for the relative difference of lift between the two cases.

It is evident the effect of the actuator on the C_L that moves the separation of the flow backwards: in fact with the actuator OFF it can be observed that separation happen at an AoA up to 18[deg] and it moves at an AoA of 19[deg] when the actuator is turned ON.

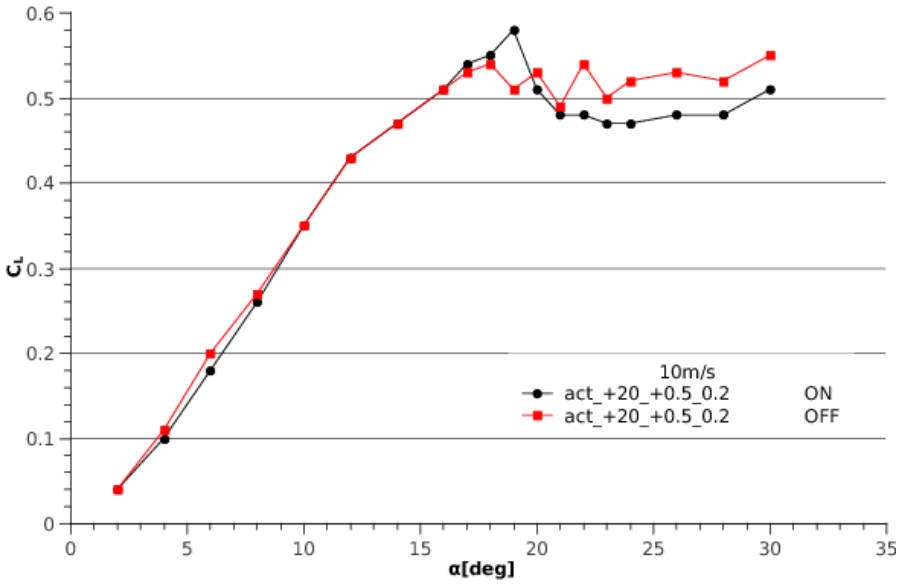

Fig. 4.3: C_L vs α up to 10m/s on a NACA-0015 in the V-tunnel @ TUDelft

At a wind speed of 20 m/s the effect of the actuator becomes more prominent as can be seen in Fig.4.4.

What it is clearly seen is that the effective C_L is increased of about the 20% of its maximum value and the separation that the flow experiences at an inclination of 17 degrees with respect to the flow direction moves forward till an angle up to 21 degrees.

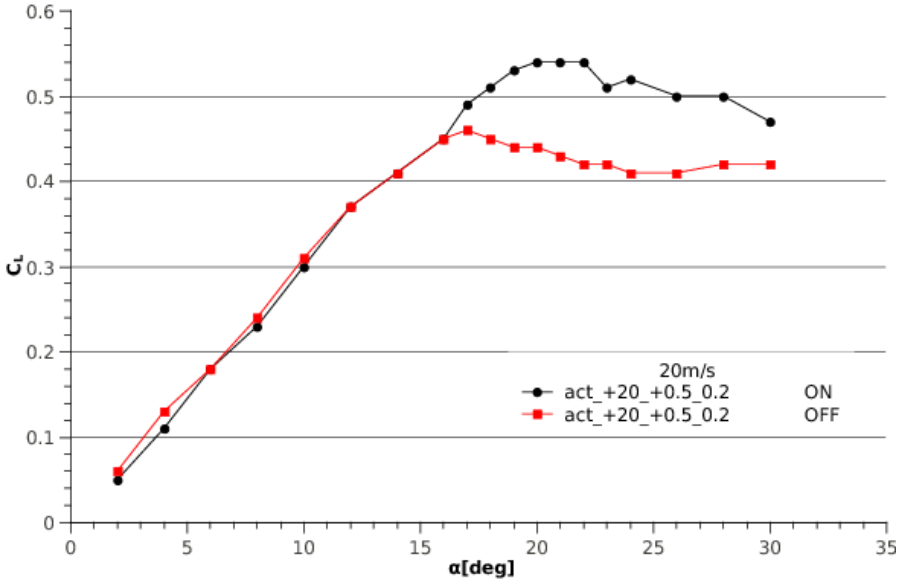

Fig. 4.4: C_L vs α up to 20m/s on a NACA-0015 in the V-tunnel @ TUDelft

Hereafter the same test with the same actuator at 30 m/s.

Also here almost the same result with respect to the case of 20 m/s has been obtained: separation delay and the C_L increasing look the same.

After this series of tests it was decided to use the case of 20 m/s as a reference, and to compare that results obtained testing other geometries at exactly the same flow conditions.

In the Fig.4.6 the result for a different geometry compared with respect to the latter one can be observed.

The actuator was: act_-5_+4_0.15 that means that the edge of the first electrode of such a geometry is placed on the lower part of the airfoil, exactly at 5 millimeter below the leading edge of the profile; the gap between electrodes is roughly 4 millimeter wide, it was wider with respect to the actuator used in the reference case. The electrical field between the two electrodes in this case must be lower with respect to the reference case since the two electrodes were placed quite far apart from each other, so, in order to increase the electrical field between the two electrodes, a thinner the dielectric layer was employed.

The improvement that the new geometry brings to this result is appreciable: explanation for such a behavior could be found either in the manipulated electrical field

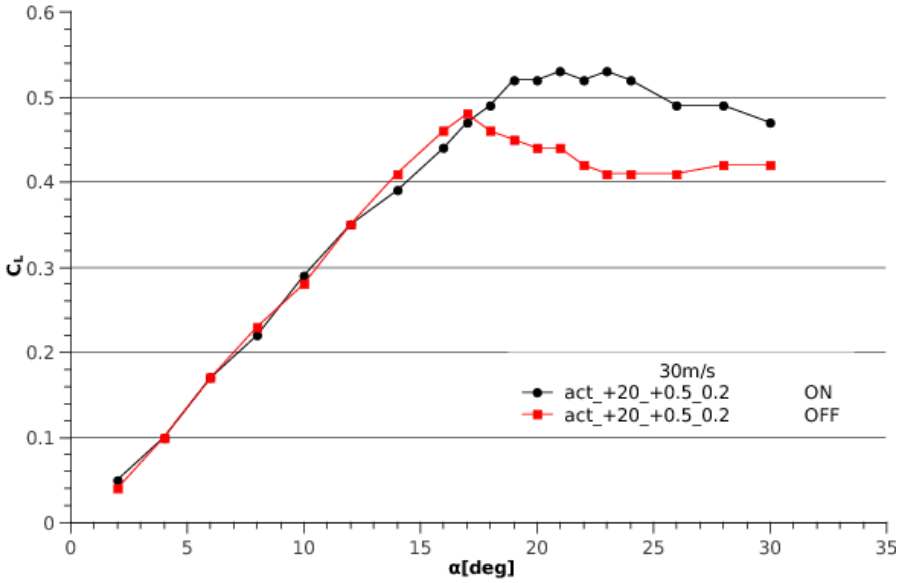

Fig. 4.5: C_L vs α up to 30m/s on a NACA-0015 in the V-tunnel @ TUDelft

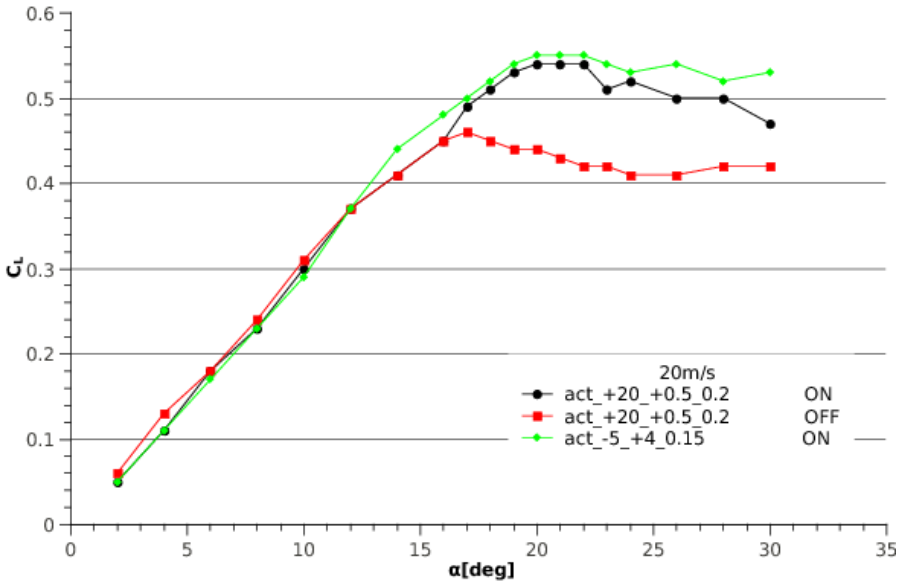

Fig. 4.6: C_L vs α up to 20m/s on a NACA-0015 with a new geometry actuator, in the V-tunnel @ TUDelft

which could have resulted to be stronger with respect to the reference case, so that the energy inputted into the flow by the discharge is higher; either the position of the actuator on the bottom part of the airfoil nose let it work in the thinner part of the boundary layer where actually it is supposed to be more effective[56].

Moreover, the gap between the electrodes was bigger which thing might affect the turbulization effect produced by the NS-DBD plasma actuator.

Hereafter, in the Fig.4.7 the previous results compared with respect to the case of a three electrodes actuator tested at the same aerodynamics conditions (velocity of the wind again up to 20 m/s) can be seen.

It could be observed that the three electrodes actuator was not able to get results as good as the two electrodes one.

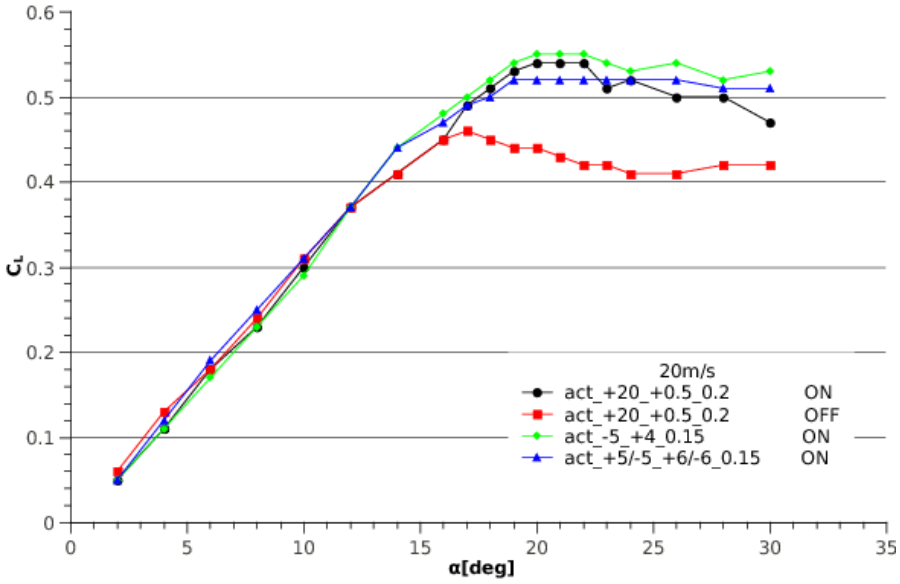

Fig. 4.7: C_L vs α up to 20m/s on a NACA-0015 with a three electrodes actuator, in the V-tunnel @ TUDelft

In the Fig.4.8 the results on an two electrodes actuator built with the gap on the leading edge is shown. It could be noticed that also such a geometry is still not able to get results as good as the actuator placed on the lower part of the airfoil nose does.

Moreover, in the following graph the mechanical effect due to the presence of the actuator itself in the flow.could be appreciated.

In the end, results of flow visualization test by means of tufts are here shown. Flow separation elimination has been demonstrated with a velocity of the flow up to 40 m/s with a Reynolds number of about $4e^5$. In the Fig.4.10 pictures of the flow visualized by tufts before and after actuation are shown.

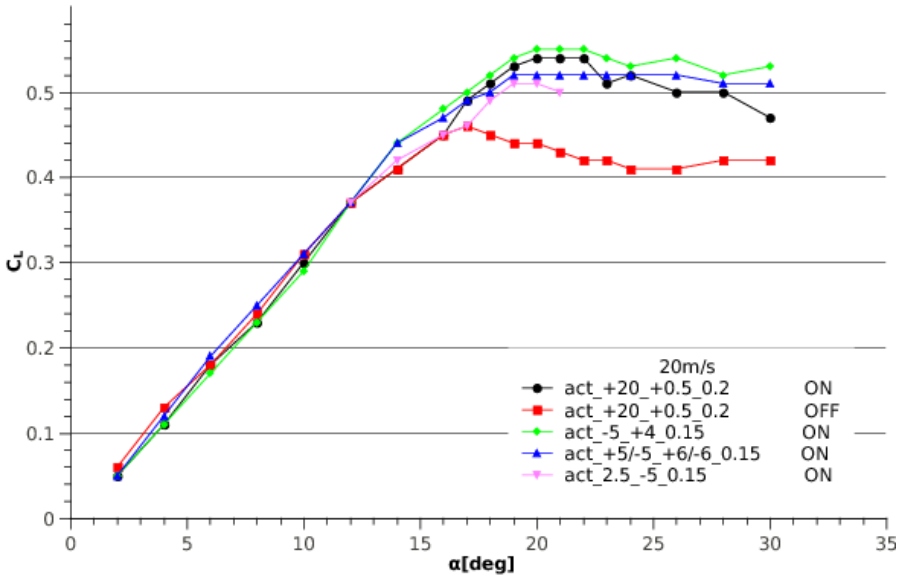

Fig. 4.8: C_L vs α up to 20m/s on a NACA-0015 with the actuator at another different position, in the V-tunnel @ TUDelft

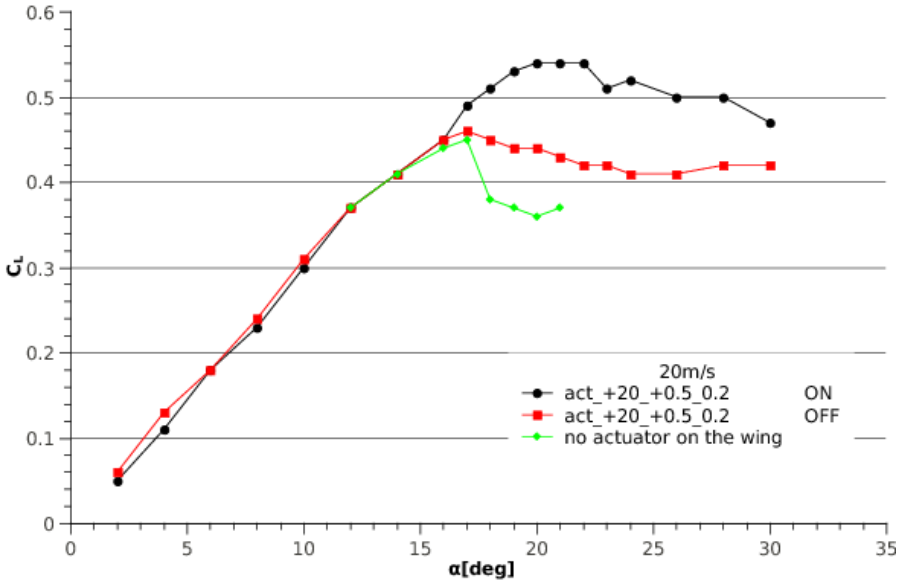

Fig. 4.9: C_L vs α up to 20m/s on a NACA-0015 without the actuator on the wing, in the V-tunnel at TUDelft

(a) Before Actuation (b) After Actuation

Fig. 4.10: Flow visualization actuator off (a) and actuator on (b), with a flow velocity at 40m/s

4.2 Tests @ LTT

In the LTT a series of tests have been carried out in order to investigate the effect of the actuator at higher velocities and Reynolds numbers. The maximum velocity reached has been 80 m/s with a Reynolds number, based on a chord of 0.6 meter, about 3.2 millions. In the Fig.4.11 a picture of the LTT.

Fig. 4.11: An overview of the Low Turbulence Tunnel (LTT) and its control station operated by the Author.

The model used for the tests was a flapped model, the NLF-MOD22, with the flap set at 0 degrees. The chord of the model with the flap retracted was 60 cm and the span was 125 cm. In order to produce separated flow the model was set at an AoA about 14.5 degrees.

By means of pressure gauges placed all along the upper and lower surface of the model, the pressure distribution on the wing has been acquired.

Moreover wake measurements by means of a wake pressure rank, placed transversally with respect to the airfoil, downstream in the far field. Such a device was capable to measure the momentum defect due to the wake. In the Fig.4.12 a picture of the pressure wake rank is shown. The picture has been taken from the inside of the wind tunnel.

The pressure gauges from the model and from the wake rank where monitored by the MMMM device. In the Fig.4.13 a picture of the MMMM is presented.

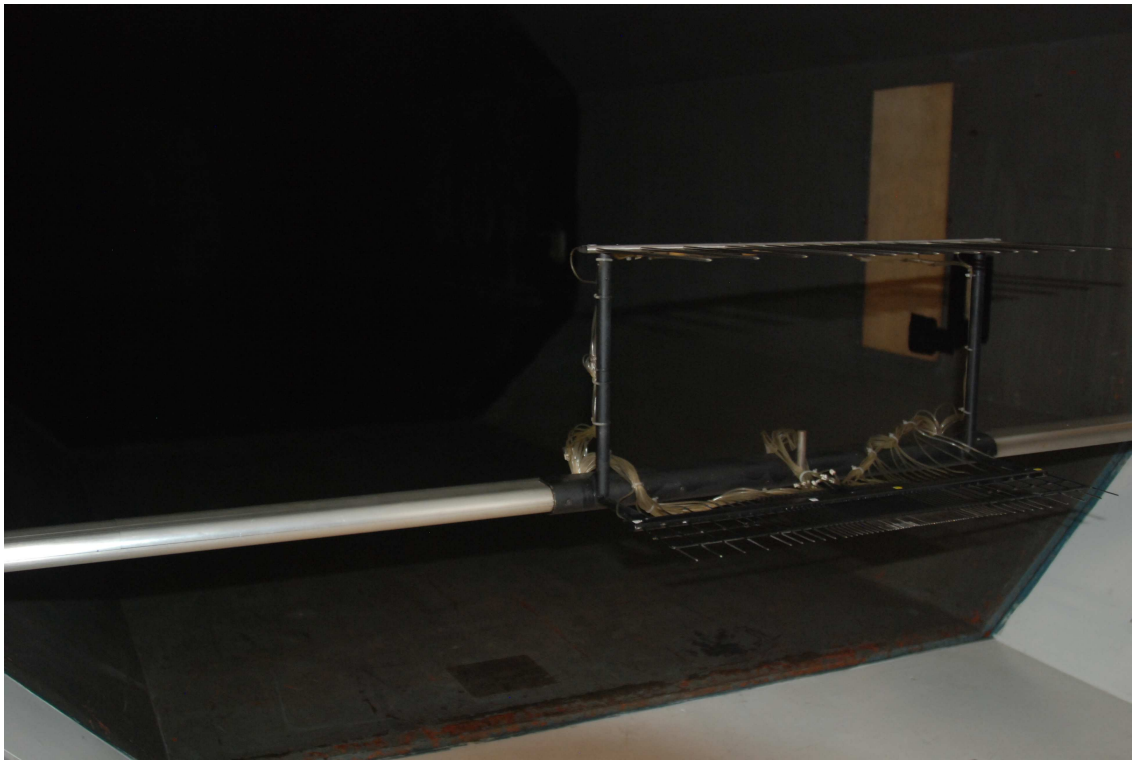

Fig. 4.12: Pressure wake rank. Picture taken from the inside of the wind tunnel

4.2.1 Description

The actuator used for the tests in the LTT was 120 cm long, on the very beginning, but since it has been no possible to appreciate any macroscopic effect of the actuator by tufts visualization applied on the upper surface of the wing, it has been hypothesized that the energy density per span centimeter could have been too low. In that respect it has been decided to make the actuator roughly 50 cm long in order to increase the energy density distribution of the discharge. The actuator was placed in such a way that its center point was about the location of the pressure gauges.

With such an set up the pressure distribution measured might be affected by the fact that the flow may not be bi-dimensional anymore. A redistribution of the pressure in the spanwise direction might reduce the value of the pressure measured by pressure gauges.Thus a lower value of pressure is expected to be measured. This will also affect the C_L and C_D since they are calculated based on the measured C_P distribution.

The test itself consisted in letting the tunnel run and taking measurements by profmeas program, a computer program installed on the LLT computer controller, consider to be part of the LTT DAS.

Such a program was able to read the pressure distribution and to return a plot of

Fig. 4.13: MMMM pressure monitoring.

the C_P along the chord and by that measurement to calculate C_L and C_D.

By a direct reading of the C_P's distribution it has been possible to check if the actuator was working (being affective) or not and in this way it has been possible to look for the conditions which the actuator could have worked, in that respect deciding the changes upon the actuator itself for further testing.

In the LTT only one kind of actuator has been investigated: the two electrodes one, with different size of the electrodes and different gaps.

4.2.2 Results @ LTT

Here below, in the Fig.4.15, the distribution of the coefficient -C_P along the upper and the lower part of the wing can be seen. It can be observed a smooth separated flow around the 35% of the chord, the presence of the retracted flap is visible on around the 70% of the chord, on the lower side of the curve.

Each curve represents such C_P's distribution with respect to the dimensionless chord at different discharge frequencies.

At the initial location (dimensionless chord about zero) it can be observed the effect of the presence of the actuator on the leading edge of the model: the Actuator closes the taps in those locations not allowing pressure measurements there. In the

Fig.4.14 a picture illustrating such a situation. In the picture the red arrow indicate one of the taps closed by the actuator.

Since the highest value of the pressure is actually expected to be at the leading edge, the presence of the actuator does not allow a complete measurement of the pressure distribution on the wing: this fact will affect the calculations of the lift since it is based on the measured C_P. Correction for this effect is possible considering, as approximation, the C_P distribution around the actuator location in condition of no actuator on the wing. Integrating this values on the uncorrected data a more realistic lift calculation might be done.

The actuator used was: act_0_3_0.15, the test has been carried out at 40 m/s and the angle of attack was 15 degrees. The width of the two electrodes was 5 millimeter.

The Figs.4.16, 4.17 and 4.18 details of the Fig.4.15 are visualized. It is clearly visible the difference between the curves.

In all these plots it is visible how the pressure distribution on the wing improves (increasing on the lower side and decreasing on the upper side of the wing) while increasing the frequency of discharge till up a value of 300 Hz. After such a frequency value the pressure start reducing

Hereafter, in the Fig.s 4.19 and 4.20, it is possible to see the differences in the C_L and in the C_D depending on the frequency of the discharge.

The effect of the actuator on the C_D, that when the discharge is up to 300 Hz goes down to 1/3 of its value with respect to the no discharge case is quite impressive.

A very interesting thing to remark out is that the same test with the same actuator but with a gap between the electrodes ten times smaller (0.3 millimeter instead of 3 millimeter, so the act_0_0.3_0.15) has not given any effect at all. This phenomenon as well as all the others will be discussed later.

By the graph it is understandable that the distribution of the pressure on the wing is affected by the NS-DBD plasma actuator. The effect gets stronger by increasing the frequency of the discharge till up to 300 Hz, above that value the effect of the actuator becomes smaller and the pressure coefficient of the wing drops.

Hereafter, from Fig. 4.21 to Fig.4.32 we can see the results of tests carried out at a flow velocity of 50, 60 and 80 m/s on an act_0_3_0.25.

4.2.3 Burst mode

In order to increase the energy inputted into the flow instead of a single pulse mode a burst mode discharge has been employed. Thus, each time the input was given, instead of using a single pulse, a burst containing several pulses was given. This trick, even if it did not increase the energy of a single pulse, was capable of inputting more energy into the flow. In the Fig.4.33 a sketch of such kind of discharge is given.

A series of tests with such a discharge has been carried out : the investigated parameters of the burst were the number of pulses of each bust, the frequency within each burst, and the frequency between the bursts themselves

The Fig.s4.34, 4.36, 4.35 and 4.37 show a small improvement of the effect of the actuator using the burst mode discharge. Such a result have suggested the possibility of scaling upwards the actuator since inputting more energy the effect looked anyhow improved.

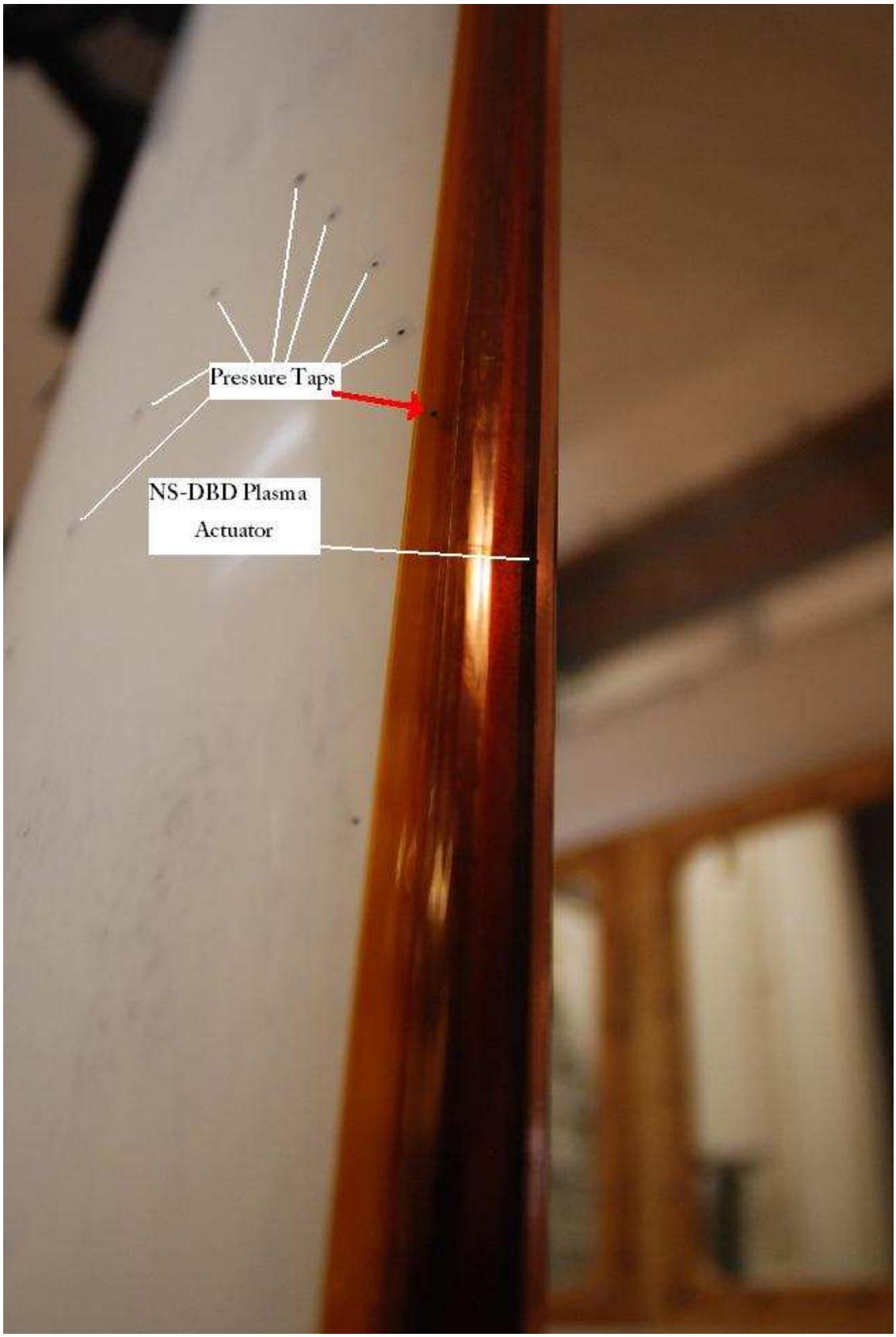

Fig. 4.14: In the picture the NLF-Mod22 with NS-DBD Plasma Actuator built on the leading edge of the airfoil. In the picture also the pressure taps are visible. The red arrow indicates one of the pressure taps closed by the presence of the Actuator.

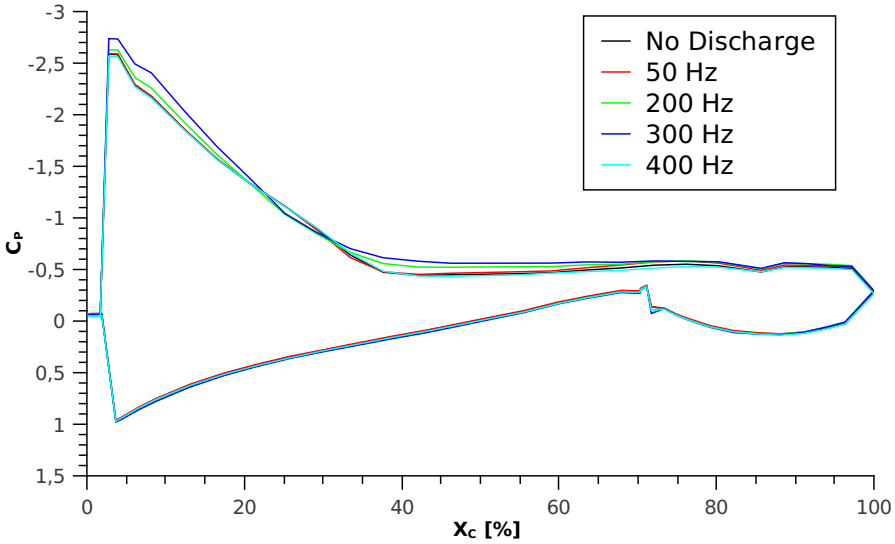

Fig. 4.15: Effect of the NS-DBD Plasma Actuator on the distribution of C_P at 40 m/s along the surface of the wing on the model NLF-MOD22A, at LLT of TUDelft

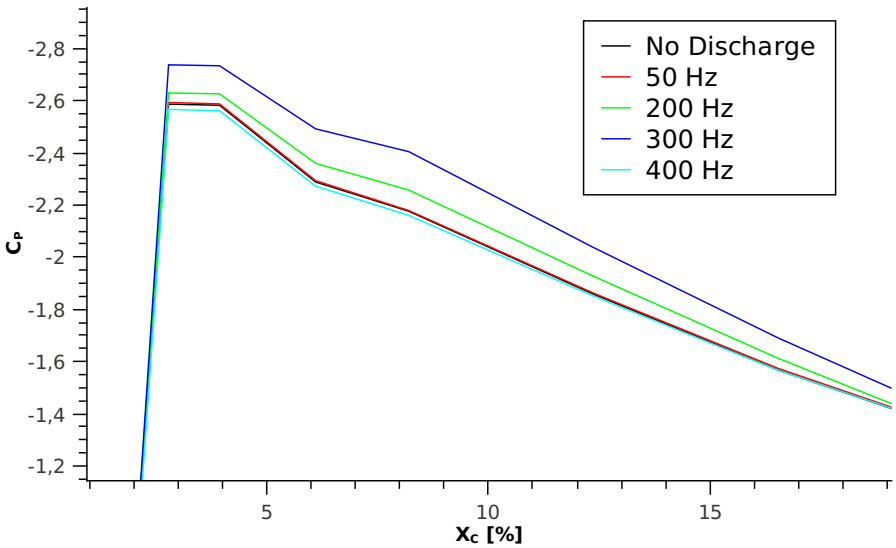

Fig. 4.16: Detail of the C_P around 5% of the chord on the model NLF-MOD22A

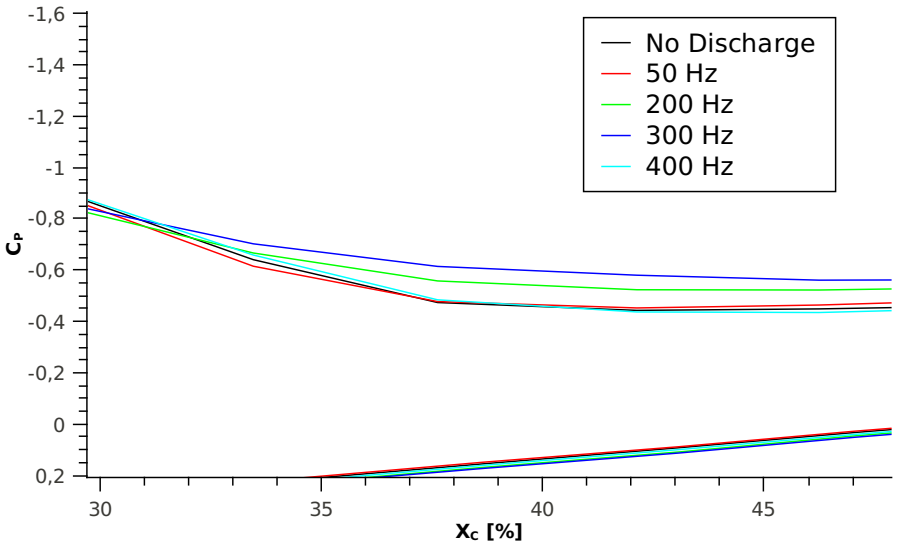

Fig. 4.17: Detail of the C_P around 35% of the chord on the model NLF-MOD22A

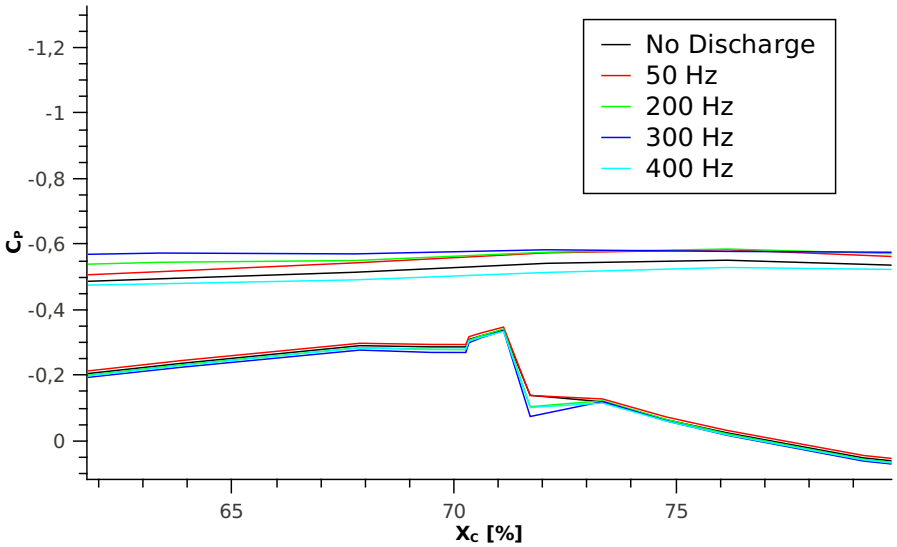

Fig. 4.18: Detail of the C_P around 70% of the chord on the model NLF-MOD22A

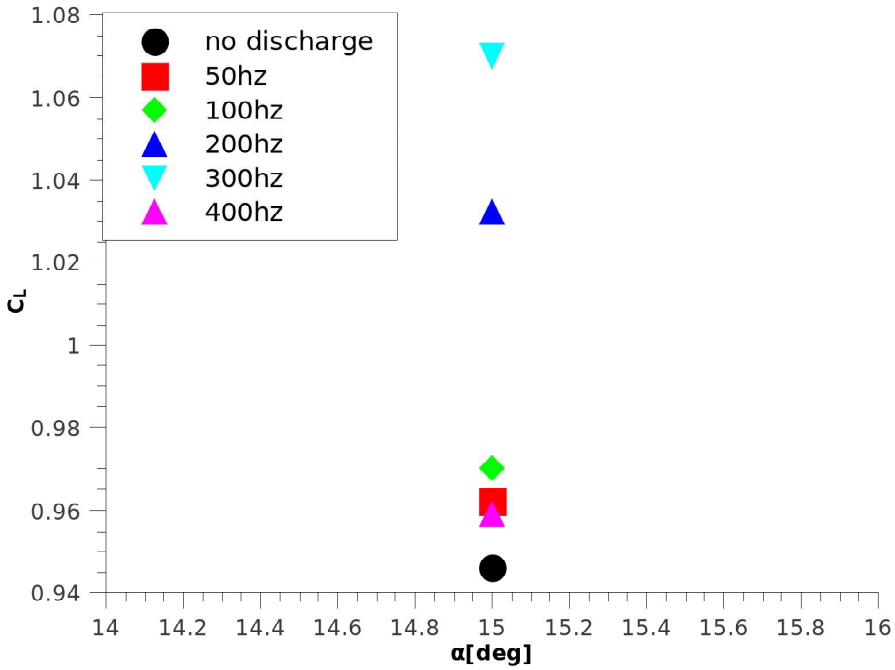

Fig. 4.19: Changing of the C_L coefficient depending on the frequency of the discharge at 40 m/s; model NLF-MOD22A

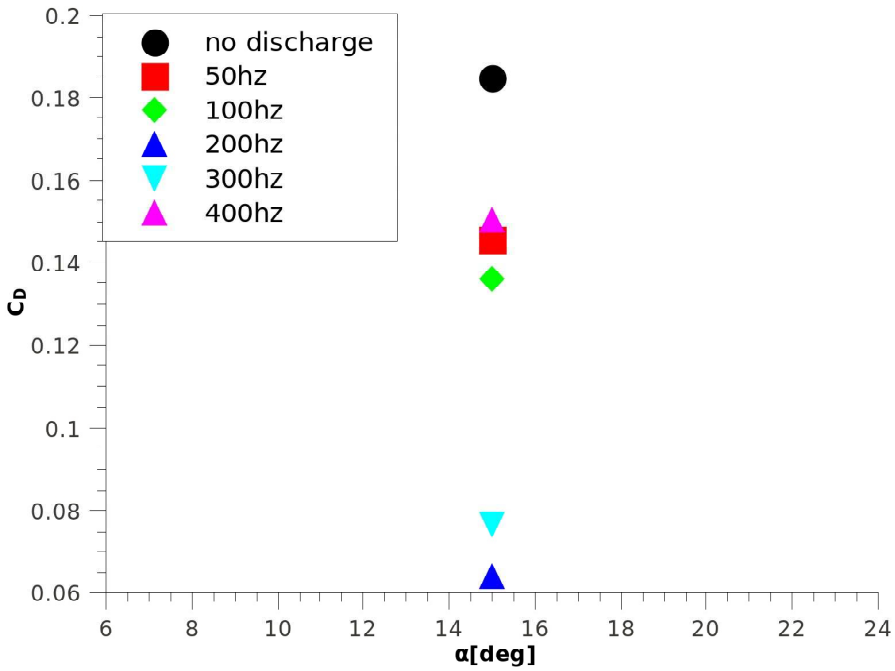

Fig. 4.20: Changing of the C_D coefficient depending on the frequency of the discharge; model NLF-MOD22A

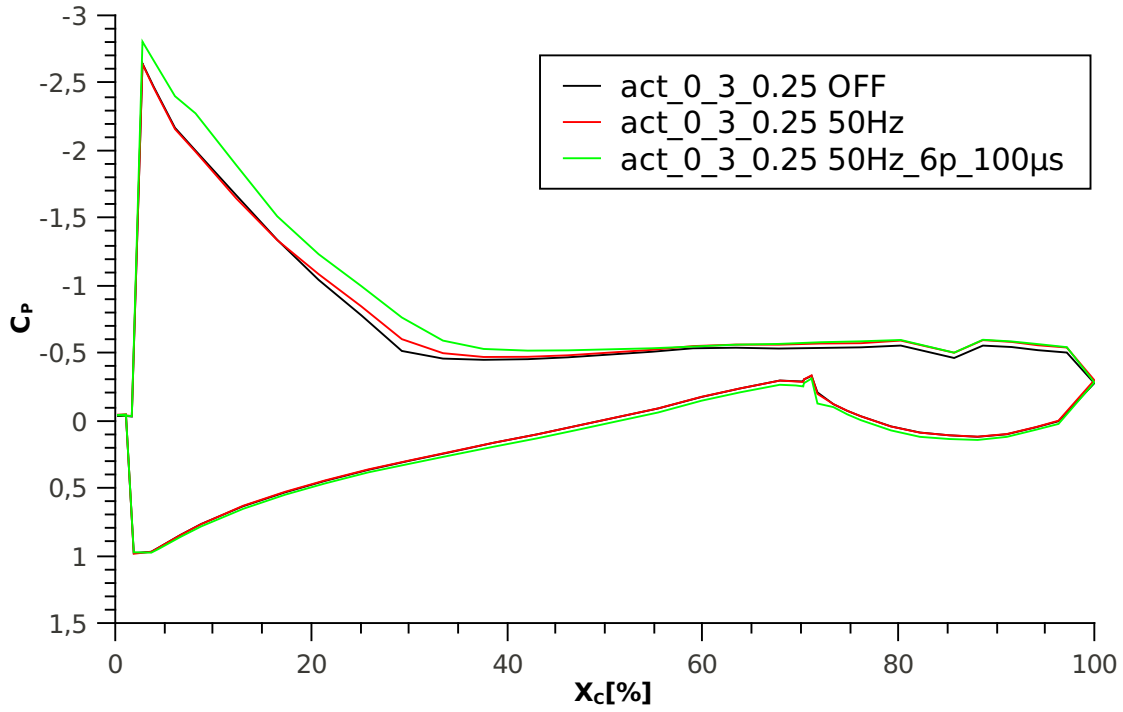

Fig. 4.21: Distribution of C_P at 50 m/s along the surface of the wing on the model NLF-MOD22A, @ LLT of TUDelft

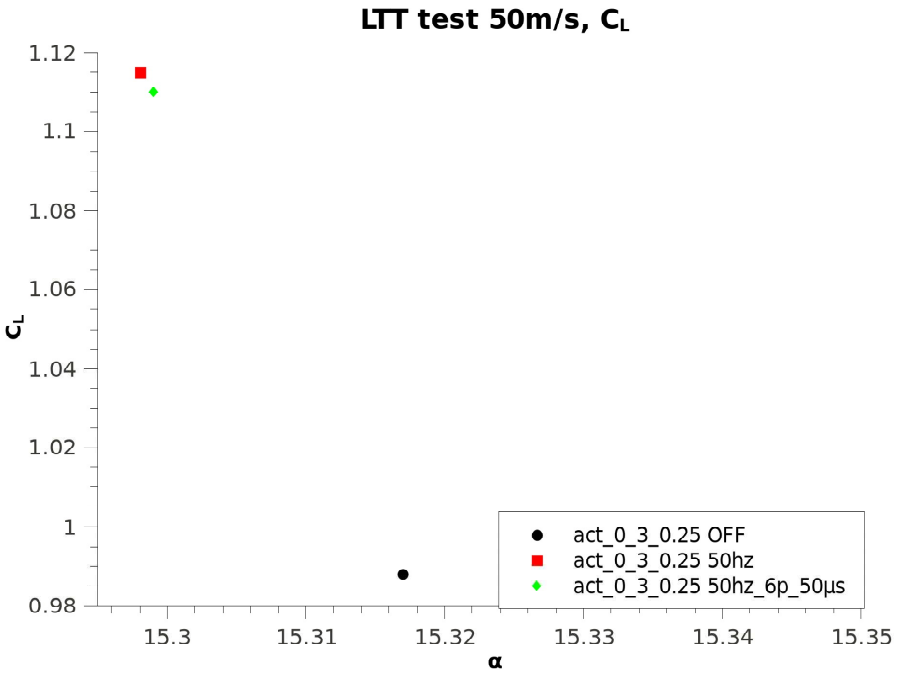

Fig. 4.22: Changing of the C_L coefficient depending on the frequency of the discharge at 50 m/s; model NLF-MOD22A

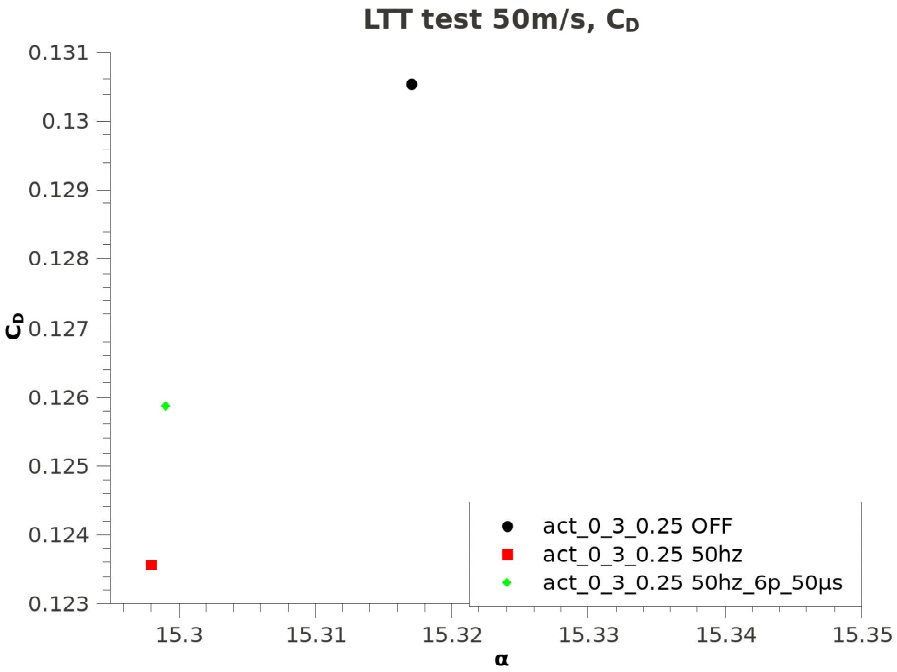

Fig. 4.23: Changing of the C_D coefficient depending on the frequency of the discharge at 50 m/s; model NLF-MOD22A

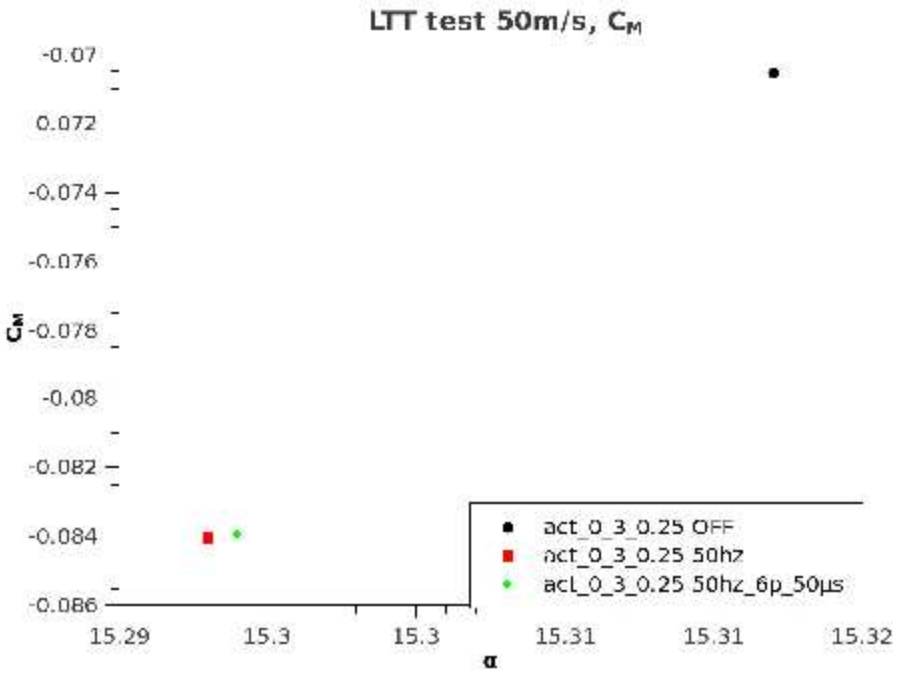

Fig. 4.24: Changing of the C_M coefficient depending on the frequency of the discharge at 50 m/s; model NLF-MOD22A

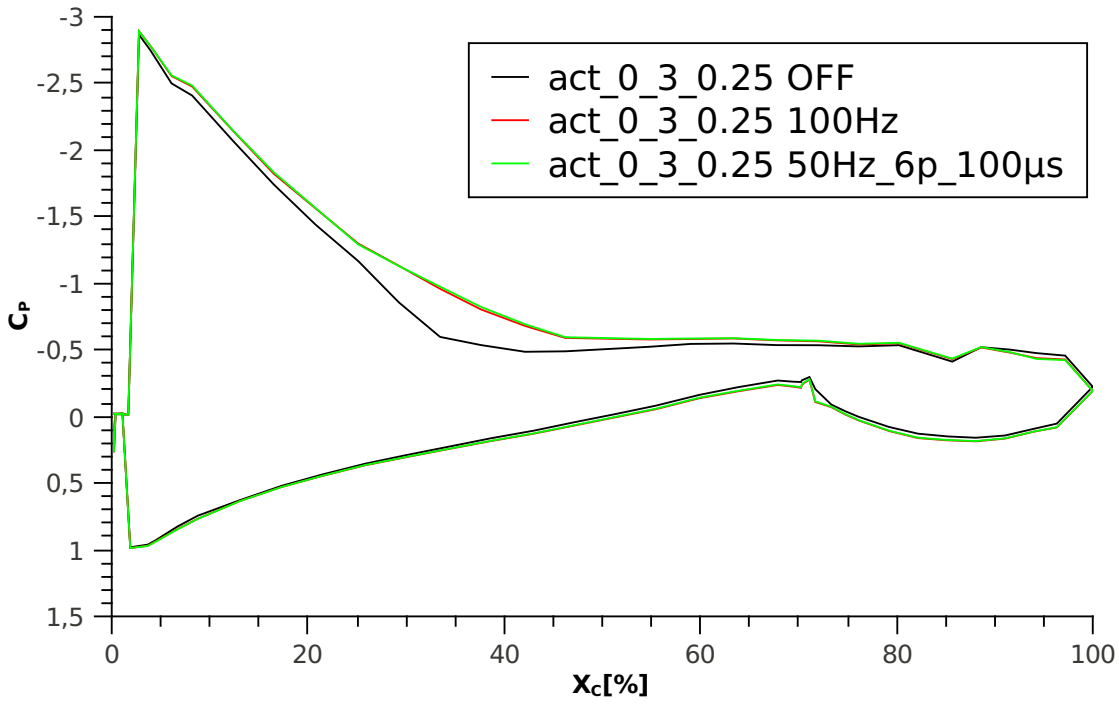

Fig. 4.25: Distribution of C_P at 60 m/s along the surface of the wing on the model NLF-MOD22A, @ LLT of TUDelft

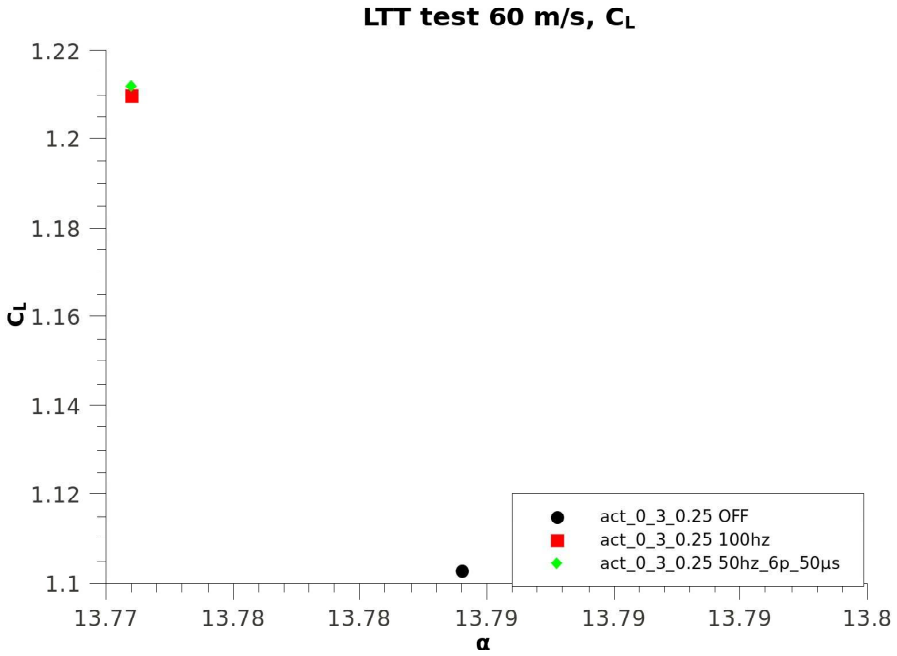

Fig. 4.26: Changing of the C_L coefficient depending on the frequency of the discharge at 60 m/s; model NLF-MOD22A

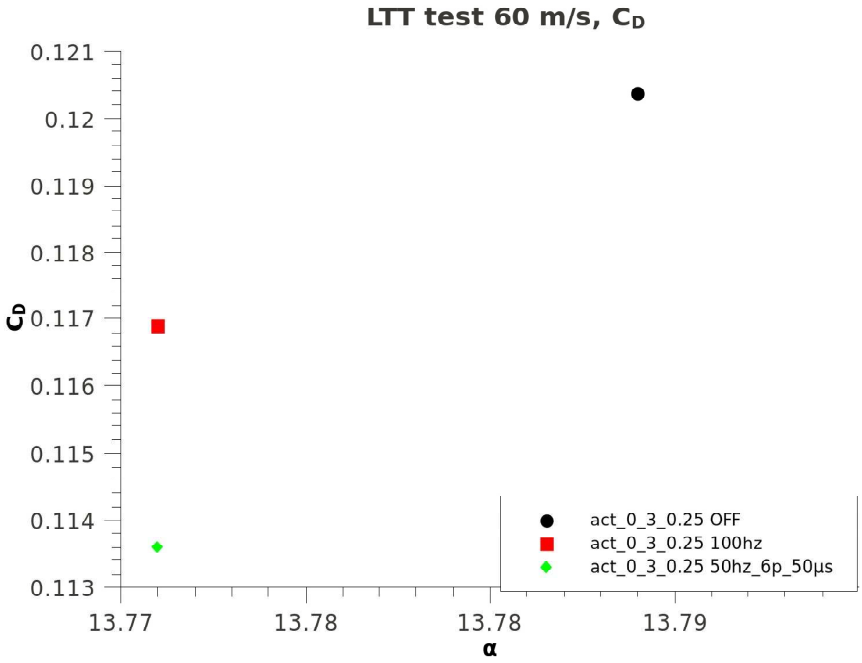

Fig. 4.27: Changing of the C_D coefficient depending on the frequency of the discharge at 60 m/s; model NLF-MOD22A

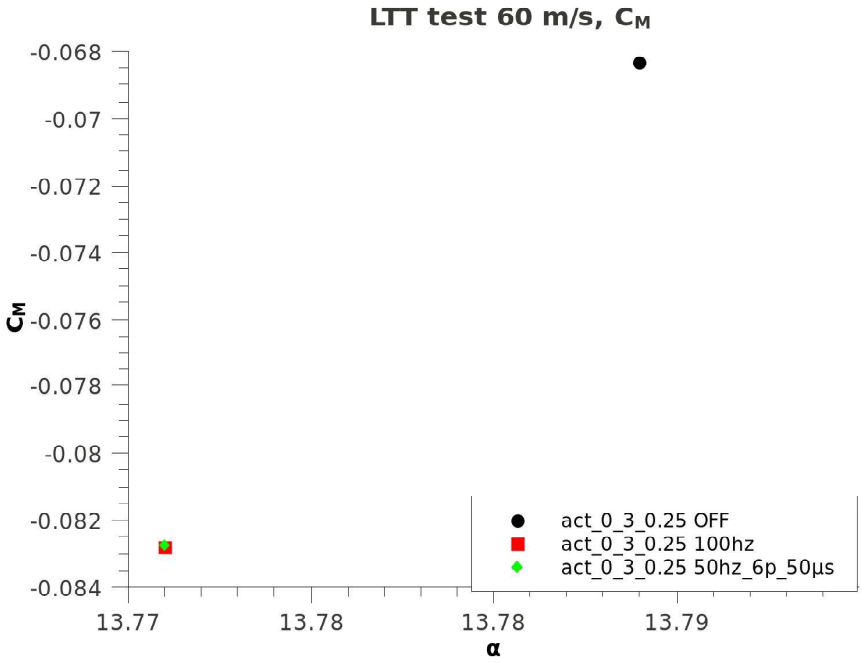

Fig. 4.28: Changing of the C_M coefficient depending on the frequency of the discharge at 60 m/s; model NLF-MOD22A

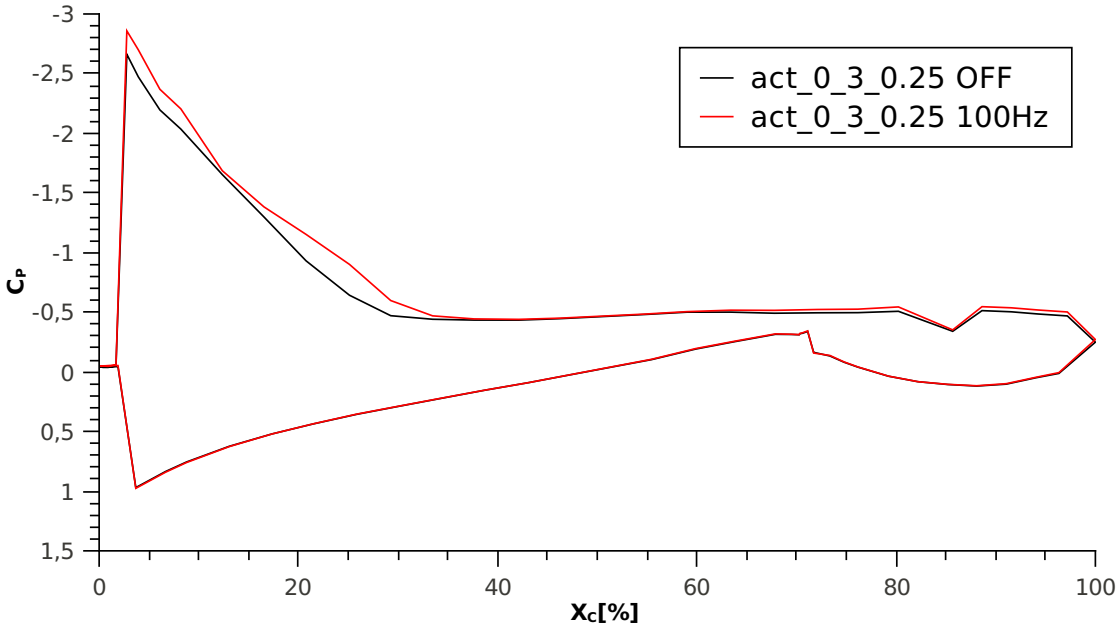

Fig. 4.29: Distribution of C_P at 80 m/s along the surface of the wing on the model NLF-MOD22A, @ LLT of TUDelft

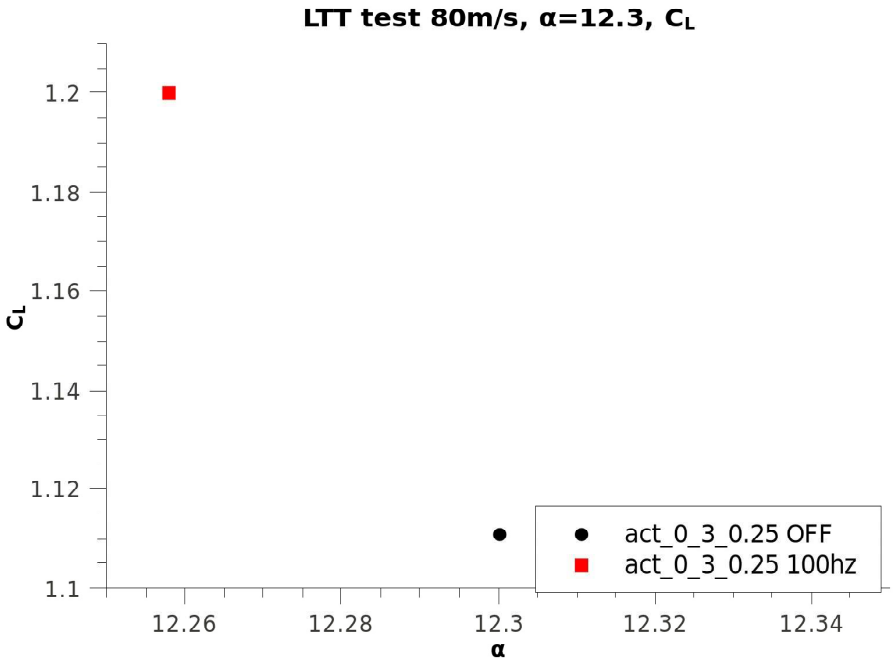

Fig. 4.30: Changing of the C_L coefficient depending on the frequency of the discharge at 80 m/s; model NLF-MOD22A

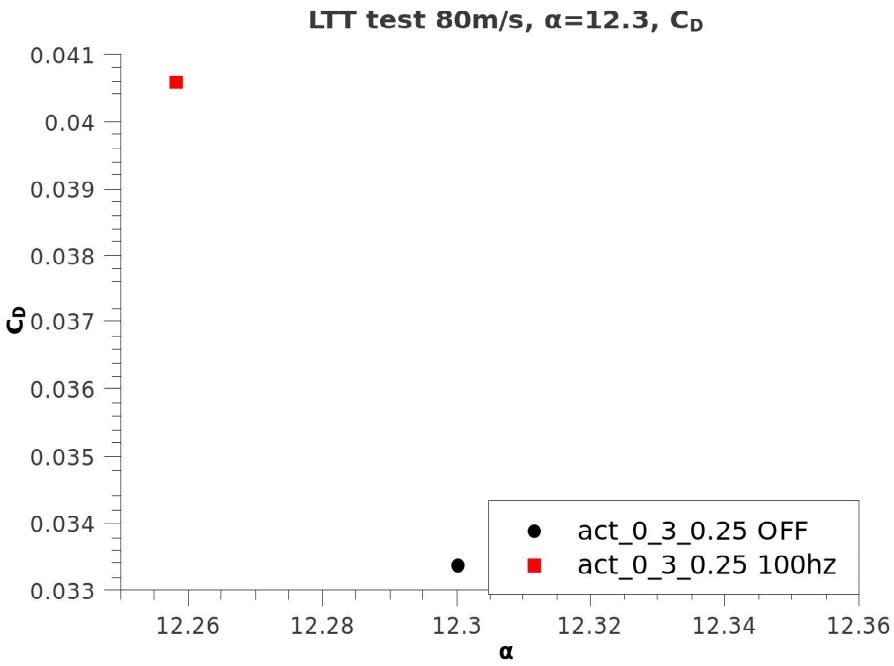

Fig. 4.31: Changing of the C_D coefficient depending on the frequency of the discharge at 80 m/s; model NLF-MOD22A

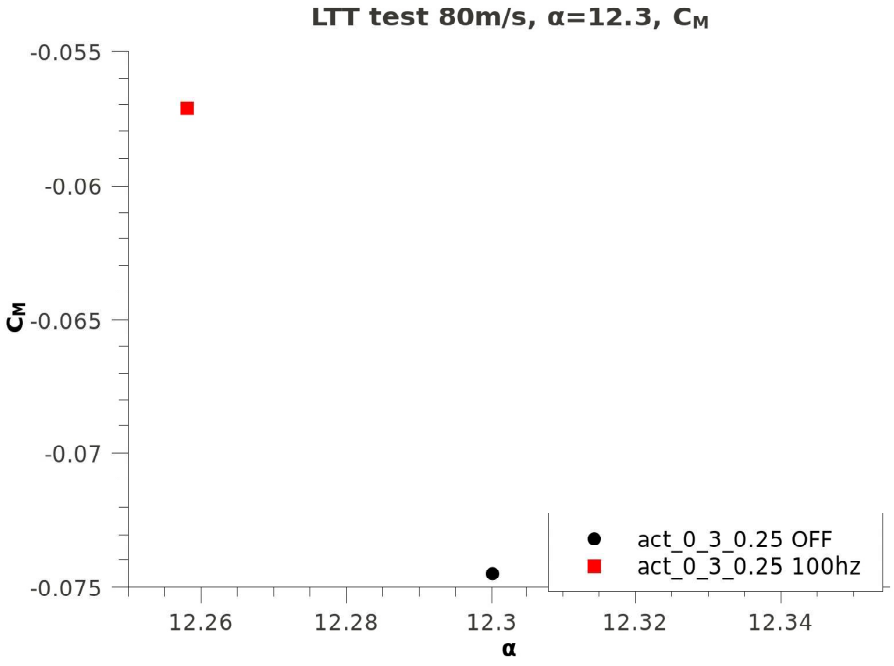

Fig. 4.32: Changing of the C_M coefficient depending on the frequency of the discharge at 80 m/s; model NLF-MOD22A

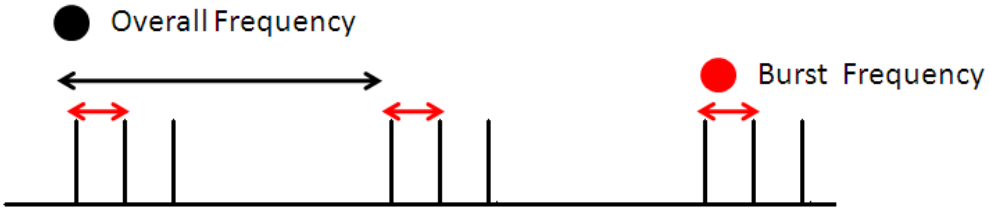

Fig. 4.33: Sketch of the Burst Mode Discharge: the black spot indicate the period between bursts, the red one the period within a single burst.

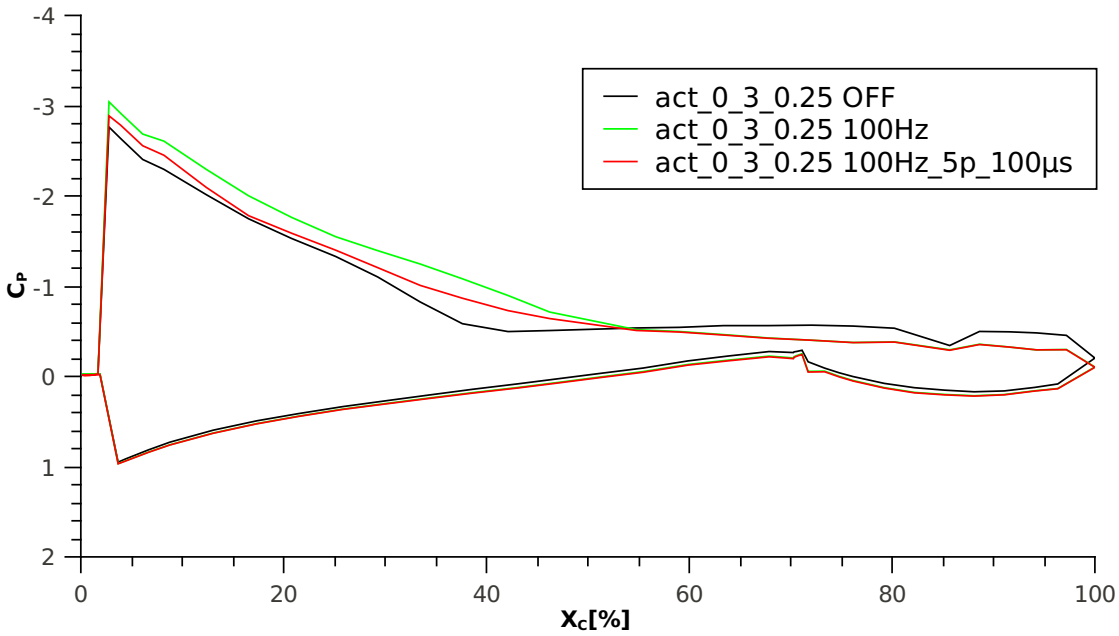

Fig. 4.34: Distribution of C_P at 80 m/s along the surface of the NLF-MOD22A, at LLT of TUDelft. Burst mode

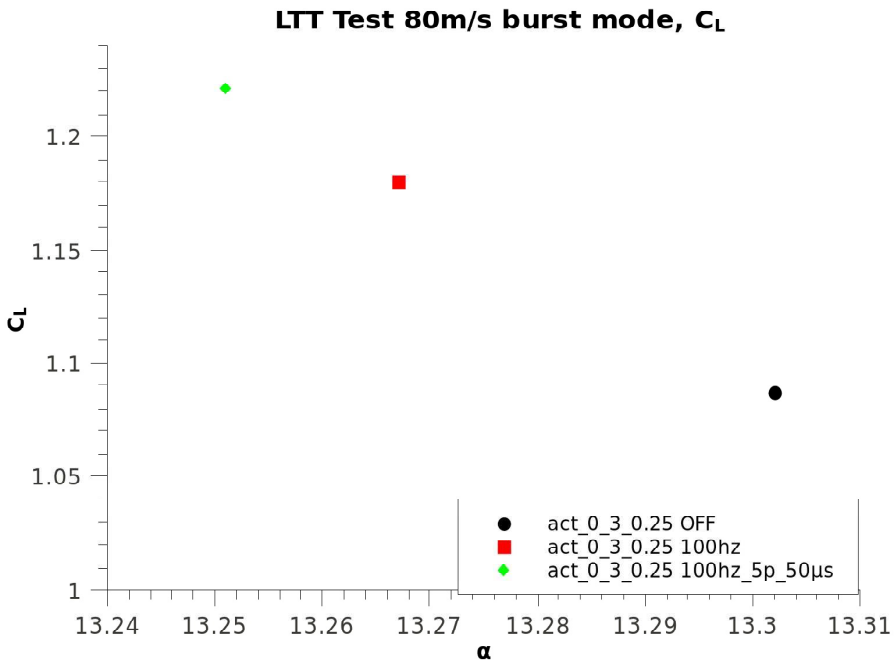

Fig. 4.35: Changing of the C_L coefficient depending on the frequency of the discharge at 80 m/s, with the Burst mode; model NLF-MOD22A

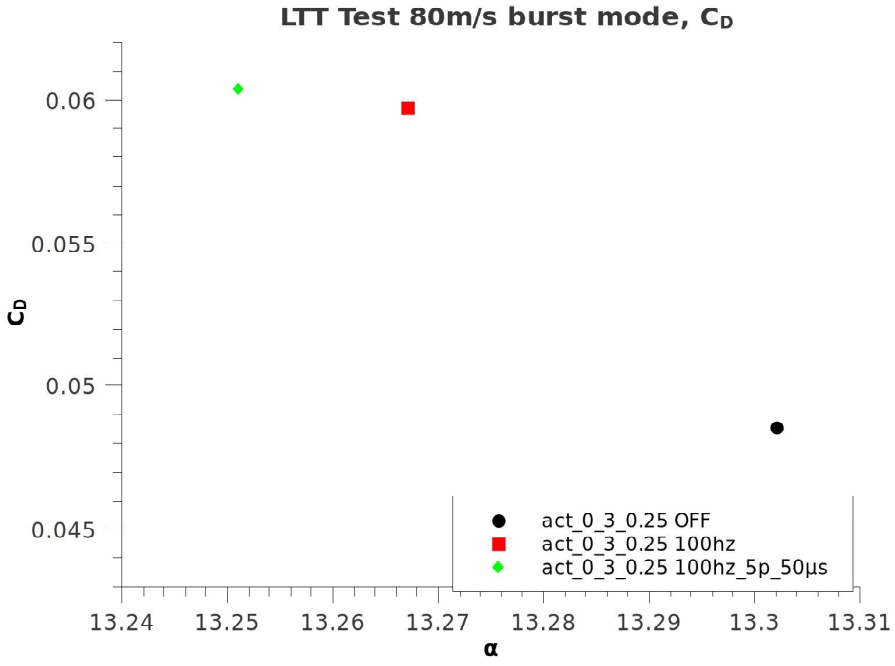

Fig. 4.36: Changing of the C_D coefficient depending on the frequency of the discharge at 80 m/s, with the Burst mode; model NLF-MOD22A

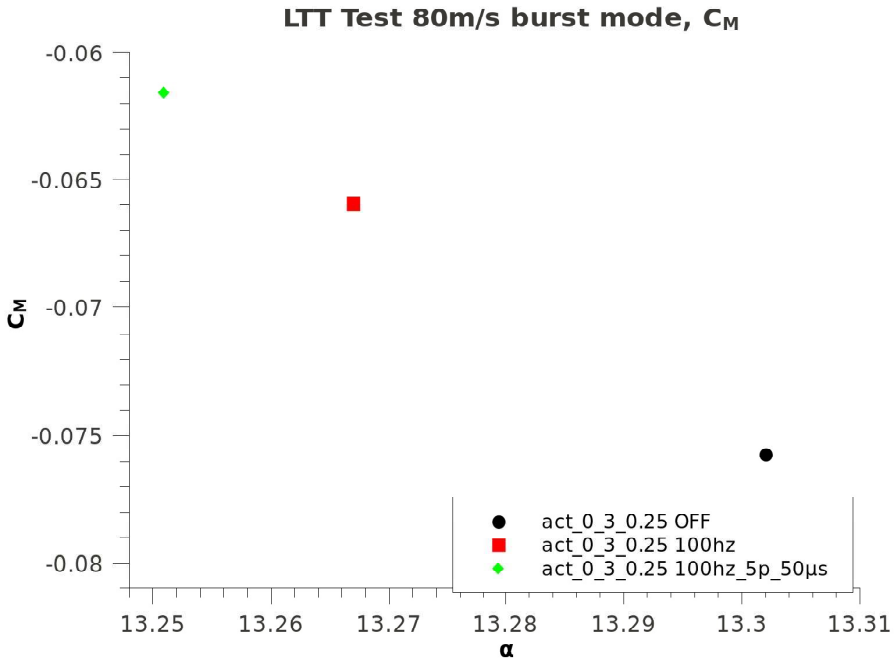

Fig. 4.37: Changing of the C_M coefficient depending on the frequency of the discharge at 80 m/s, with the Burst mode; model NLF-MOD22A

4.3 Test @ M-Tunnel

4.3.1 Description

The actuator used for the tests in the M-tunnel was 40 centimeter long and the model used was a NACA 63618, a 5-digit NACA airfoil, typically employed for wind turbines blades. Such a model has been used for its characteristic trailing edge separation, this means that the separation of the flow along the upper surface of the airfoil happens smoothly which thing might imply that small changes in the pressure distribution on the model might be enough for appriciating small reattached portions of the flow on the airfoil itself.

The model was made out of a dielectric material, thermal resistant, very rigid. The test itself consisted in letting the tunnel run and taking measurements by means of a balance of forces which was monitored by Data Acquisition System(DAS).

The DAS was controlled by a computer which was able to calculate C_L and C_D.

In the M-tunnel only one kind of actuator has been investigated: the single one.

These tests have been carried out applying a test section, made out of Plexiglas, to the test outlet jet section of the wind-tunnel, so for the taken measurements corrections for downwash effect is not necessary. Such Plexiglas test chamber was designed in such a way that it is applyable on both the M-tunnel and the W-tunnel.

In the Fig.4.38 is shown the set-up of the tests carried out at the M-tunnel.

Moreover in the Fig.4.39 is shown the Plexiglas test chamber and the balance of forces. Such balance has six degrees of freedom so it is able to acquire data of the three component of both the Aerodynamics force and momentum acting on the model.

4.3.2 Results @ M-Tunnel

Regarding the lift polar the results of these tests were quite expected. As it could be observed in the Fig.s 4.41,4.40, 4.43 and 4.42 that the stall angle is delayed, lift is enhanced and an appreciable reduction of the drag is achieved. Such results were expected based on the earlier results gotten in the LTT and V-tunnel test campaigns.

Test presented results in the Fig.s 4.40, 4.41, 4.42 and 4.43 are for a flow velocity up to 20 and 30 m/s. The acquired data demonstrate active flow leading edge separation control with a Reynolds number about $2\text{x}e^5$ and $3\text{x}e^5$ respectively, with a increase of the C_L, a delay of the stall angle and a reduction of the calculated C_D are appreciable in both the cases.

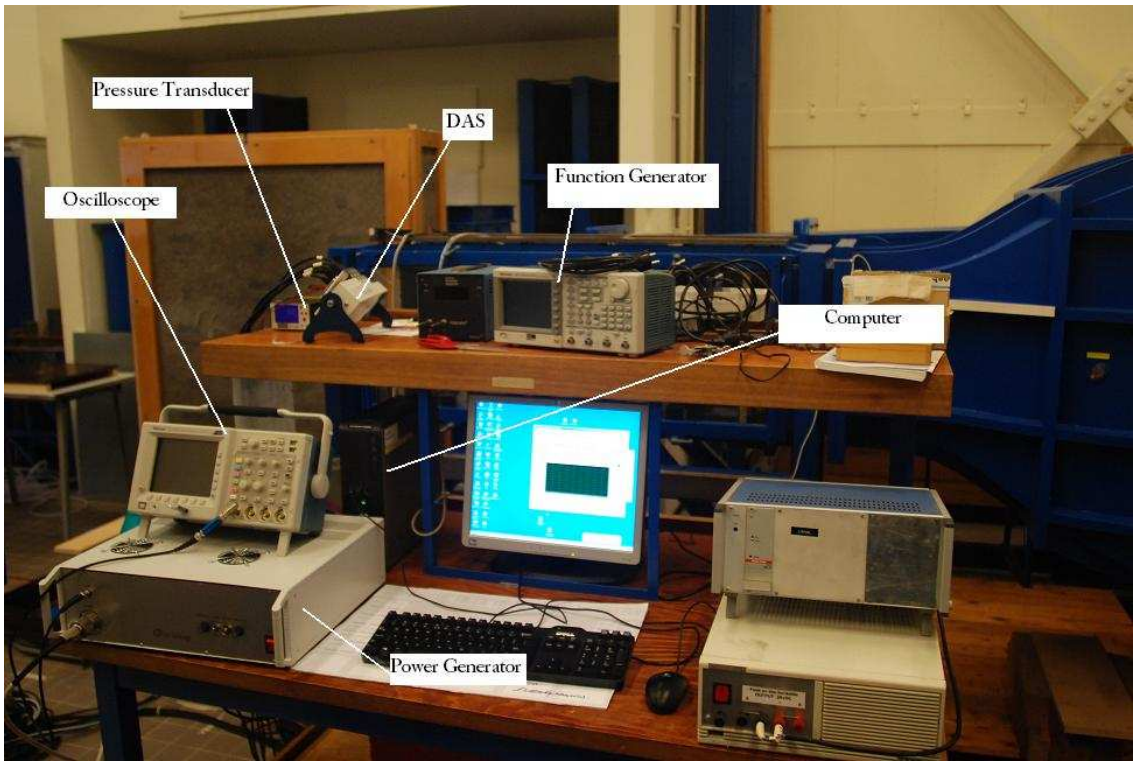

Fig. 4.38: Set-up of the M-Tunnel test campaign.

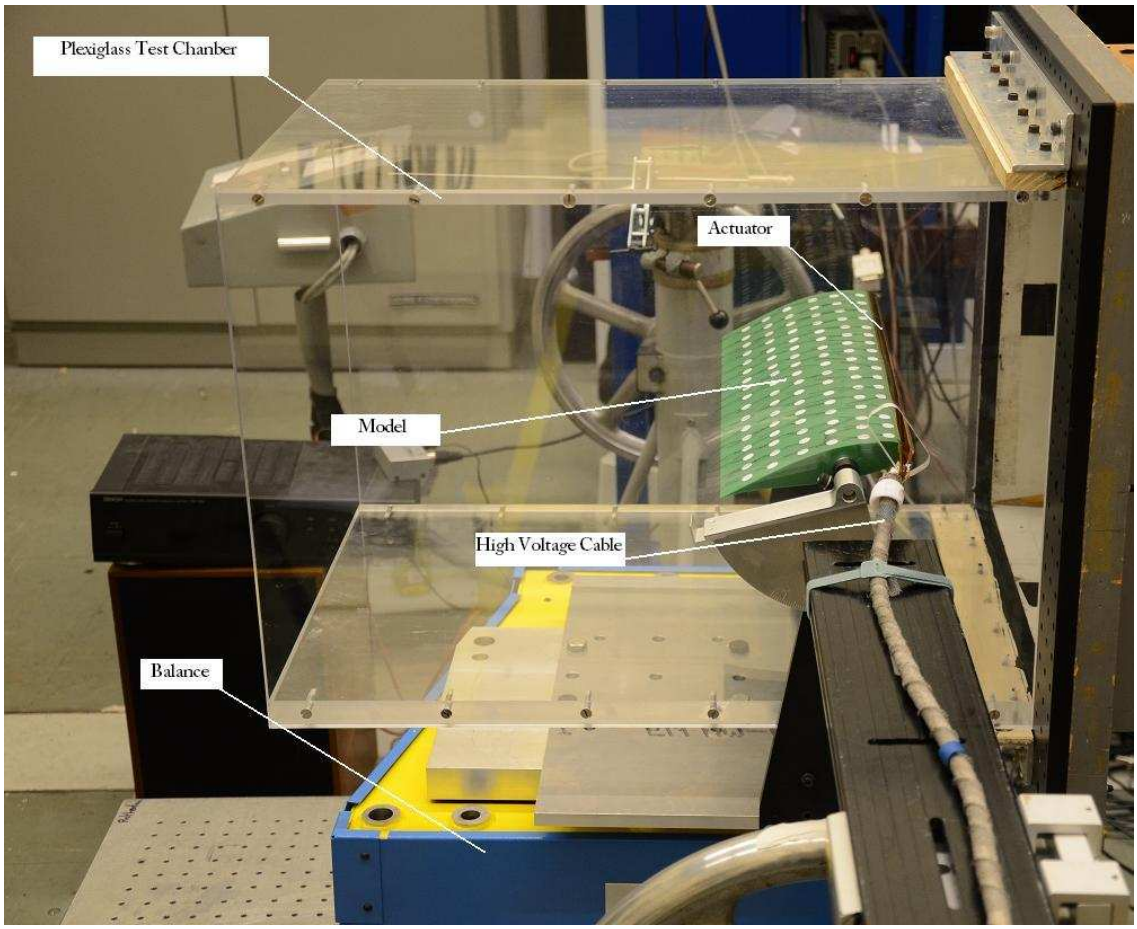

Fig. 4.39: In the picture the plexiglas test chamber and the six component Balance of forces supporting the airfoil.

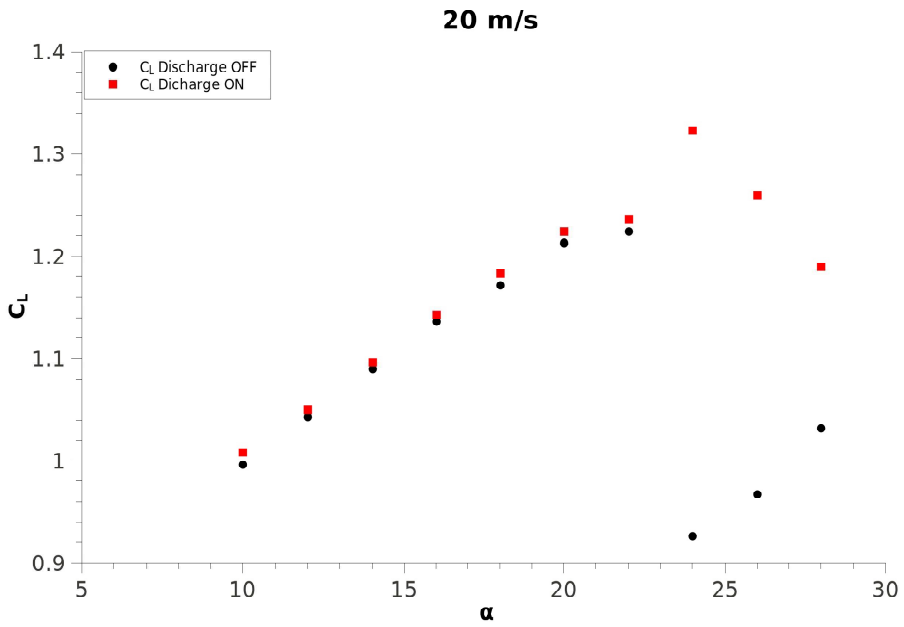

Fig. 4.40: Lift polar for the NACA 63-618 model in the M-tunnel at 20m/s. Data comparison of actuator On and Off.

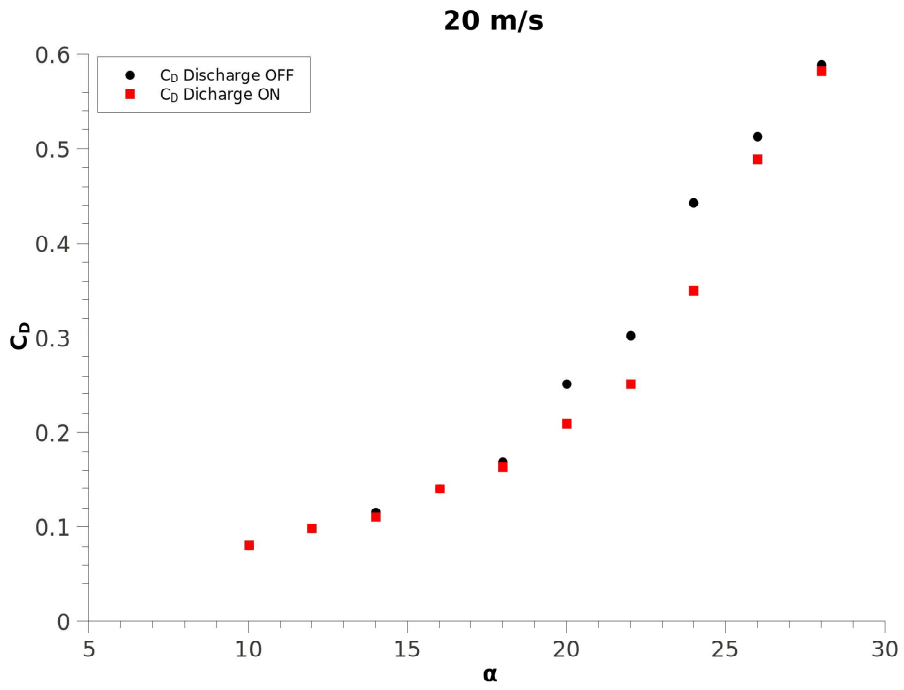

Fig. 4.41: Drag polar for the NACA 63-618 model in the M-tunnel at 20m/s. Data comparison of actuator On and Off.

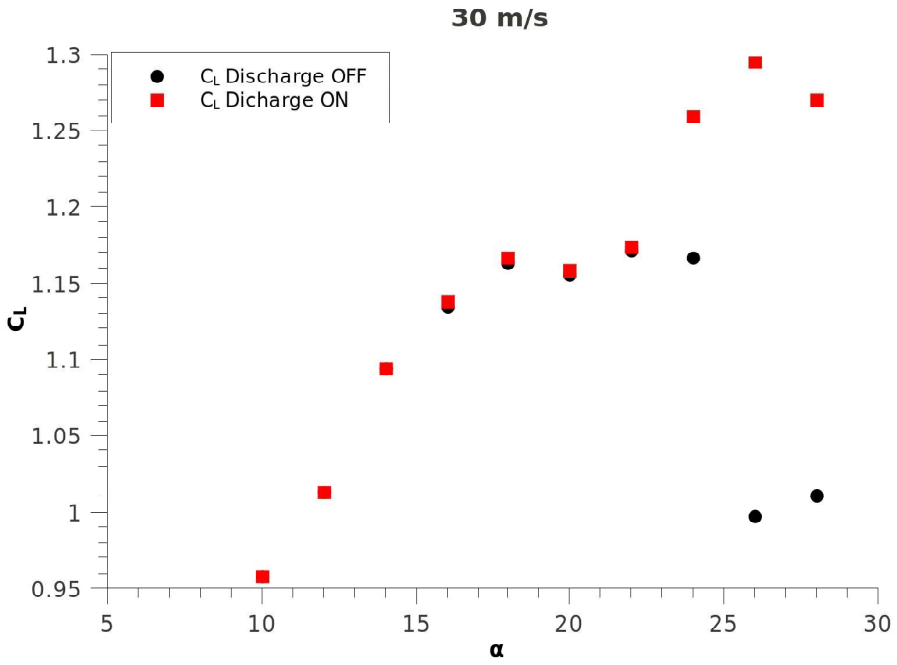

Fig. 4.42: Lift polar for the NACA 63-618 model in the M-tunnel at 30m/s. Data comparison of actuator On and Off.

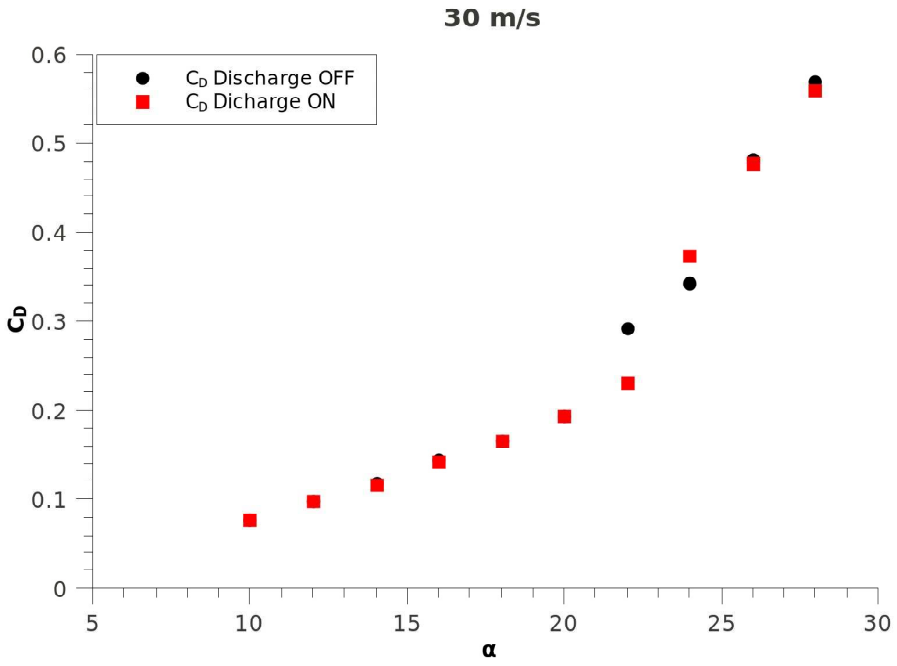

Fig. 4.43: Drag polar for the NACA 63-618 model in the M-tunnel at 30m/s. Data comparison of actuator On and Off.

4.4 Test @ W-Tunnel

4.4.1 Description

The actuator used for the tests in the W-tunnel was roughly 40 centimeters long tested on the same model used for the tests at the M-tunnel, the NACA 63-618; also the balance of forces was used but this time only as support of the airfoil.

In this tunnel two different series of tests have been carried out, a Schlieren champaign and a PIV campaign test. They will be treated separately.

The first series of test was carried out using the Schlieren Technique. This series of experiments was aimed to observe the mechanism of the actuation given by the NS-DBD pulsed discharge actuator, in order to qualify it.

The test itself consisted in letting the tunnel run and recording the event of the actuation by a particular set-up of light, lenses and a fast camera.

The system was controlled by a computer that, thanks to a software, was able to cut useless parts of the acquired movies and store the data at a different frame rate.

During the same test section, series of tests aimed to study the scalability upwards of the actuator were performed. For such a goal several configuration of actuators has been investigated: the single one, double one and a triple one.

For all these geometrical configuration five parameters have been investigated: Angle of Attach (AoA)(between 20 and 32 with a stepwise of 3 degrees), Speed Flow (15 and 30 m/s), overall frequency (0, 50 Hz, 100 Hz, 200 Hz, 400 Hz, 800 Hz), number of pulses for the burst mode(from 1 till up to 10 pulses per burst) and period (frequency) between the pulses of each burst (100μs, 200μs, 300μs).

These tests have been carried out with an open-jet configuration of the tunnel.

In the same tunnel a second test champaign has been carried out, this time using a PIV acquisition technique.

Actually this section could be divided in subsections: a planar PIV in the plane of the airfoil with a field of view of 10x10 centimeters, in a flow with a velocity up to 30 m/s has been carried out, and, beside this test it was recognized to be very useful a more typical study case. So the set-up was changed and the PIV was carried out in a still air box and the actuator was built on a flat plate. However the results of these test will be treated in separate subsections later in this chapter.

4.4.2 Results @ W-Tunnel(Schlieren)

The first section of test carried out in the W tunnel, as it has been already said in the introduction to this section, was aimed to study the scalability of the actuator and to give a qualification to the mechanism of the actuation. In order to do so

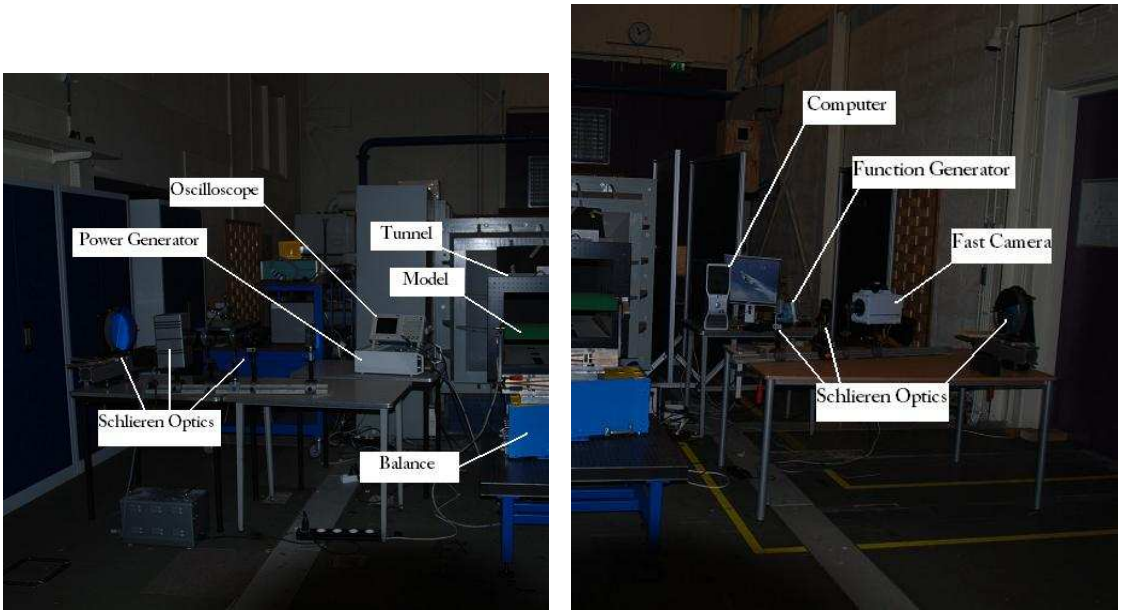

Fig. 4.44: In the picture is shown a typical set-up of a schlieren test.

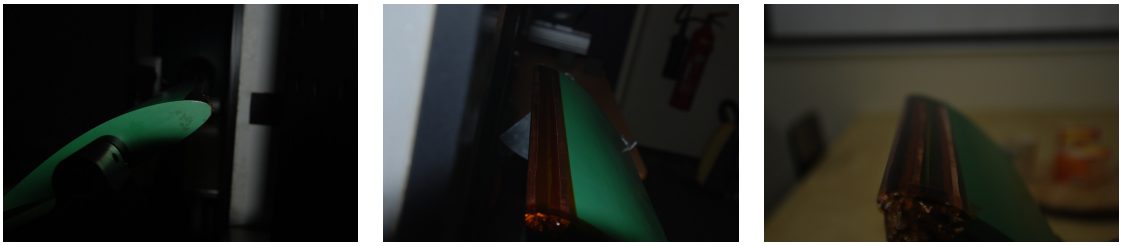

(a) Single Actuator (b) Double Actuator (c) Triple Actuator

Fig. 4.45: In the pictures are shown the three different configurations of actuator used for the schlieren test campaign.

a Schlieren acquisition technique has been selected, and the peculiar set-up was carefully executed, also thanks to the professionalism of the technician of TUDelft. In the Fig.4.44 the set-up of the Schlieren test campaign is presented:

The schlieren acquisition technique had been used for studying three different configurations: single, double and triple NS-DBD Plasma actuator. The three configurations are given in the Fig.4.45

The results have been analyzed and here only an overview of the most significant obtained results will be given. For a check in more details of all the results the reader is addressed to the Appendix D of this thesis, where all the most significant test results are presented in more details.

In the Fig.4.46 it is presented a table of pictures comparing different cases. The differences for the different aerodynamics tested conditions are visible.

Because of the frames size only a limited number of tests are comparable at the

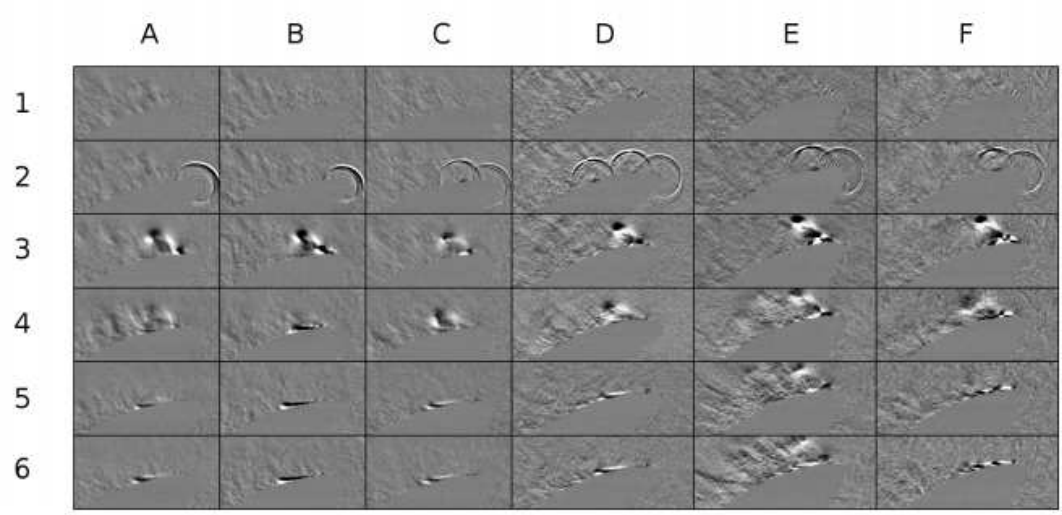

Fig. 4.46: Schlieren imaging of the actuator in different cases: A — α = 26 deg, single actuator, no burst; B — α = 26 deg, single actuator, burst 10 pulses, Δt = 100 μs; C — α = 26 deg, double actuator, no burst; D — α = 26 deg, triple actuator, no burst; E — α = 29 deg, double actuator, burst 2 pulses, Δt = 300 μs; F — α = 29 deg, double actuator, burst 5 pulses, Δt = 300 μs; Images taken at moments in time: 1 — 0 μs (before the first pulse); 2 — 40 μs (shock wave propagation); 3 — 1 μs (vortex formation after 1^{st} burst); 4 — 6 μs (after 2^{nd} burst); 5 — 11 μs (after 3^{rd} burst); 6 — 16 μs (after 4^{th} burst); In all cases burst-to-burst frequency was 200 Hz, pulse voltage 10 kV. Velocity of the flow 30m/s and Reynolds number based of the chord of the model about $4e^5$

same time in one table as in Fig.4.46, so a more wide test analysis has been carried out and the result of such an analysis is shown in the table.

In the table "α"is the angle of attack between free stream and airfoil; "type"indicates the kind of actuator configuration distinguishing between single, double and triple actuator; "n_{burst}"indicated the number of pulses within a burst, given per pulse input; "Δt"is the period within one burst, when it is not given is because within one burst there is only one pulse, the period is measured in μs; "N_{reatt}"indicates the number of bursts needed in order to get the flow reattached; "x/c"indicates the portion of flow reattached on the airfoil in percentage with respect to the chord length of the model.

α	**type**	n_{burst}	**Δt,μs**	N_{reatt}	**x/c**
26	single	1	—	3	25%
	single	3	100	3	30%
	double	1	—	2	38%
	double	3	100	2	41%
	triple	1	—	2	45%
	triple	3	100	2	49%
	triple	3	300	2	51%
29	triple	10	100	4	24%
	triple	10	300	4	35%

The scalability has been shown: it is possible to archive more and more an active control on the separated flow increasing the number of actuators, or increasing the number of pulses inside a burst. It has been observed that for more burdensome conditions (like AoA up to 32 degrees) a bigger amount of energy needs to be spent in order to achieve the control on the flow. Moreover an interesting gas-dynamic limit of the actuation mechanism has been observed: increasing the period between two consecutive pulses inside the same burst helps in order to control the flow. It means that with a bigger period between two consecutive pulses it is possible to get a better result (reattaching the flow spending less energy with respect to the time interval). This gas-dynamic limit will be discussed later on in the next chapter. From the 'qualification of the actuation mechanism' point of view it has been observed, for all the different configuration (single, double, triple), that when the control on the flow happens always the same series of events is record: after the discharge the volume enclosing it warms up, this, after few μs leads to an adiabatic expansion, so a shock wave is formed. The velocity of this shock wave has been calculated and found to be roughly 370 m/s, so the shock wave velocity is a bit higher than a sonic shock, it is a compression wave. This shock wave propagates perpendicularly to the shear layer (generated by the separated flow): the free stream flow has an higher velocity with respect to the flow between the airfoil and the shear layer (in the recirculation flow region), so the shock wave propagates in the two regions with two different velocities.

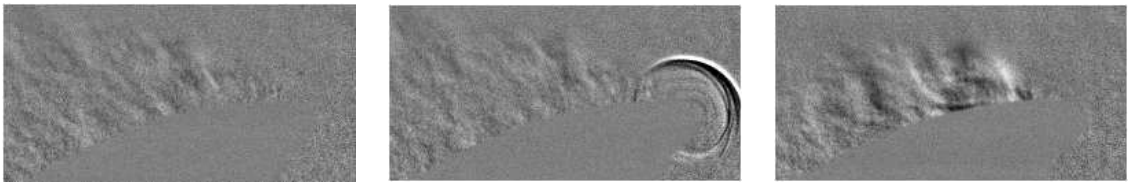

(a) Flow separated (b) Shock wave (c) Instability propagation

(d) Generated vortex (e) Flow reattached (f) Flow reattached

Fig. 4.47: Single actuator configuration. In the pictures are presented six processed frames showing the several phases of the actuation. It could be observed that after the flow is reattached it stays in that way. In this test the velocity of the free stream is 30m/s with $\alpha = 26$ deg.

Since the total momentum of the system needs to be conserved this phenomenon generates a pressure gradient throughout the shear layer which generates itself a disturbance that propagates downstream. The generation of such a disturbance has been explained in the section regarding the Phenomenology (par.2.5.2) of the NS-DBD plasma actuator.

Now, going back to the gas-dynamic limit mentioned earlier, when the distance between two consecutive pulses, so between two consecutive shock waves, is bigger, this disturbance has more time for growing up before the next shock destroys (or compensates) it. Actually it could be hypothesized that the disturbance produced by the oncoming SW will affect every disturbance already generated by the previous SW, but if the previous disturbance is big enough it does not really get much affected by the oncoming one.

Thus to a bigger period between pulses corresponds an bigger disturbance for which corresponds, as well, a better result in terms of flow controlled.

This brings with it the idea that the instability is the 'Key' for the actuation phenomenon.

All these results will definitely be analyzed later on, at the light of a more complete set of data.

Eventually, in Fig.s 4.47 and 4.48, significant processed result for a single and a triple actuator respectively are presented aimed to help the visualization for the qualification of the mechanism.

In the Fig.s 4.47 and 4.48 is shown a typical result: after the actuation the flow stays attached on the model. This phenomenon might be due to a strong down-wash effect generated after the actuation due to the fact that the controlled flow

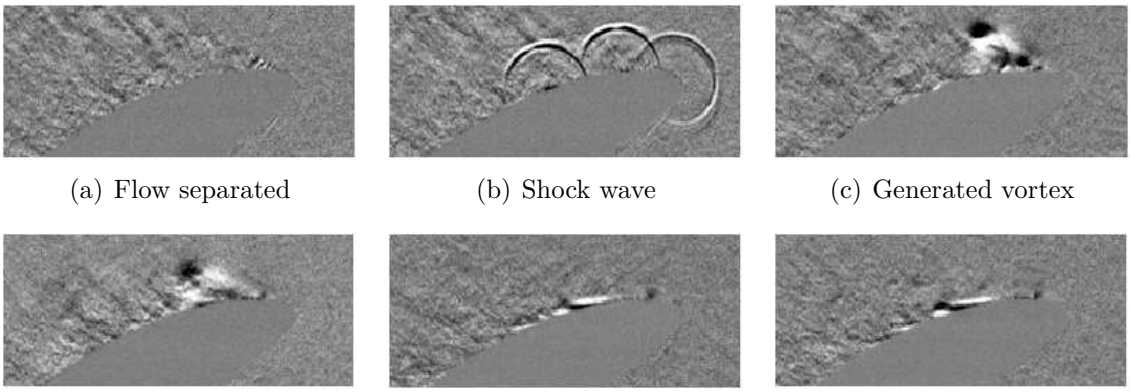

(a) Flow separated (b) Shock wave (c) Generated vortex

(d) Generated vortex (e) Flow reattached (f) Flow reattached

Fig. 4.48: Triple actuator configuration. In the pictures are presented six processed frames showing the several phases of the actuation. It could be observed that for more extreme boundary conditions one vortex is not enough in order to reattach the flow. Also in this case, after the flow is reattached it stays in that way. In this test the velocity of the free stream is 30m/s with $\alpha = 29$ deg.

acquires some three-dimensionality. A different explanation for this phenomenon might be found in the stall behavior characteristic of the model itself which might be such that a stable equilibrium is created controlling the flow.

For the sake of clarity hereafter, in Fig.4.49 are shown processed frames with a single SW propagating and the vortex later generated by the pressure disturbance traveling backwards into the SL.

Moreover, the Fig.4.50 shows a frame acquired with the model inclined about 90 degrees with respect to the flow direction. Such a result is shown in order to clearly show the gradient created by the shock wave propagating into the shear layer.

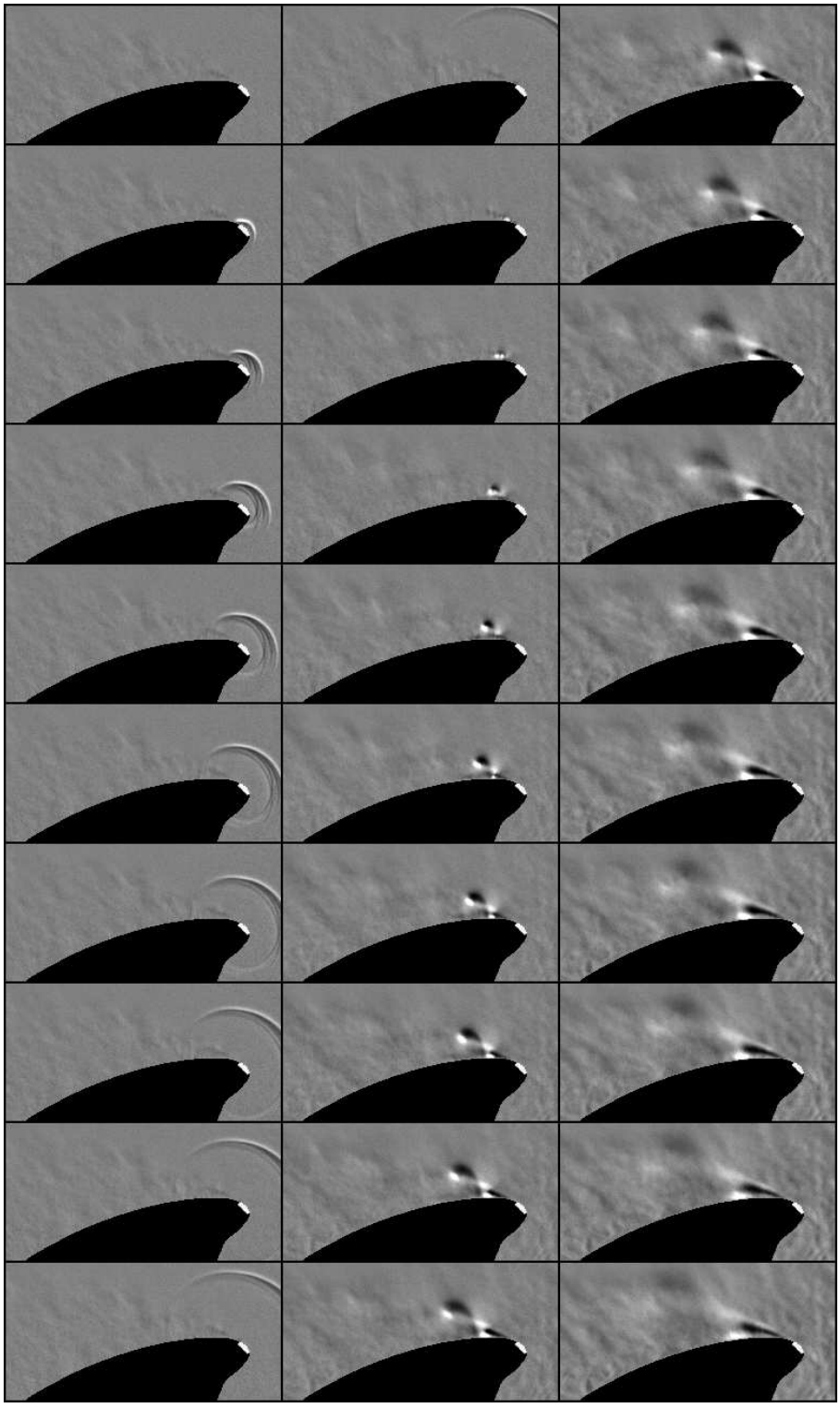

Fig. 4.49: Processed Schlieren images: SW propagation and Vortex generated afterward, by the pressure disturbance propagating backward into the SL. Time forwarding going downward from the top-left frame.

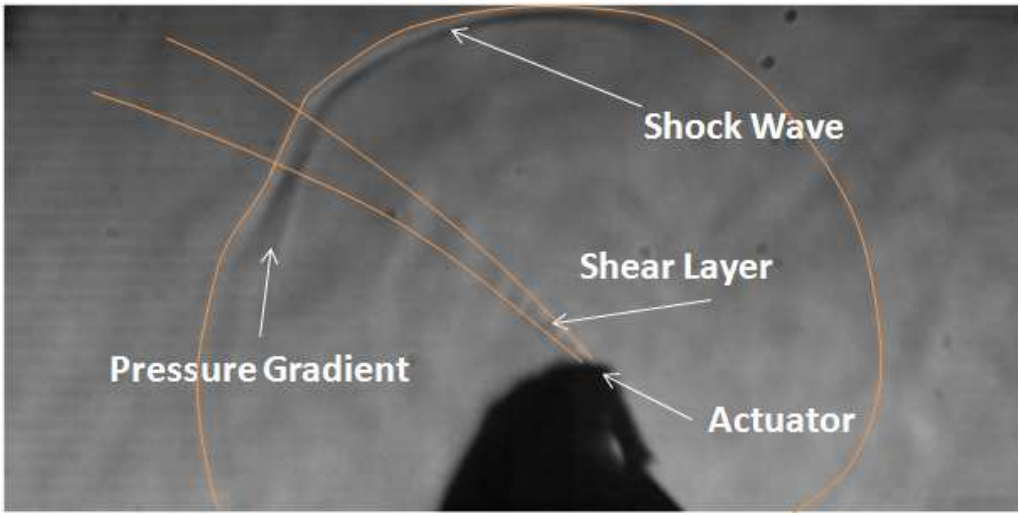

Fig. 4.50: Visualization of the gradient produced by the shock wave propagation into the shear layer. In the picture the Shock Wave and the Shear Layer are annotated with orange lines.

4.4.3 Results @ W-Tunnel(PIV)

The second test section carried out at the W tunnel was aimed to give a quantification to the mechanism of actuation due to the NS-DBD plasma actuator. In order to do so a PIV acquisition technique has been selected, and the peculiar set-up was carefully execute, also thanks to Mr.Sina Ghaemi. a PhD student at TUDelft, expert in PIV acquisition tests. His tips and suggestions have been priceless also during the phase of data processing.

As already said, this section can be actually split in two separate subsections since two different PIV test have been carried out: PIV test of an airfoil in a flow with a velocity up to 30 m/s and PIV test on a flat plate in still air.

Test in the flow

With the NS-DBD plasma actuator mounted at the leading edge of a 5-digit NACA airfoil, the NACA63-618, the same one used for the Schlieren test section, a PIV measurement has been performed in order to quantify anyhow the actuation mechanism.

This test has been performed on a field of view of 10 by 10 centimeter.

Hereafter, in Fig.4.52 is presented the most significant result in form of matrix of pictures and a brief description coming along with it. The test set-up was a typical PIV set-up, with a magnification of 1 and a acquisition frame rate of 1 kHz. The discharge frequency of the NS-DBD plasma actuator, placed on the leading edge of the model, was about 200 Hz.

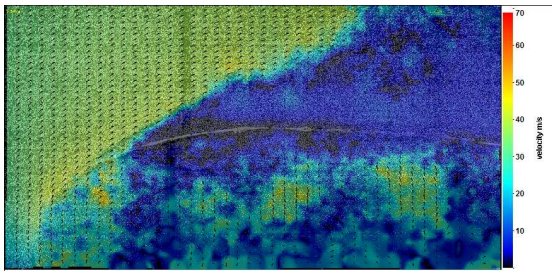

(a) t = 0 ms

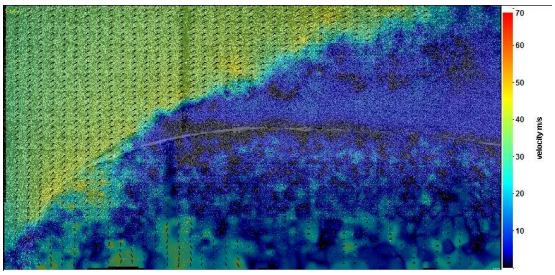

(b) t = 0.2 ms

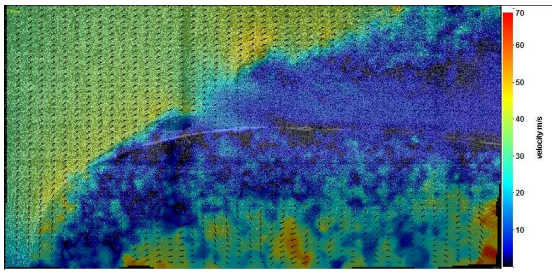

(c) t = 0.4 ms

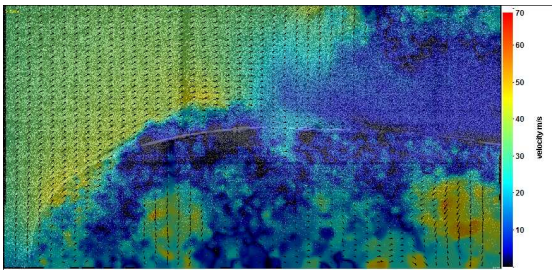

(d) t = 0.6 ms

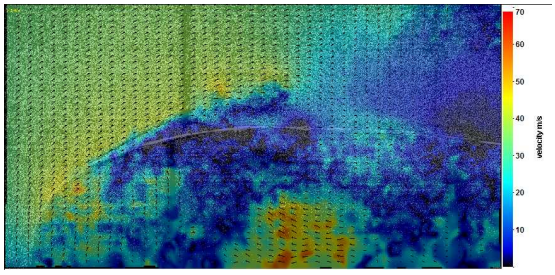

(e) t = 0.8 ms

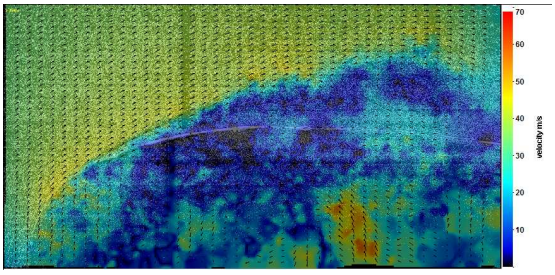

(f) t = 1.6 ms

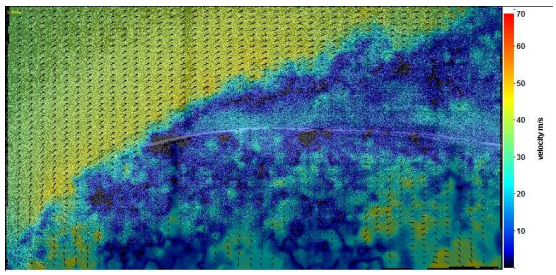

(g) t = 4.6 ms

Fig. 4.51: The figure continues on the next page

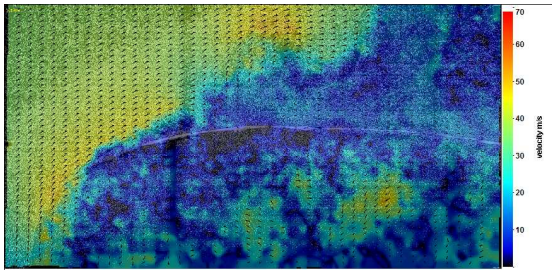

(a) t = 5.8 ms

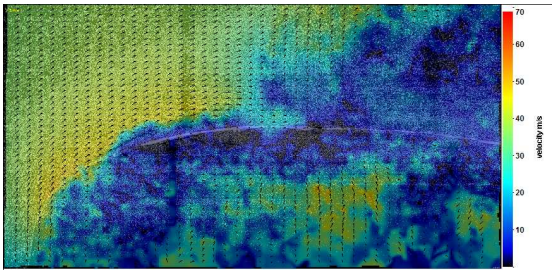

(b) t = 6 ms

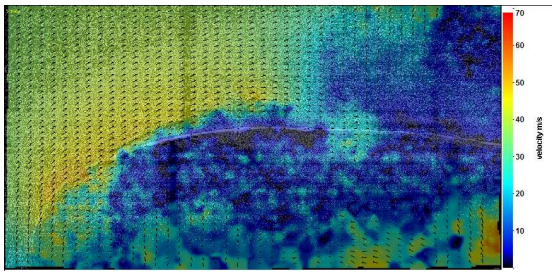

(c) t = 6.2 ms

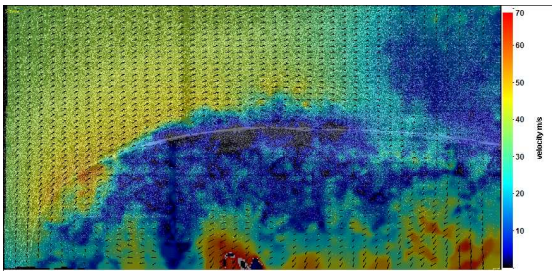

(d) t = 6.4 ms

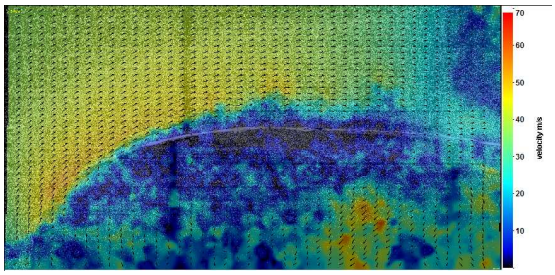

(e) t = 6.6 ms

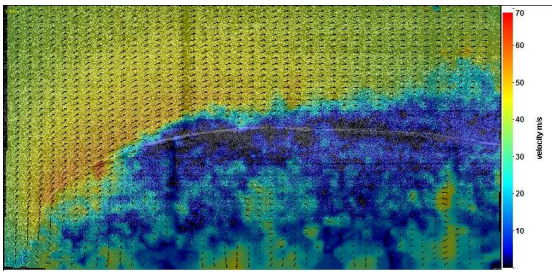

(f) t = 7.4 ms

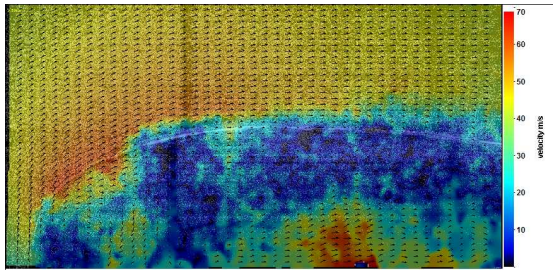

(g) t = 9.8 ms

Fig. 4.52: In this table of pictures it is possible to observe a processed PIV result. It is shown that within two pulses the flow reattaches. After each pulse a disturbance produces a vortex into the shear layer which is visible in this result. Frames:(a) initial condition; (b) first pulse; (c-d-e) first vortex; (f) situation after one pulse; (g) second pulse; (h-j-k-i-l) second vortex; (m) flow reattached; (n) final situation.

In the Fig.4.52 the result for the planar PIV test on a 10x10 centimeters field of view is shown. Remarkable result is that the flow speed increases after the reattachment. Initially the flow is up to 30 m/s and after the reattachment it gets up to about

65-70 m/s. Since in the flow it has been not possible to catch any of the events observed performing the Schlieren tests it was thought to be useful to switch to an other kind of test: the actuator was tested on a flat plate in the still air box.

Test in the still air Box

A PIV test has been carried out with the actuator mounted on a flat plate, in a still air condition. The field of view is very small, about 5 by 5 millimeters. The employed magnification was about 3. This test is aimed to observe and quantify the event of the actuation from its very beginning

Hereafter, in Fig.4.54, the most significant result in form of matrices of pictures and a brief description coming along with it below are presented. The acquisition rate was 5 kHz while the discharge frequency was 1 kHz, so one pulse each 5 frames:

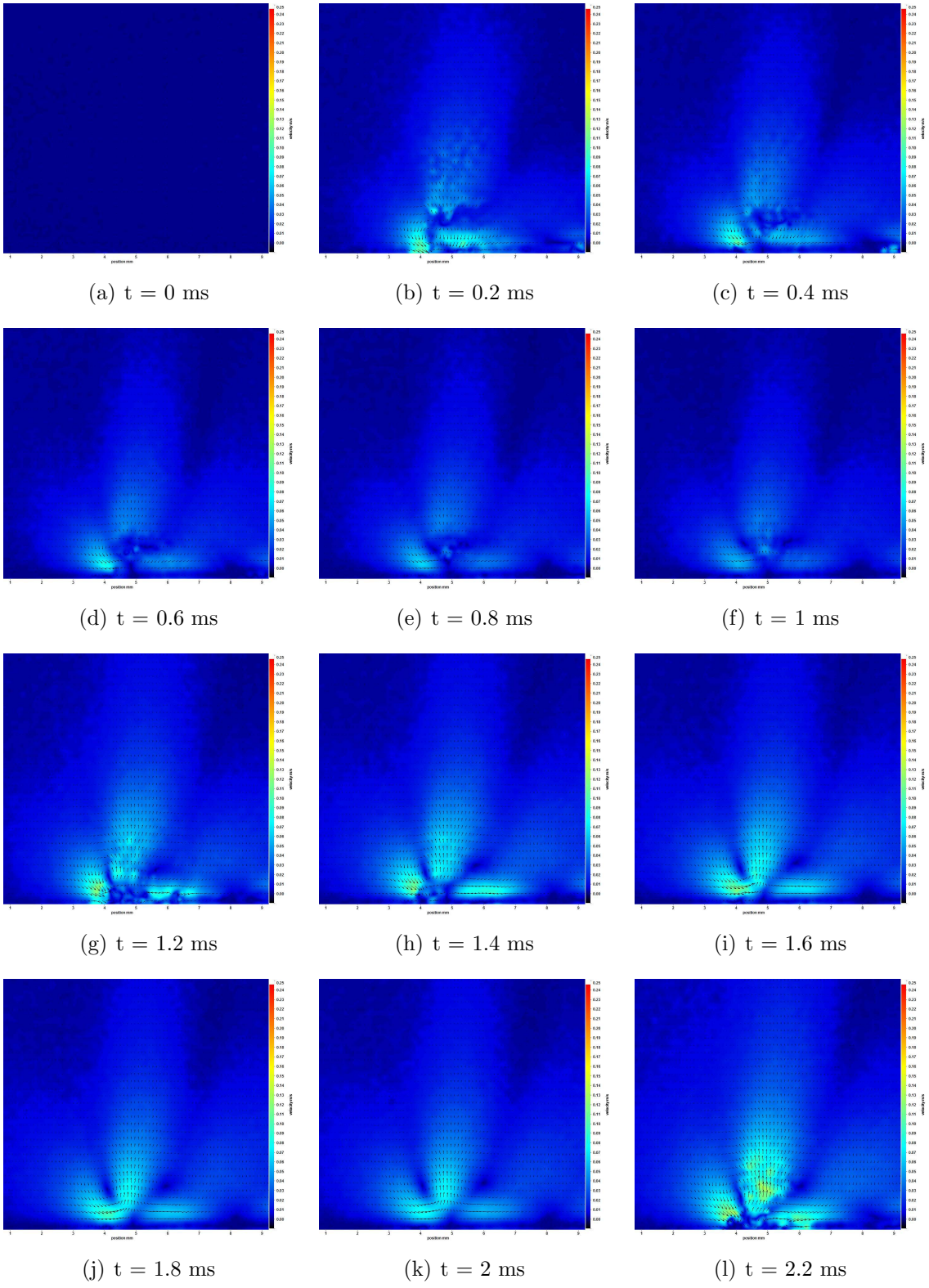

(a) t = 0 ms (b) t = 0.2 ms (c) t = 0.4 ms

(d) t = 0.6 ms (e) t = 0.8 ms (f) t = 1 ms

(g) t = 1.2 ms (h) t = 1.4 ms (i) t = 1.6 ms

(j) t = 1.8 ms (k) t = 2 ms (l) t = 2.2 ms

Fig. 4.53: The figure continues on the next page

In the Fig.4.54 the discharge from its very beginning is shown. Here a new phenomena have been found. First of all it is visible in Fig.4.55 that the formation, and expansion, of consecutive shock waves creates a jet of air, probably warmer then the rest of it. This effect translates in a quite weak momentum transferred upwards, in the vertical direction, in a plane perpendicular to the flat plate. The formation of the jet, for a momentum conservation principle, drives suction of air from the side-air-jet regions. Such a suction produces the formation of two vortexes which also are observable in Fig.4.55.

Moreover, it is very interesting to see, in all the frames following a pulsed discharge, in the Fig.4.54 the frames (b-g-l-q-v), a downwards pointed velocity. Since these velocity vectors begin at a certain height from the flat plate the small momentum they transfer could play a rule in the flow reattaching mechanism. Even if the momentum that those velocity vectors are able to transfer is pretty low it is still comparable to the momentum that a flow could have in that region of the boundary layer, very close to the surface (no slip condition at the wall).

Explanations for the latter phenomenon could be several: maybe the discharge does not happen very close to the dielectric surface and the downwards pointing velocity vectors results from the expansion of the hit volume; maybe the oil particles, used for the PIV test, get charged and attracted by the electromagnetic field created by the discharge.

This phenomenon will be discussed later on in the next chapter.

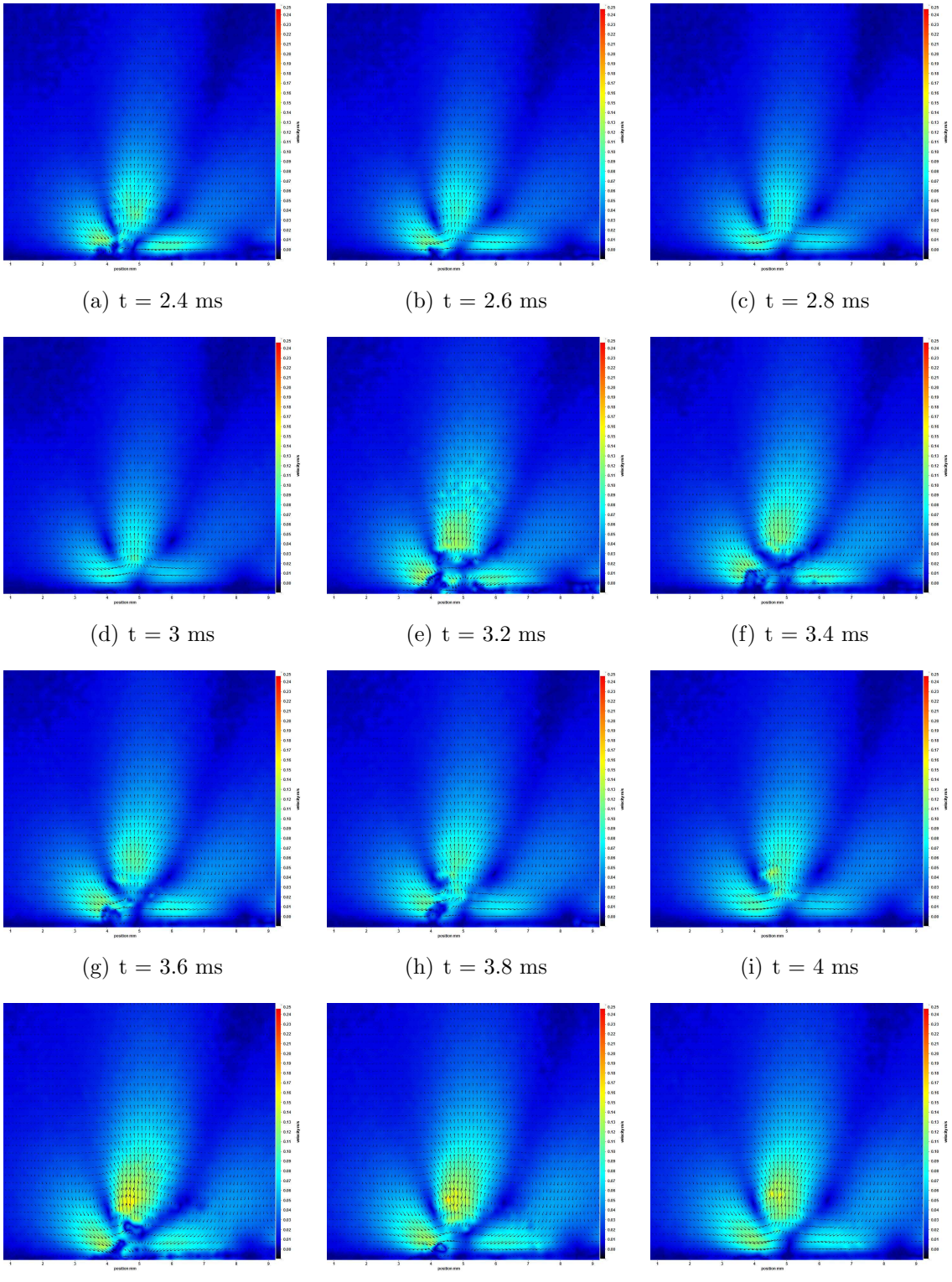

(a) t = 2.4 ms (b) t = 2.6 ms (c) t = 2.8 ms

(d) t = 3 ms (e) t = 3.2 ms (f) t = 3.4 ms

(g) t = 3.6 ms (h) t = 3.8 ms (i) t = 4 ms

(j) t = 4.2 ms (k) t = 4.4 ms (l) t = 4.6 ms

Fig. 4.54: PIV result of an NS-DBD Plasma Actuator on a Flat Plate in still air. The frames following a pulsed discharge are b-g-l-q-v. These frames reveal a downwards pointed velocity vector generated by the discharge.

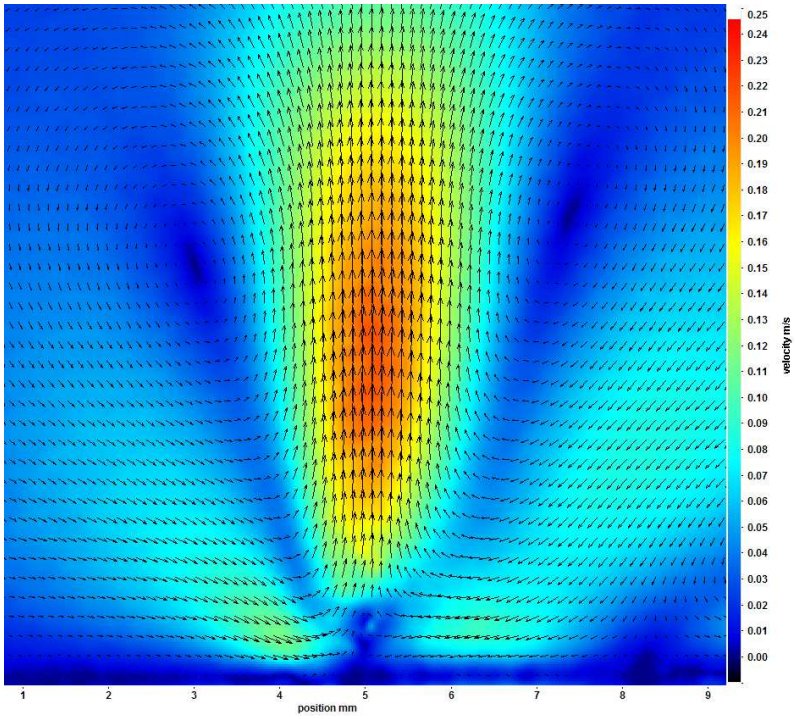

Fig. 4.55: From the still air box test the velocity distribution after 20 pulses is presented. The formation of a vertical jet is visible, just above the location of the dircharge region. The flow into the jet gets accelerated to the velocity of 0.25 m/s, depicted in red in the picture.

4.5 Additional Tests

Several tests have been carried out in order to investigate the extent of applicability of the NS-DBD plasma actuator for industrial applications.

4.5.1 Structural Test

A structural test aimed to investigate the thermal-structural impact of the actuator on the wing during the actuation has been carried out since no reference has been found in the literature about that.

The test itself was quite easy: based on a long duration discharge, after a while the thermal status between the working actuator, the flow and the wing becomes stationary.

To obtain an actuation frequency that is relevant for a full scale application a Strouhal number of 1 was selected ([54] [56]). This leads the frequncy to be $f = \frac{V}{L}$ where V is the velocity of the flow and L is a characteristic length of the system.

Since the max velocity which an airplane could get is, in the cruise mode, up to 250 m/s and since the average chord of the models that have been testing is roughly 20 cm the frequency which the actuator has been tested at was between 50 and 1500 Hz.

Description

In order to perform such a test an actuator 15 centimeter long has been built up on purpose. The actuator was glued on a model and the discharge was actuated (always without the flow). After 5 minutes of discharge, with a thermo-couple a direct measurements was taken and annotated, and an average temperature on ten values have been calculated for each case. Five discharge frequencies have been selected for the tests: from 250 Hz till 1.5 kHz, with a stepwise of 250 Hz.

Five different models made out of different materials have been tested: aluminum, wood, apoxie resin, foam covered by a plastic shell and carbon fiber.

Structural Test Result

In the Fig.4.56 it can been seen the averaged temperature that each model reached, depending on the frequency of the discharge and on the material that the model itself was made of.

This test might be enough in order to give a clue about the impact of the NS-DBD plasma actuator on a wing. The temperatures gotten by the wood and the foam ones are quite high. When testing a model made out of such materials it could very

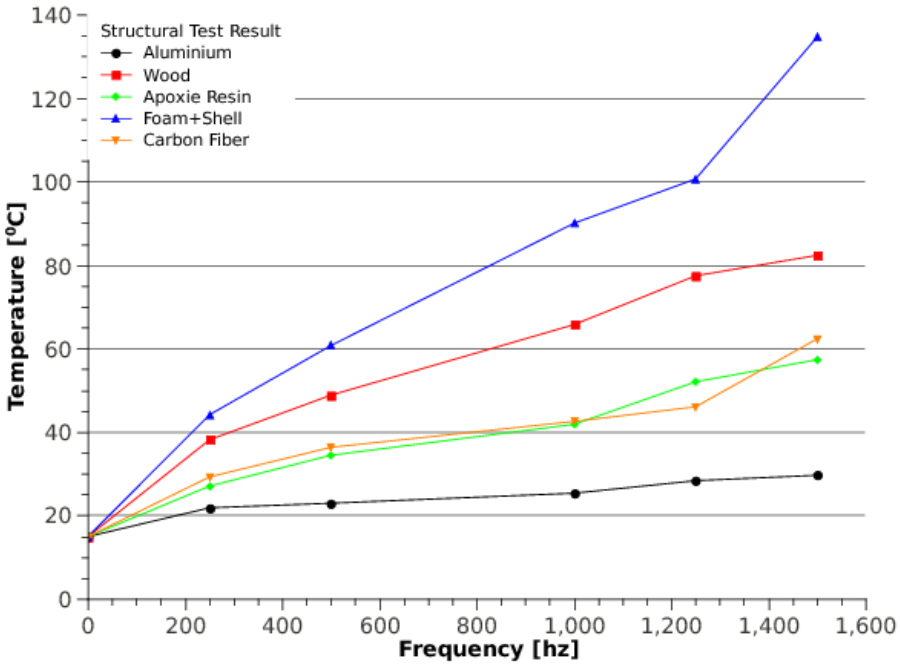

Fig. 4.56: Temperature vs Frequency on different materials without flow

important to keep in mind this result in order to protect the wing and do not let the model get damaged. Of course the test has been performed in absence of flow, which might be able to cool the temperature down quite quickly.

4.5.2 Rain Test

In order to investigate the extent of applicability of the ND-DBD plasma actuator a rain test has been performed. The test is aimed to demonstrate the functionality of the NS-DBD plasma actuator in severe conditions such as the presence of drops of water in the flow.

Description

The test has been carried out just after the Schlieren test campaign, so the visualization technique used for this test is the Schlieren one as well. Such a test gave the chance to observe in slow motion the propagation of shock waves, produced by the nanosecond discharge, and the formation of the consequential disturbance, with the airfoil at an AoA of 29 degrees, and drops of water in a flow with a velocity up to 30 m/s.

The test has been performed two times, one with discharge ON and the other with the discharge OFF in order to see if any mechanical effect on the shear layer could have been caused by the water drops of water themselves.

The test itself consisted in letting the tunnel run, injecting upstream into the flow nebulized water by an electrical nebulizer, in order to simulate rain drops, and taking measurements. The nebulized water jet was directed transversally with respect to the flow direction.

Even if the test itself is not really representative for the rain case, it still proves the functionality of the NS-DBD plasma actuator in conditions of high humidity.

Rain Test Result

It is very difficult to visualize the water drops in the results, this is why it is not worth to show them. However the results of these two rain tests could be summarized: when the discharge is OFF the flow has been observed to be slightly affected by the presence of the water drops, although the flow does not get reattached; when the discharge is turned ON reattachment has been achieved, even if an higher frequency (so more energy) was required for achieving the actuation in this situation with respect to the same case with a clean flow.

4.5.3 Ice Test

During the cruise-mode flight an airplane could experience very low temperatures depending on the height it is flying at. This phenomenon brings with it the issue of the ice formation on the flow stagnation point of a wing.

In order to investigate the extent of applicability of the NS-DBD plasma actuator, a still air test has been carried out with the presence of ice in the discharge region. Such a test was aimed to observe if and how the plasma actuator was working in such severe condition.

Description

For the ice test an actuator 20 cm long has been built on a flat plate, then water has been placed on both the electrodes enclosing the discharge region. The sample was put in a refrigerator for two days.

The test has been very short. It basically consisted in just letting the discharge go on an actuator with presence of ice on its surface and recording it.

The test was not aimed to acquire data but only to observe the behavior of the NS-DBD plasma actuator dealing with ice. The discharge frequency was kept constant at 1 kHz and the size of the the ice layer from the actuator surface was about 2 mm, which is about two times the size of the actuator itself.

Ice Test Result

The result of such test did not only show that the discharge happen normally, even through the ice, but it also revealed the capability of the NS-DBD plasma actuator to melt it. The test has been performed in the refrigerator itself, in order to prevent the ice from melting because of the room temperature. The frequency of the discharge was kept constant at 1 kHz and the ice got melted completely in about 2 seconds. Unfortunately no reference has been found in the literature in order to make any comparison.

Such result might open the way for a further research about possible application of the NS-DBD plasma actuator for de-icing applications. It might be though an Active Safety De-icing System which could highly increase the safety feeling of any user of aerodynamics devices. For instance such a de-icing system might be applied on wind turbines in arctic regions where the issue of de-icing is quite important.

Chapter 5

Discussion and Conclusions

5.1 Results Summary

Summarizing all the results obtained during this experimental research about NS-DBD Plasma Actuator for Leading Edge Separation Control it could be stated that:

- Boundary Layer Separation delay or elimination has been demonstrated
- Scalability has been demonstrated
- Lift Coefficient increased about 20% of its maximum value
- Drag due to wake reduced about 300%
- Lift-to-Drag ratio enhanced about 3.2 times
- Capability to work in severe conditions such as high humidity or ice
- Capability to work at Reynolds Number up to 3.3 millions
- Non-linear dependence of the optimal discharge frequency on the AoA has been observed
- New phenomenology has been observed
- Low Energy Consumption Demonstrated
- Applicable on existing devices without big modifications
- No severe constrains for the constructive elements
- Actuation Mechanism has been proposed

5.2 Discussion

The first step of this research has been to make sure of the capability of the NS-DBD plasma actuator to work properly. The second step has been to measure the aerodynamic enhancement that such a device could produce. The third step has been to prove the scalability of the actuator in order to understand the applicability extent of it. Afterward an observation study has been performed aimed to characterize the actuation mechanism qualitatively and quantitatively. Such study brought to the light several phenomena: the barrier discharge does produce a shock wave which creates a pressure gradient into the shear layer. Only after few tens of microsecond from the gas expansion a vortex get formed into the shear layer at the leading edge, in a condition of leading edge separation. This fact makes the Author believe that the hypothesized phenomenology regarding the pressure disturbance transmitted upstream into the shear layer is valid. The vortex, together with other vortexes formed just after the first one due to the continuous propagation of the shock wave through the shear layer, breaks down the viscous region of the flow field allowing so the free stream to pass through.

Nevertheless this phenomenon does not look enough for the actuation itself, since in many tests it has been observed the breaking down and the reformation of the shear layer several times before getting the flow reattached. This may be explained by the downward pushing phenomenon, also hypothesized and confirmed by the experimental results. In fact if the downward pushing phenomenon advances the separation, it does change the direction of the free stream in the neighborhood of the leading edge, making the shear layer expanding, so reducing the velocity in its upper region. This eventually might affect the disturbance upstream propagation, reducing the strength of the induced vortex.

Another effect that may be taken into account is the formation of an air jet, perpendicular with respect to the actuator plane, induced by the gas expansion. Such a jet, moving upward, induces a momentum injection downward, from its sides, into the expanded region. This phenomenon induces the formation of two counter rotating vortexes, on the sides of the air jet, in a still air box. Such a phenomenon created in a separated flow condition might change the direction of the free stream velocity vector such that it might become able to pass through the shear layer once it is broken down. On the other hand the velocity induced by the air jet is about 0.25 m/s, so the momentum induced by it may not be big enough to affect a flow with a free stream velocity about hundred times bigger.

However, the relative direction of the free stream, once the shear layer is broken down, looks to be a parameter that plays a very important role in the actuation mechanism.

Moreover it has been observed a dependency of the optimal frequency of actuation on the AoA: the more the AoA is increased the higher is the frequency required for controlling the flow. Nevertheless this dependency did not look linear.

Such a dependency actually makes sense: in fact the more the angle of attack increases, from an aerodynamic point of view, the bigger changes need to be actuated on the flow in order to control it. The bigger is the change one is aimed to get, the higher is the prize one must pay in terms of energy spent for achieving the flow control.

Beside the actuation mechanism itself, during this study several effect produced by the NS-DBD plasma actuator have been observed and recognized, and some of them look very similar to already existing flow control devices: the downward pushing of the SW produced by the gas expansion looks like a Suction System at the wall; the perpendicular air jet looks like a Zero Net Mass System, the possible vibration of the actuator's body, induced by the gas expansion, looks like a Vibrating String Actuator, the gas hearting might locally affect the velocity profile like an heated wall flow control technique.

Thus as it could be seen in the equation 2.1 the several "flow control related terms" are all affected by the actuator itself. Moreover a very high unsteady term may be considered since the Δt in which the velocity profile is affected is of the order of the microsecond.

Also looking at the Crocco equation one might conclude that the vorticity level after each pulse of the discharge get increased since all the terms of the Crocco equation are increased: entropy gradient due to the shock wave, total Enthalpy since the thermal phenomena, and the unsteady term which, again, might be very significant.

5.3 Conlusions

In conclusion it could be stated that the NS-DBD plasma actuator, having such a wide range of applications and being so constructively simple, is a cutting edge technology very promising in the Flow Control field.

If properly designed it could increase the efficiency of any existing aerodynamic application. Furthermore application of the plasma actuator might be taken into consideration in the design stage of any aerodynamic device. In this case the ND-DBD actuator might bring with it a drastic change in the concept design itself.

It does not require extra mechanical elements and it is able to provide an active control on the flow, with a reaction time being a fraction of a millisecond, very cheap and low energy consuming.

It is able to increase not only the aerodynamics performances but it also might increase the lifetime of the device itself through gust load alleviation.

The key for an optimization strategy for the control of the flow is in the understanding of the physical mechanism of actuation. With such a knowledge an optimal design may be obtained.

Although quite some aspect of the nanosecond-pulsed actuators still have to be studied in more detail, the technique may be close to an industrial application. Moreover, the Electromagnetic Noise problem, which hinders a direct implementation of nanosecond-pulsed actuators, has been overcome during this research.

As soon as the relation between the optimal frequency of discharge, angle of attack and airfoil shape is found, trial-and-error applications may be started, using an engineering approach.

A combination of AC and NS DBD plasma actuator might be considered as an interesting step. As such the combination of the two different kind of actuators leads to complementary actions which may be required for a specific flow problem (i.e. transition in combination with flow separation). A feedback control loop might be further developed in order to better optimize the two plasma actuators working together.

It is judged likely that an "industrial application design" could be achieved in about one year of work.

Chapter 6

Outlook and Future Research

Understanding the actuation mechanism of the NS-DBD plasma actuator would open the way for implementing it in many different technology fields. Its peculiar features such as the low energy consumption or the very easy layout, make the plasma actuator a very appealing cutting edge technology.

The possible applications, which a researcher could come up with, are several: it might be thought to be applied for separation flow control as well as separation delay, or flow turbulizator or perhaps it may be used for reducing the wake drag of bluff bodies.

Its secondary effects such as de-icing capability, shock wave interaction or high frequency induced vibrations could be further studied and a wide range of possible applications might be thought.

Of course several investigations are still required for getting the plasma actuator to the stage of industrial applications. In the next section several outlooks of the NS-DBD plasma actuator will be proposed and discussed. Further in this chapter next stages for this research will be proposed, motivated and discussed.

6.1 Outlooks

Regarding the primary effect of the NS-DBD plasma actuator several applications, and several outlooks, may be sought. Moreover, the secondary effect, further studied and developed might also be used for several useful applications.

It might be applied on airplanes: wings, tails, flaps, rudders, fuselage, engine nacelles. Such an application might bring several advantages: increasing the possible angle of attack of wings may reduce the take-off required time, since at the same

take-off velocity a bigger lift may be produced, so it would also reduce the required take-off strip: this may also imply a reduction of fuel consumption during the take-off of an airplane. Applications on flaps may make the maneuverability of the aircraft improve as well as applications on tail's radder. In the cruise mode, applications on fuselage or engine nacelles may reduce the drag due to the wake. Feedback loops might be developed for fast active reaction to sudden gusts or atmospheric turbulence so increasing the flight safety.

Moreover the possible capability to prevent the ice formation or to melt formed ice might make an anti-ice system develop. This may increase not only the safety of the flight itself but also it may greatly increase the safety feeling of any kind of user, from pilot to passengers.

Moreover, the possible capability to induce high frequency vibrations might make an anti-flutter system develop. This system might be able to prevent structural fluttering problems, increasing the safety of the flight itself and increasing the operational lifetime of the aircraft.

Moreover, the possible capability to interact with shock waves may make noise suppression system develop. This may be able to reduce the loud sound produced by the engines thus solving a nowadays big issue of airports.

All these applications may bring to a drastic change of the concept design of an aircraft which may become smaller and lighter, less fuel consuming, more safe and more environmental friendly. Moreover, airports might have smaller take-off strips and be less annoying for their neighbors.

It may be applied on rotors: helicopter flight, wind turbine, propellers. The capability of the plasma actuator to increase the possible angle of attack could bring a drastic change of the concept design also of these devices. Rotors may increase their blade/wing splice angle increasing in this way the mass flow, and so the momentum, they are able to transfer.

Moreover, possible shock wave interaction might help the aerodynamics at the tips of the rotor itself in such a way to either increase the tip AoA either increase the size of the blade/wing itself.

Moreover root aerodynamics might be improved such that bubble separation might be prevented and possible vortex interaction might reduce the aerodynamic drag in that region.

These effects all together may increase the operational lifetime of a rotor, increasing it efficiency, maneuverability and safety.

It may be applied on cars and trucks: both normal cars and racing cars may get a substantial improvement of their aerodynamics performances using NS-DBD Plasma Actuator. Flow separation delay may reduce the drag due to the wave of a bluff body such as a normal car, so reducing the fuel consumption, making the car itself less consuming and environmental friendly.

Even higher advantages may be gotten by a racing car, since its performances are strongly related to its aerodynamics. The actuator may be applied on any part of a racing car, increasing its downwards pushing at a fixed velocity, so increasing the safety of the car. Its maneuverability may get positively improved, and a fuel consumption reduction may be achieved.

Many other applications might be figured out, like applications on space launchers, or applications for flow control around bridges or high buildings, or flow control for inner flows like metanoduct.

All the possible industrial applications of NS-DBD plasma actuator need to be further studied and implemented. For this reason the next section is devoted to the proposal of a study aimed to develop a stronger understanding of the actuator mechanism, trying eventually to prove it. Afterward a study about the capability of implementation of the plasma actuator for industrial applications will be proposed and discussed. The final goal of such a research will be to bring the studied device to an industrial applications stage. Eventually several flow control strategies will be developed with respect to the industrial field of applications that the NS-DBD plasma actuator will be sought for.

6.2 Future Research

In order to further continue this research and bring the NS-DBD Plasma Actuator at an "industrial application" stage few other tests are suggested.

A systematic Boundary Layer parametric study on a well know flat plate is required, perhaps supported by a CFD calculation. Such a test campaign is necessary in order to understand the interaction of the plasma actuator with the Boundary Layer. For real application, in fact, it must be considered that the size of the boundary layer produced in the TUDelft facilities is not even comparable with one generated on the wing of a big airplane. The relative effect of the actuator with respect to the size of the controlled BL is a very important information. It might affect the optimal position of the actuator itself. Moreover a study about the effect of the actuator on the skin friction is very important as well in order to be able to estimate the total overall effect that a NS-DBD actuator might have in a real application.

Further on, in order to finally be able to design a flow control strategy, finding out the relation between the angle of attack and the optimal frequency of discharge is necessary in order to get the actuation happening.

With such an aim again flat plate tests are suggested: placing in a wind tunnel two flat plates, consecutively, and placing the second one at an angle with respect to the first one as well as with respect the flow direction, one might be able to reproduce the "flow separated"conditions. With such a configuration two series of tests might be designed.

First of all the optimal frequency of discharge is studied. Based on the observations done in the presented experimental work, the optimal frequency of discharge is considered to be related to the frequency of oscillation of the separated shear layer, which itself must be related to the velocity of the free stream and the velocity of the flow in the separated region. The velocity of the flow in the separated region must be dependent on the angle at which the second plate is set. So changing the angle of the second plate, and so changing the frequency of oscillation of the shear layer, a parametric study could be performed.

Second of all, since the mechanism has been thought to act on a laminar separated shear layer, changing the size of the first plate a turbulent separated shear layer could be achieved and a study on the effect of the actuator in such a situation also is necessary for possible industrial applications.

With such a complete set of information strategies for real applications of flow control might be designed for any kind of outlook that has been already discussed in the previous section.

Appendix A

Windtunnel wall corrections for NACA0015 model in the V-tunnel

Based on reference [61] and [62] a correction may be obtained for the angle of attack in case a rectangular model spans a circular test section. The ratio of measured lift over the lift obtained in a free stream can be written as

$$\frac{L}{L_0} = \frac{8\pi R}{a_1 c}\left(\frac{2}{\pi^2} - \sum_{n=0}^{\infty}\frac{b_n}{2n+3}\right) \tag{A.1}$$

where

- R is the wind tunnel jet radius ($0.3m$)
- c is the wing chord (in the case of the NACA-0015 model $c = 0.24m$)
- a_1 is the 2-dimensional lift curve slope (assumed to be 2π)
- b_n are the coefficients that determine the span-wise loading of the wing [61] [62].

In this case the correction to the angle of attack becomes

$$\Delta\alpha = -C_{L_u}\frac{1}{a_1}\left(\frac{L_0}{L} - 1\right) \tag{A.2}$$

where $C_{L_u}$is the uncorrected lift coefficient.

With $\mu = \frac{8\pi R}{a_1 c} = 5$ and $b_0 = 0.31968$, $b_1 = 0.0222$, $b_2 = 0.0698$ from [62] we find an angle of attack correction which is linear with the lift coefficient

$$\Delta\alpha(C_L) = -13.2\, C_L \quad (deg) \tag{A.3}$$

Appendix B

Discharge Characteristics

The characteristic of the discharge pulse inputted into the plasma actuator might affect the functionality of the device itself, and its applicability and scalability upwards.

Its has been observed in the several researches about the plasma actuator that only a nanosecond discharge is actually able to generate such a mechanism able to actively control the flow. In fact the very small energy content of a picosecond discharge pulse would create a not enough strong shock wave or a millisecond discharge pulse might not even create a shock wave at all.

Important characteristics of the nanosecond pulse are the rising time and the duration of the pulse. Moreover the voltage applied and the frequency of the discharge itself are key parametres for the actuation of the mechanism as well. The pulse rising time can affect the compressibility effect: in fact the slower the inputted pulse rises the weaker will be the shock wave produced in term of Δp of the shock wave itself.

The duration of the pulse can affect the thermal energy inputted in the flow: a long pulse could increase the raised temperature, increasing in this way the strength of the shock wave.

Several tests carried out on long actuators showed that the velocity of propagation of the pulse into the electrodes is half of the speed of light, which means that a pulse with a duration of about 20 nanoseconds can travel to a length of about 6 meters, which actually gives an up limit to the upwards scalability. In actuators shorter than 6 meters, with such a pulsed discharge, the pulse will reach the end of the electrodes and will be reflected backwards. Doing so the energy inputted get multiplied as much as the pulse get reflected.

It has been observed that a parallel system of actuator, developed for proving the scalability, is able to reduce the energy expense required in order to achieve

the actuation mechanism. Physically it might be explained as a more distributed energy over the actuators might increase its efficiency. This effect can be observed in the Fig.B.1.

The energy input is calculated based on the time integral of the curve in Fig.B.1. It has been calculated that for a Reynolds number up to $4e^5$ the energy expense is about 2 W/m^2 at an AoA of 26 degrees. This value rises up to 20 W/m^2 when the AoA is up to 32 degrees.

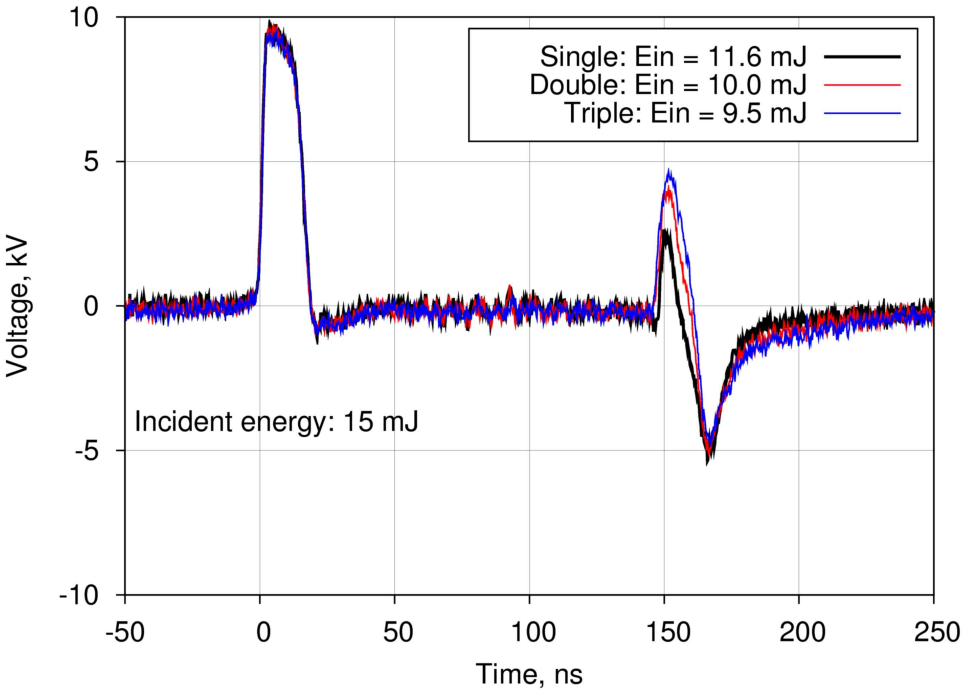

Fig. B.1: In the graph is shown the energy input given into the actuator for a single, double and triple configuration. For acquiring such information a Back Current-Shunt technique has been applied.

It has been observed that a minimum of 7 kV are required for achieving control over a flow up to 30 m/s. A frequency and a burst mode discharge studies have shown that more important than the voltage inputted per pulse is the total energy content that get inputted into the flow.

Appendix C

Dealing with Electromagnetic Noise

Carrying out experiments about NS-DBD plasma actuator a researcher will experience the very annoying interference of the Electromagnetic Noise produced by the discharge of the actuator itself.

This electromagnetic (EM) Noise travels like a wave, propagating in all the directions from its source point, its strength is depending on the discharge characteristics such as voltage applied or frequency and it will be amplified by all the cablings of the experimental setup which will work as antennas for the EM noise.

The EM wave, travelling in the laboratory space meets on its way electronics such as computers, transducers, extensometers, cameras and many others electronic equipments of the acquisition system.

As a result the electronics may freeze in a short or somewhat longer period depending on their own quality.

Even if the interaction is quite short it increases the difficulty of peforming experiments with nanosecond-pulsed actuator considerably. Considering that the phenomenon under study takes less then a millisecond it might be seen how much this EM emission is an issue for a researcher.

Unfortunately it is impossible to get rid of the EM noise, so one has to live with it.

In fact, in order to carry out many of the tests done during this research a home made Faraday Cage has been designed and built. Such a device was not always needed but it turned out to be extremely useful when the EM noise was too big. Usually it was used for protecting deviced such as computers, transducers and anything else was being affected by EM. In fact thanks to it the tests in the V-tunnel and in the M-tunnel, and some of the tests in the W-tunnel, have been possible.

In order to reduce the EM emission some tricks could be performed such as: minimizing the length of all the required cables and wires, positioning when possible

the electronics as far as possible away from the noise source and reducing at the minimum the discharge duration. Moreover a good shielding and grounding of all the electronics is strongly recommended in order to reduce the noise and preserve the correct functioning of the electronics.

In fact all these measures are needed to enable wind tunnel test with nanosecond-pulsed actuators. Especially for future applications it is needed to investigate efficient ways to incorporate them in the particular setup.

Appendix D

Schlieren Results

From the Schlieren Imaging important conclusions were drawn out in this report with respect to the working principle of the nanosecond- pulsed actuators. To enable the reader to get a clear picture of particular actuator and flow conditions all Schlieren images have been presented in subsequent Fig.s D.1 to D.21 as is.

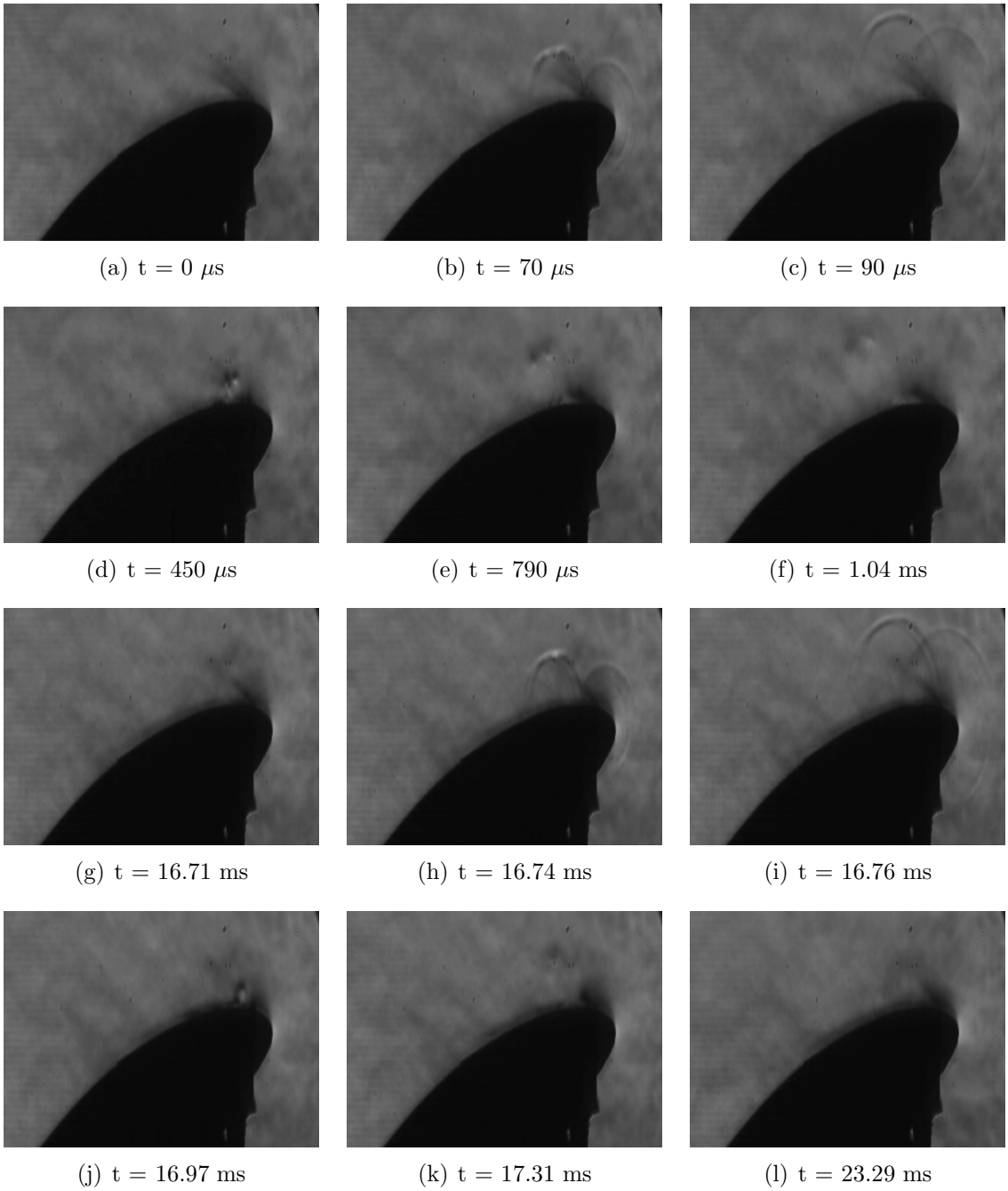

(a) t = 0 μs (b) t = 70 μs (c) t = 90 μs

(d) t = 450 μs (e) t = 790 μs (f) t = 1.04 ms

(g) t = 16.71 ms (h) t = 16.74 ms (i) t = 16.76 ms

(j) t = 16.97 ms (k) t = 17.31 ms (l) t = 23.29 ms

Fig. D.1: AoA26.50hz.30ms.act 0-20 +0.2 0.15

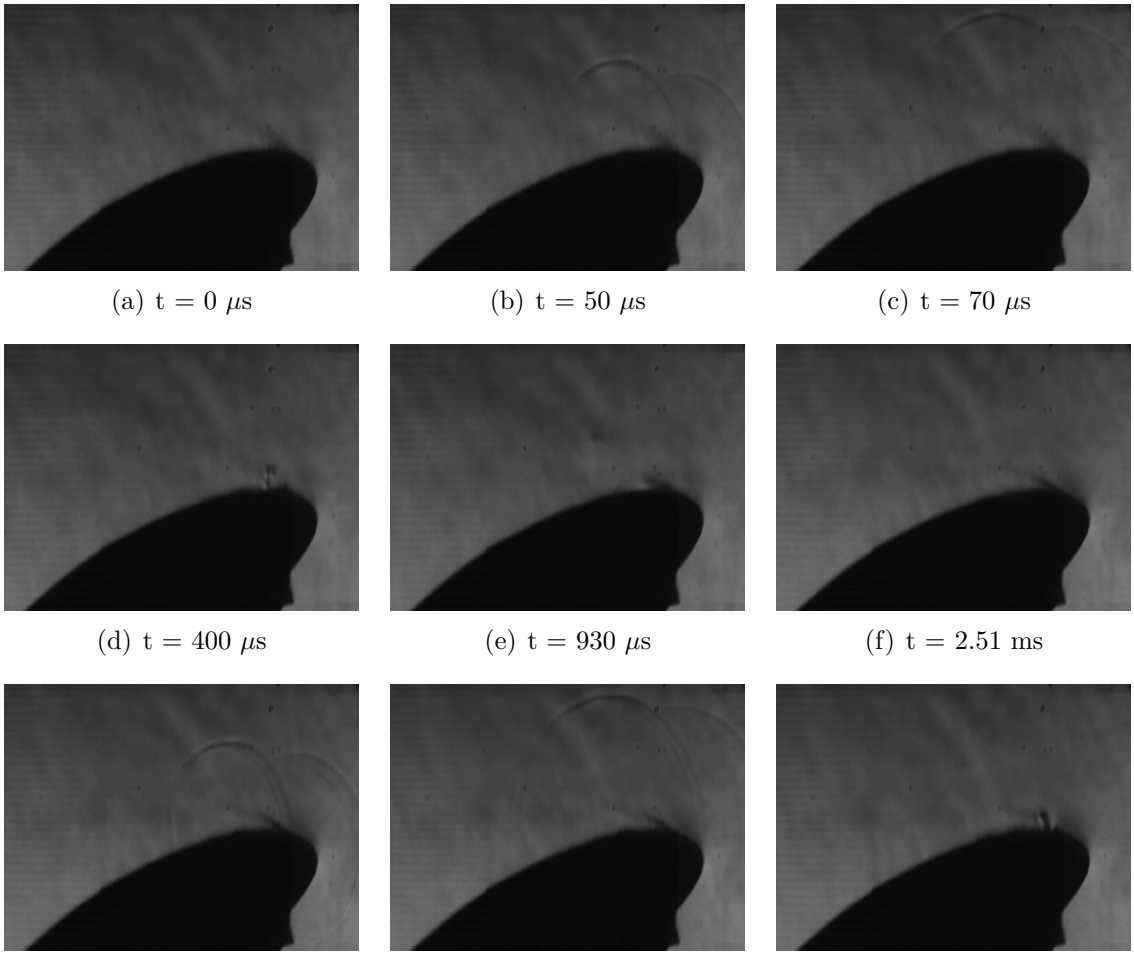

(a) t = 0 μs (b) t = 50 μs (c) t = 70 μs

(d) t = 400 μs (e) t = 930 μs (f) t = 2.51 ms

(g) t = 5.26 ms (h) t = 5.28 ms (i) t = 5.53 ms

Fig. D.2: The figure continues on the next page

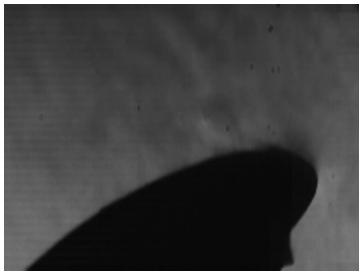

(a) t = 5.99 ms

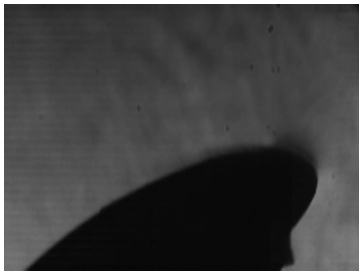

(b) t = 10.41 ms

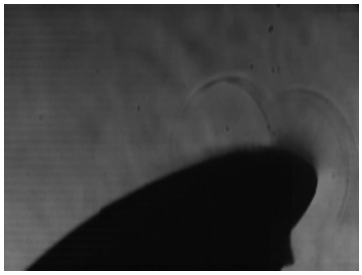

(c) t = 10.46 ms

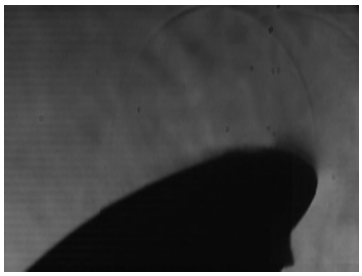

(d) t = 10.50 ms

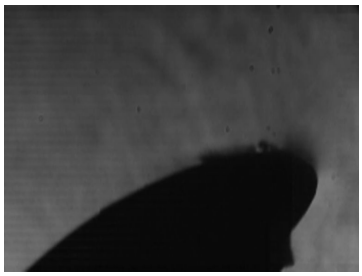

(e) t = 10.72 ms

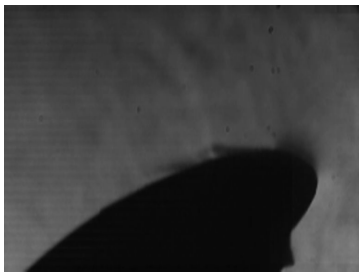

(f) t = 11.05 ms

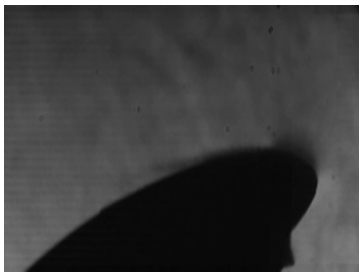

(g) t = 11.55 ms

Fig. D.3: AoA26.200hz.30ms.act 0-20 +0.2 0.15

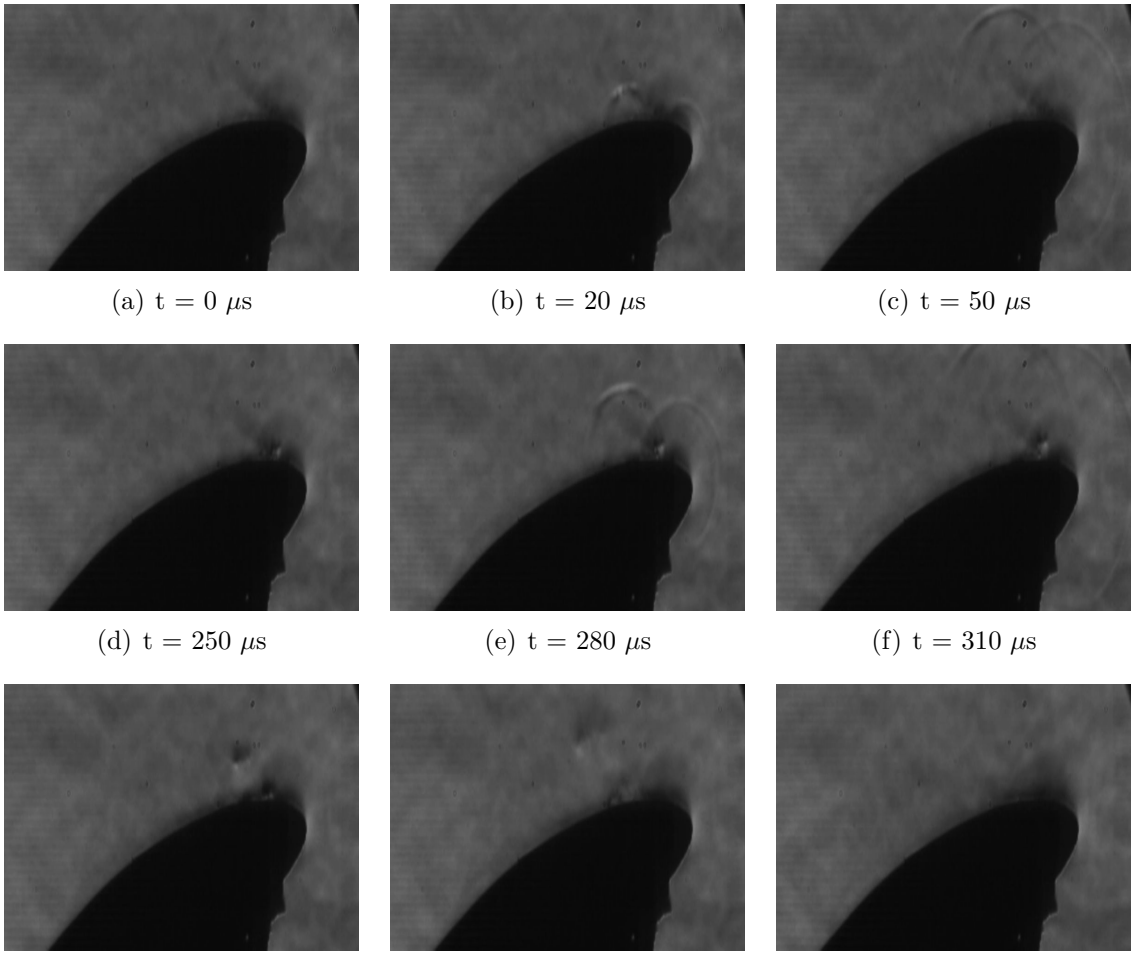

(a) t = 0 μs (b) t = 20 μs (c) t = 50 μs

(d) t = 250 μs (e) t = 280 μs (f) t = 310 μs

(g) t = 570 μs (h) t = 930 μs (i) t = 4.17 ms

Fig. D.4: The figure continues on the next page

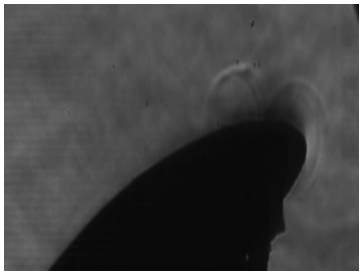

(a) t = 4.19 ms

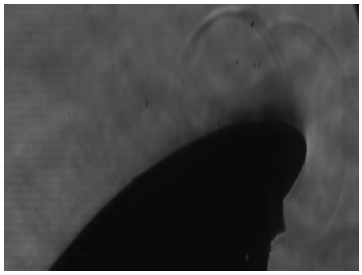

(b) t = 4.22 ms

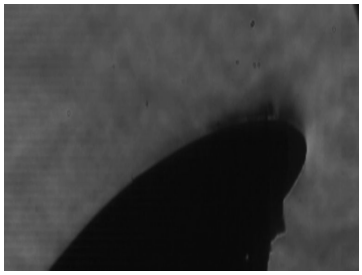

(c) t = 4.42 ms

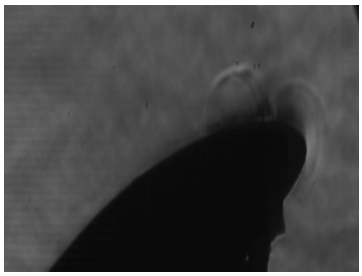

(d) t = 4.44 ms

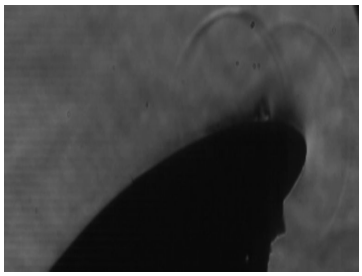

(e) t = 4.47 ms

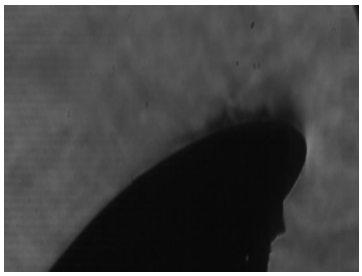

(f) t = 4.71 ms

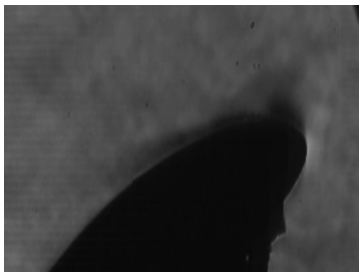

(g) t = 8.33 ms

Fig. D.5: AoA26.200hz.2p.300μs.30ms.act 0-20 +0.2 0.15

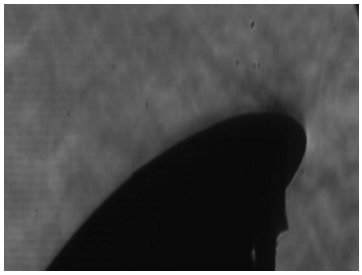

(a) t = 0 μs

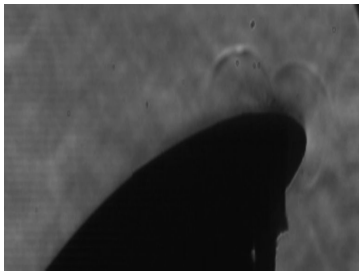

(b) t = 30 μs

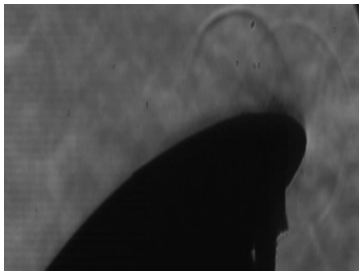

(c) t = 50 μs

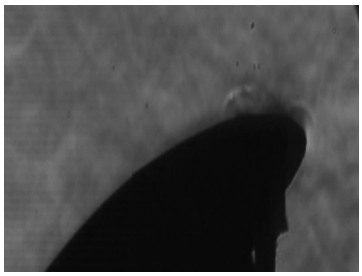

(d) t = 100 μs

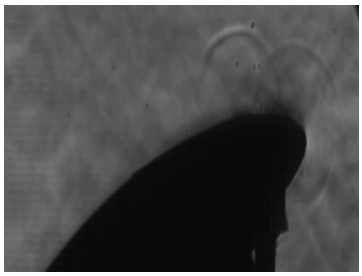

(e) t = 120 μs

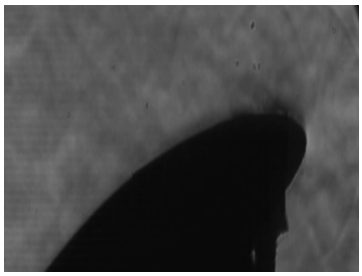

(f) t = 150 μs

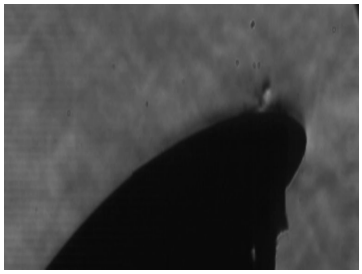

(g) t = 350 μs

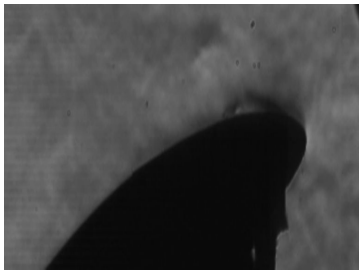

(h) t = 920 μs

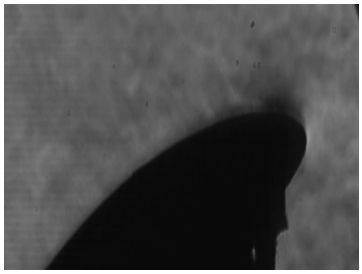

(i) t = 4.16 ms

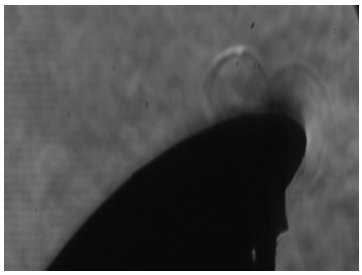

(j) t = 4.20 ms

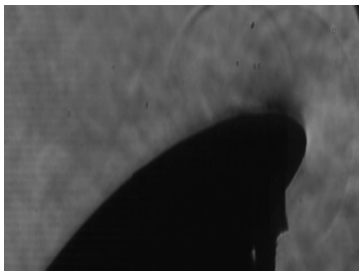

(k) t = 4.22 ms

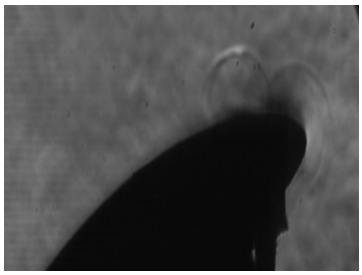

(l) t = 4.28 ms

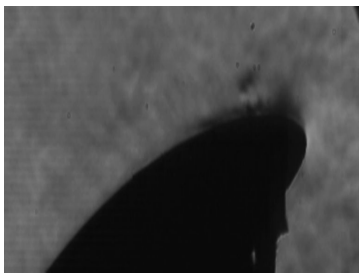

(m) t = 4.60 ms

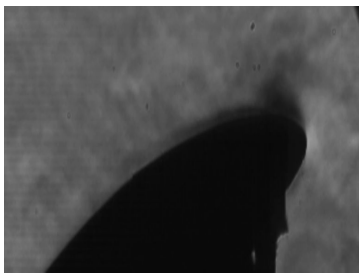

(n) t = 8.33 ms

Fig. D.6: AoA26.200hz.2p.100μs.30ms.act 0-20 +0.2 0.15

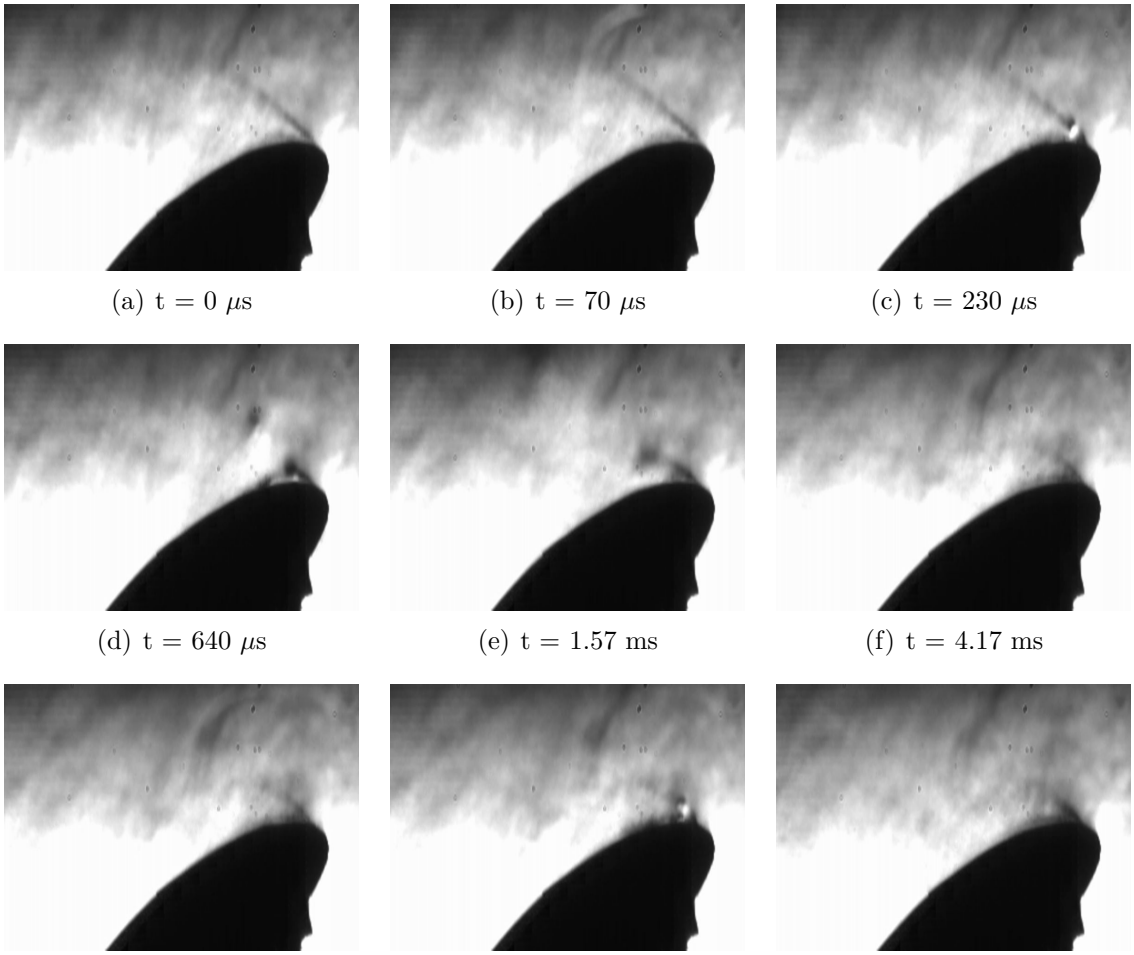

(a) t = 0 μs (b) t = 70 μs (c) t = 230 μs

(d) t = 640 μs (e) t = 1.57 ms (f) t = 4.17 ms

(g) t = 4.23 ms (h) t = 4.40 ms (i) t = 8.33 ms

Fig. D.7: AoA29.200hz.30ms.act 0-20 +0.2 0.15

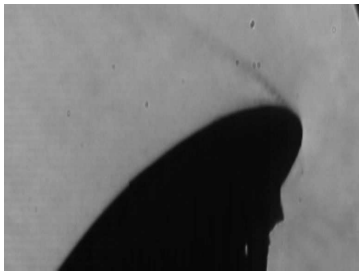

(a) t = 0 μs

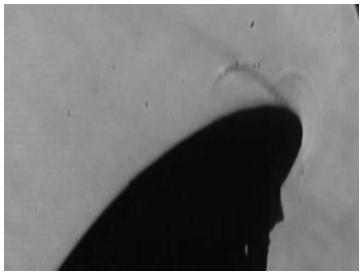

(b) t = 20 μs

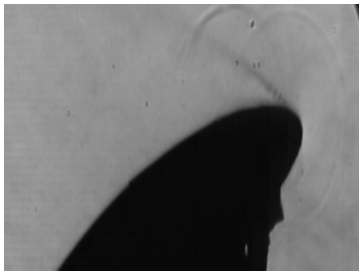

(c) t = 50 μs

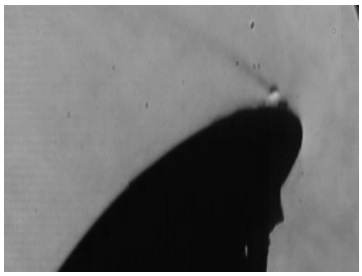

(d) t = 230 μs

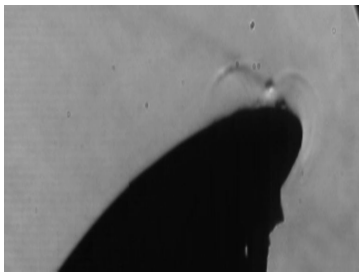

(e) t = 270 μs

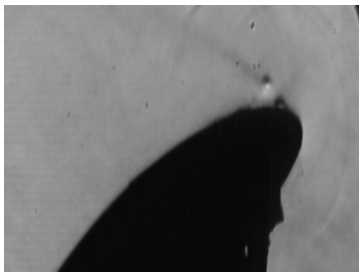

(f) t = 310 μs

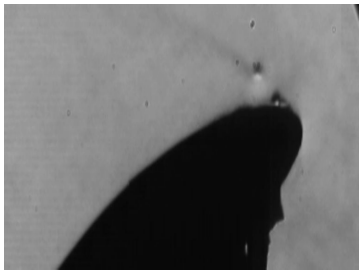

(g) t = 390 μs

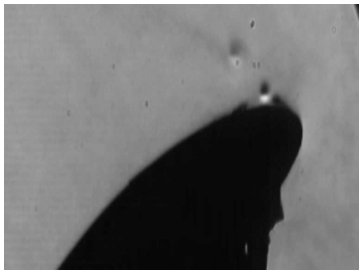

(h) t = 600 μs

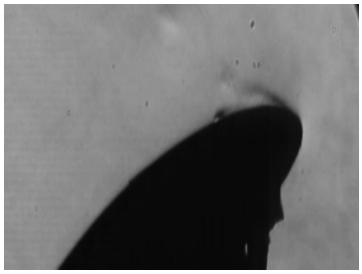

(i) t = 1.20 ms

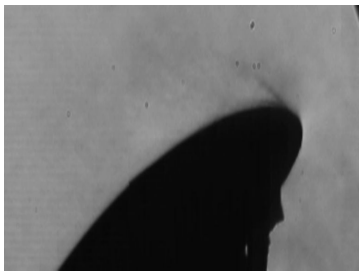

(j) t = 4.16 ms

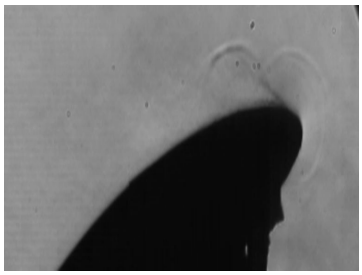

(k) t = 4.20 ms

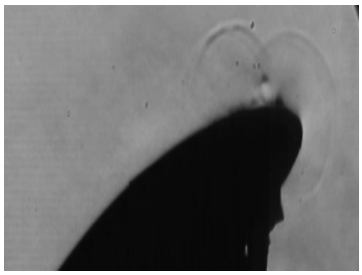

(l) t = 4.46 ms

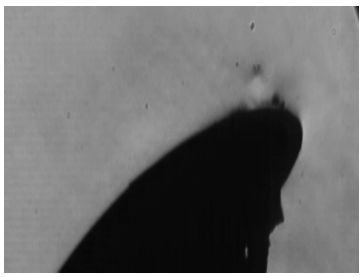

(m) t = 4.53 ms

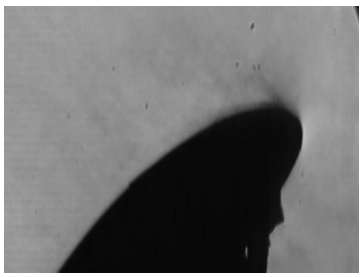

(n) t = 8.33 ms

Fig. D.8: AoA29.200hz.2p.300us.30m s.act 0-20 +0.2 0.15

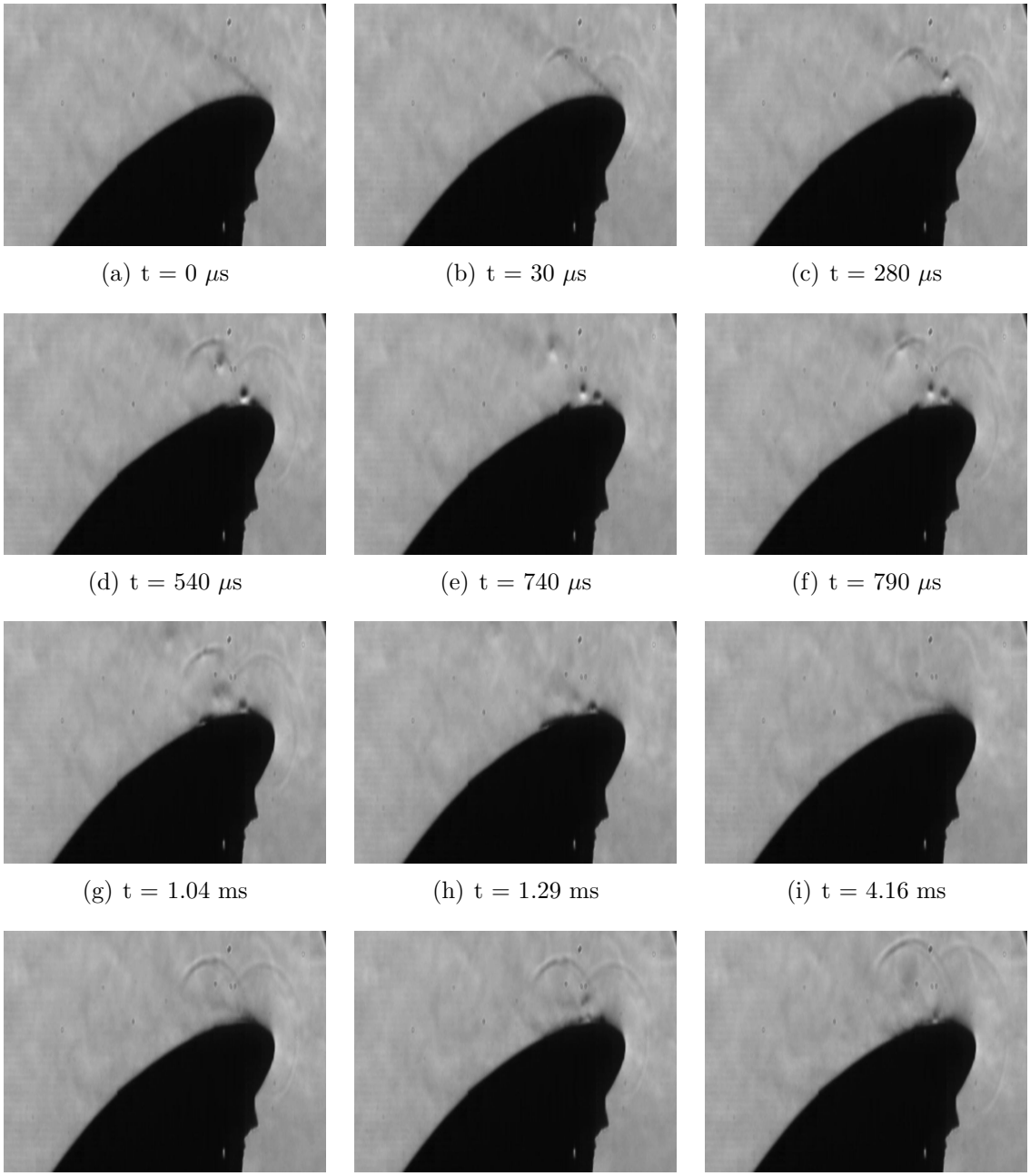

(a) t = 0 μs (b) t = 30 μs (c) t = 280 μs

(d) t = 540 μs (e) t = 740 μs (f) t = 790 μs

(g) t = 1.04 ms (h) t = 1.29 ms (i) t = 4.16 ms

(j) t = 4.20 ms (k) t = 4.45 ms (l) t = 4.71 ms

Fig. D.9: The figure continues on the next page

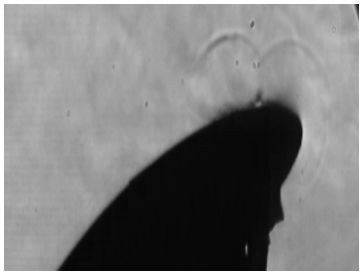

(a) t = 4.95 ms

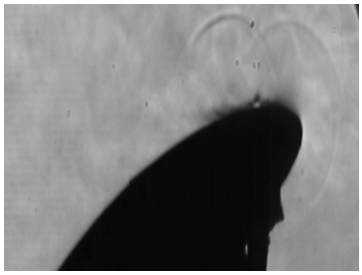

(b) t = 5.21 ms

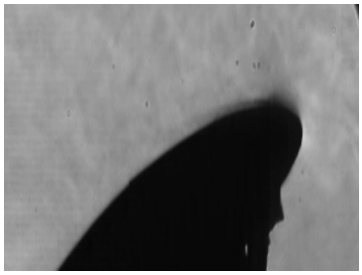

(c) t = 8.33 ms

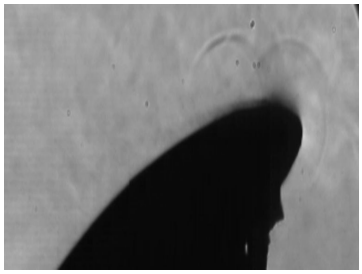

(d) t = 8.37 ms

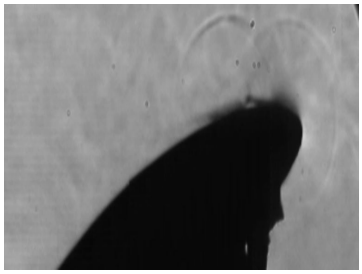

(e) t = 8.63 ms

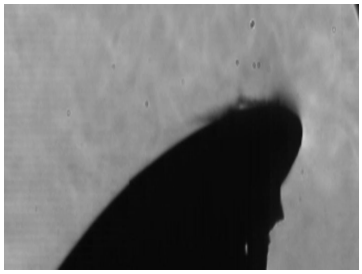

(f) t = 8.69 ms

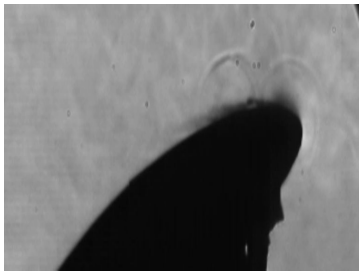

(g) t = 8.86 ms

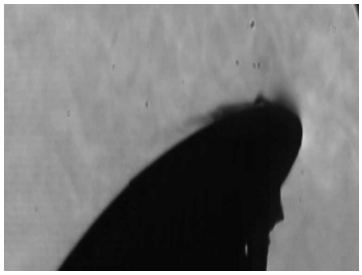

(h) t = 9.06 ms

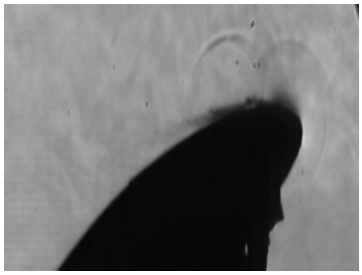

(i) t = 9.12 ms

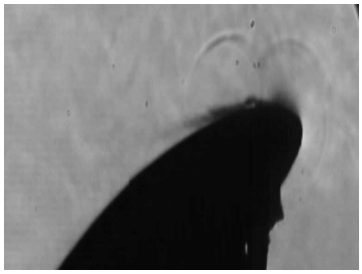

(j) t = 9.37 ms

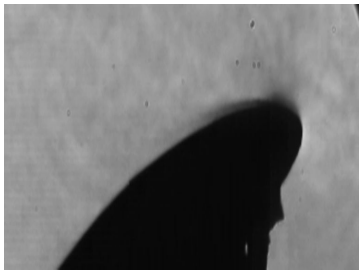

(k) t = 12.49 ms

Fig. D.10: AoA29.200hz.5p.300us.30m s.act 0-20 +0.2 0.15

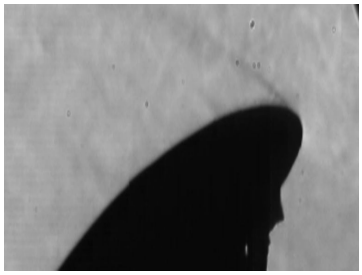

(a) t = 0 μs

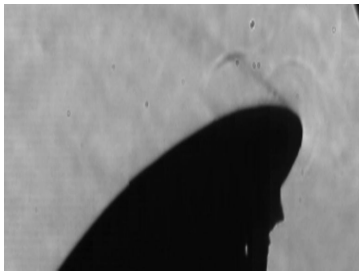

(b) t = 50 μs

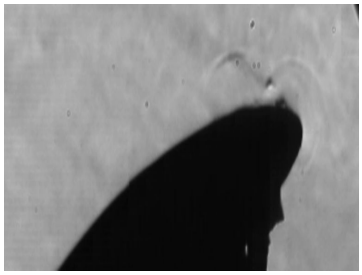

(c) t = 140 μs

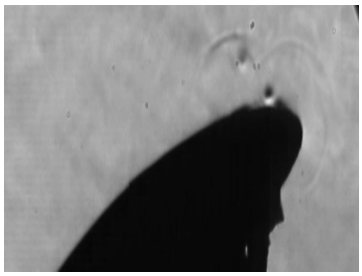

(d) t = 220 μs

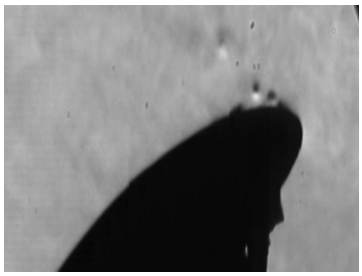

(e) t = 300 μs

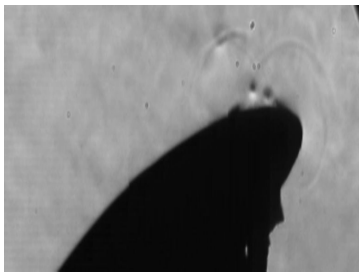

(f) t = 400 μs

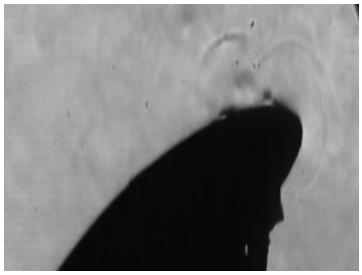

(g) t = 870 μs

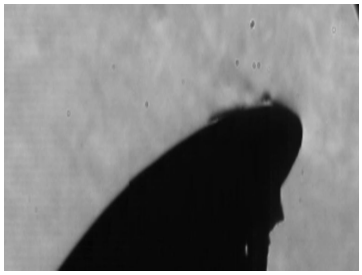

(h) t = 4.17 ms

Fig. D.11: AoA29.200hz.5p.100us.30m s.act 0-20 +0.2 0.15

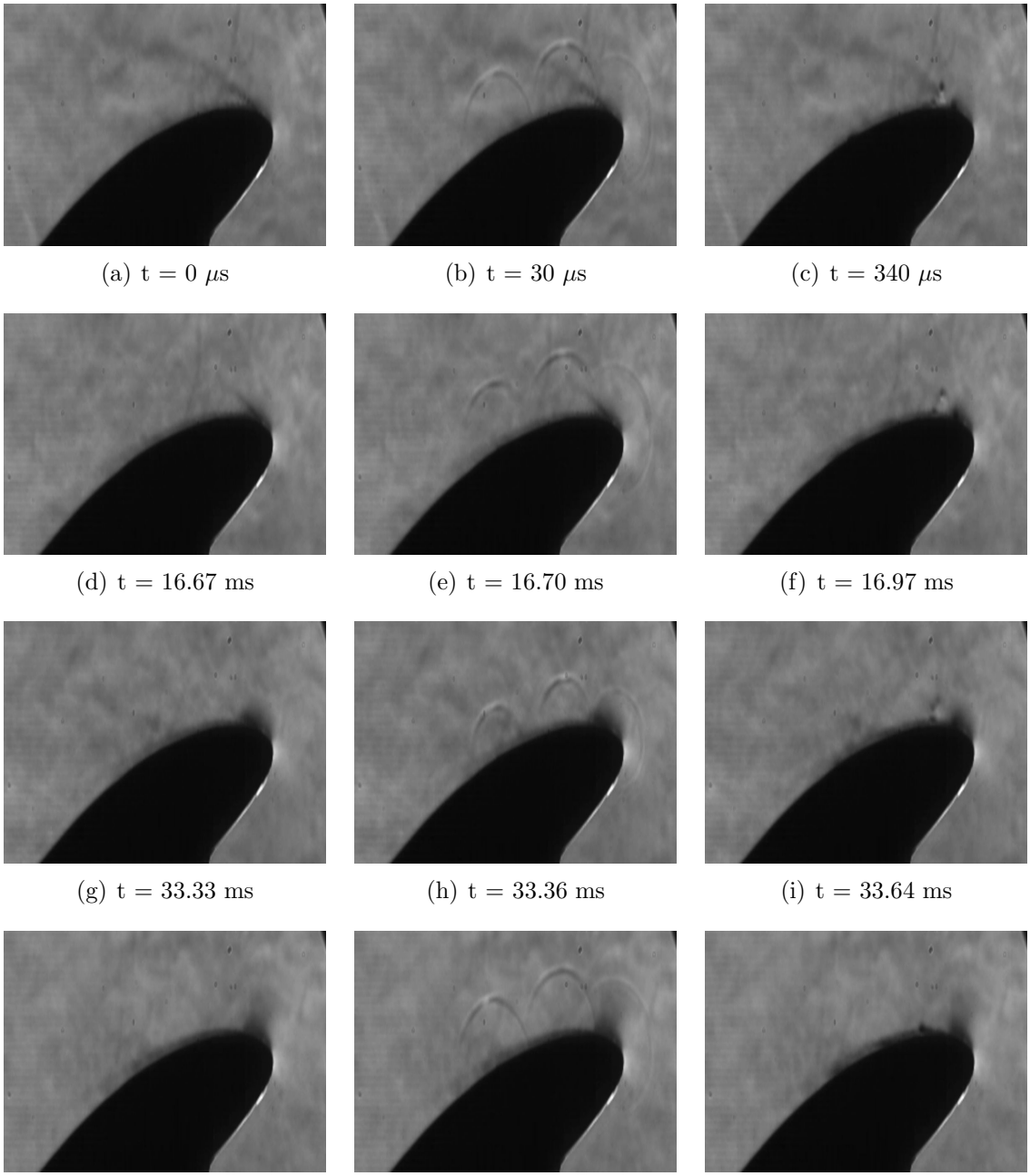

(a) t = 0 μs (b) t = 30 μs (c) t = 340 μs

(d) t = 16.67 ms (e) t = 16.70 ms (f) t = 16.97 ms

(g) t = 33.33 ms (h) t = 33.36 ms (i) t = 33.64 ms

(j) t = 50.00 ms (k) t = 50.03 ms (l) t = 50.36 ms

Fig. D.12: AoA26.50hz.30ms.act 0-20-45 +0.2 0.15

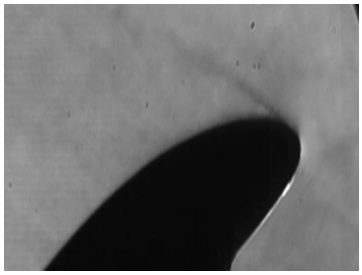

(a) t = 0 μs

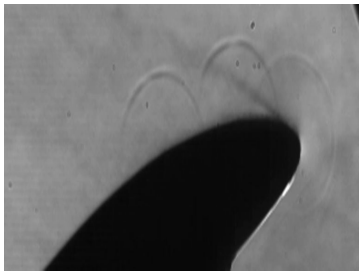

(b) t = 40 μs

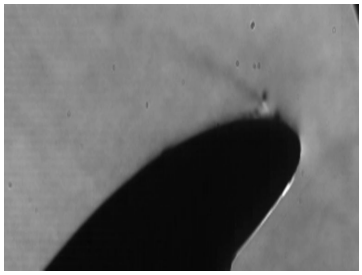

(c) t = 360 μs

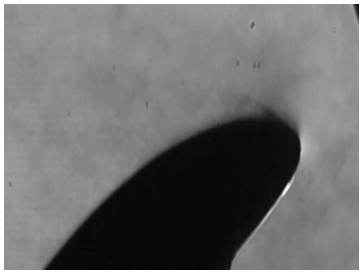

(d) t = 4.17 ms

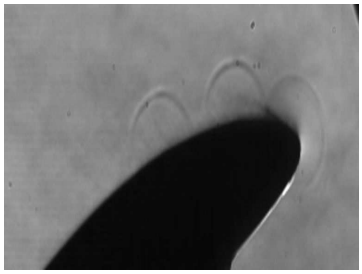

(e) t = 4.20 ms

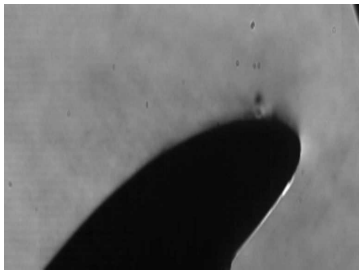

(f) t = 4.50 ms

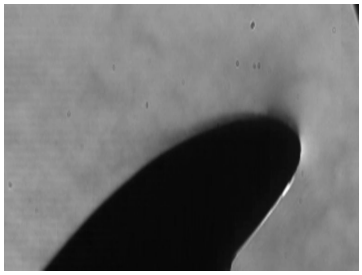

(g) t = 8.33 ms

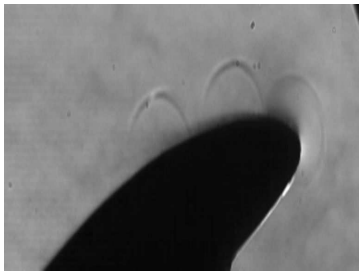

(h) t = 8.37 ms

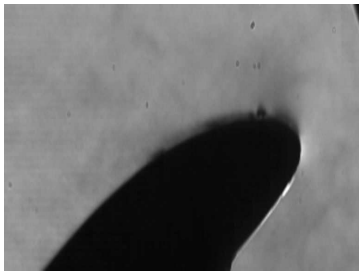

(i) t = 8.60 ms

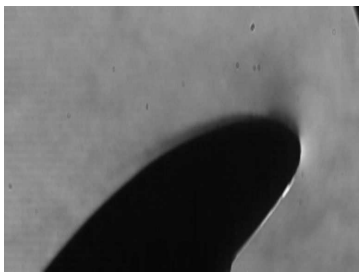

(j) t = 12.50 ms

Fig. D.13: AoA26.200hz.30ms.act 0-20-45 +0.2 0.15

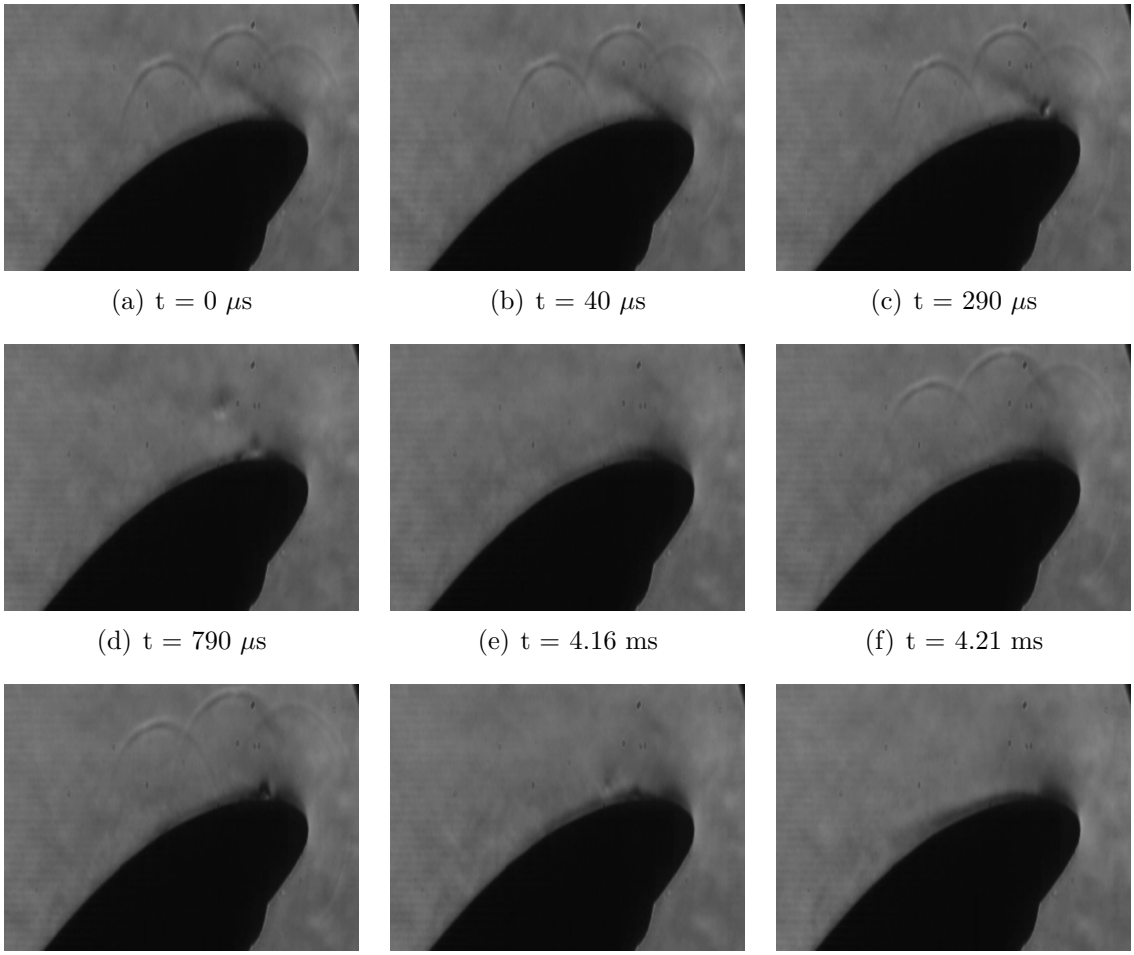

(a) t = 0 μs (b) t = 40 μs (c) t = 290 μs

(d) t = 790 μs (e) t = 4.16 ms (f) t = 4.21 ms

(g) t = 4.46 ms (h) t = 4.82 ms (i) t = 8.33 ms

Fig. D.14: AoA26.200hz.2p.300us.30ms.act 0-20-45 +0.2 0.15

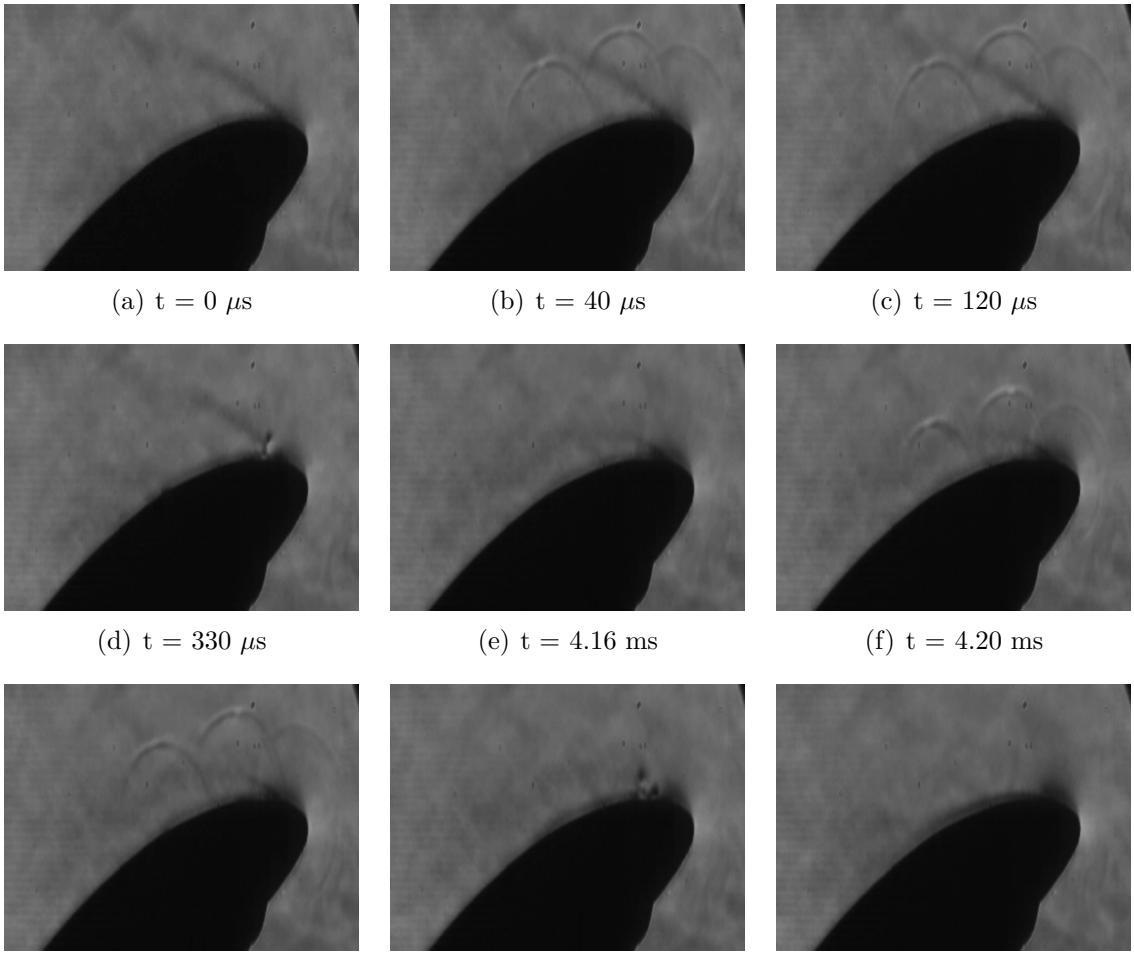

(a) t = 0 μs (b) t = 40 μs (c) t = 120 μs

(d) t = 330 μs (e) t = 4.16 ms (f) t = 4.20 ms

(g) t = 4.29 ms (h) t = 4.54 ms (i) t = 8.33 ms

Fig. D.15: AoA26.200hz.2p.100us.30ms.act 0-20-45 +0.2 0.15

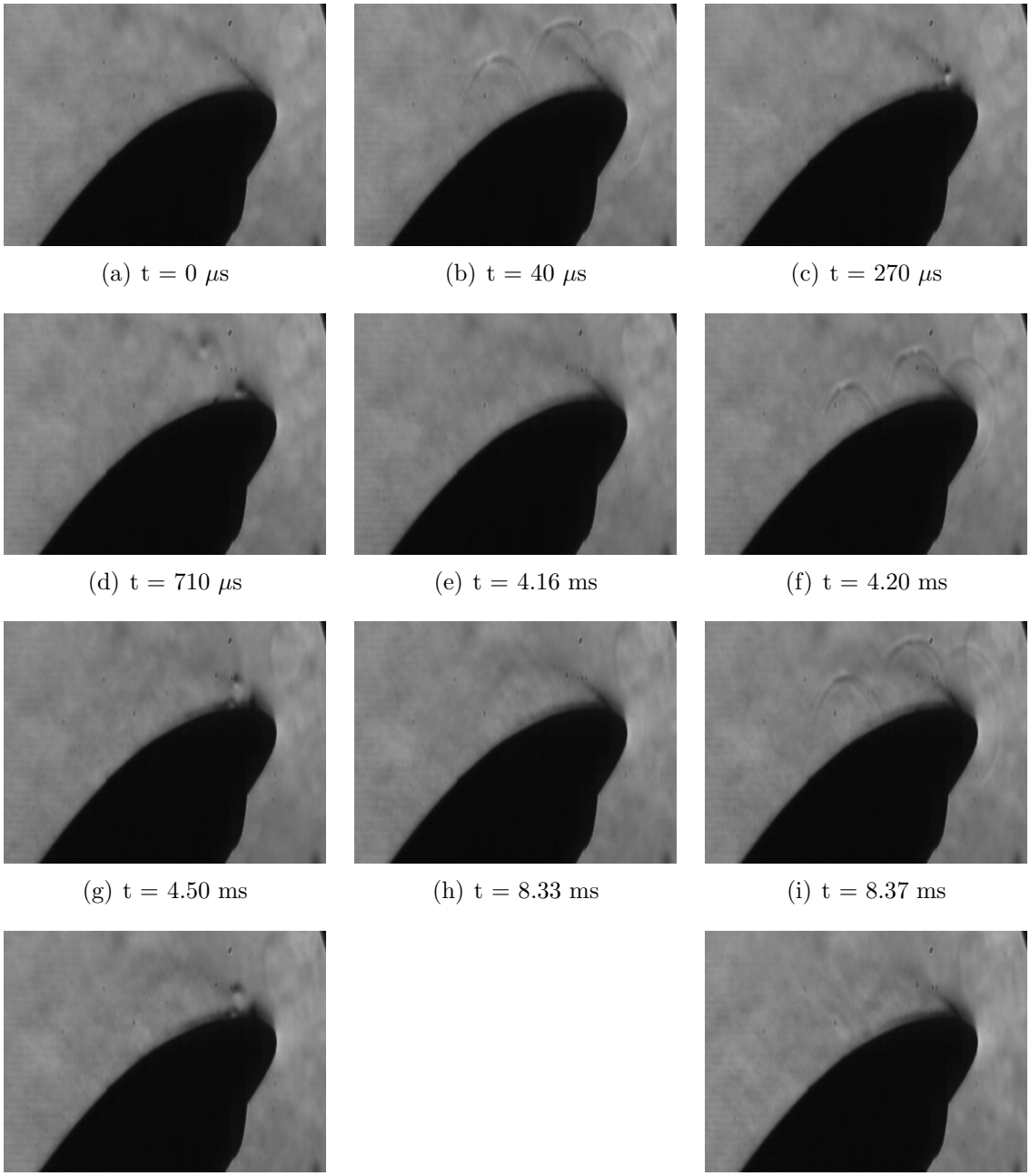

(a) t = 0 μs (b) t = 40 μs (c) t = 270 μs

(d) t = 710 μs (e) t = 4.16 ms (f) t = 4.20 ms

(g) t = 4.50 ms (h) t = 8.33 ms (i) t = 8.37 ms

(j) t = 8.62 ms (k) t = 12.50 ms

Fig. D.16: AoA29.200hz.30ms.act 0-20-45 +0.2 0.15

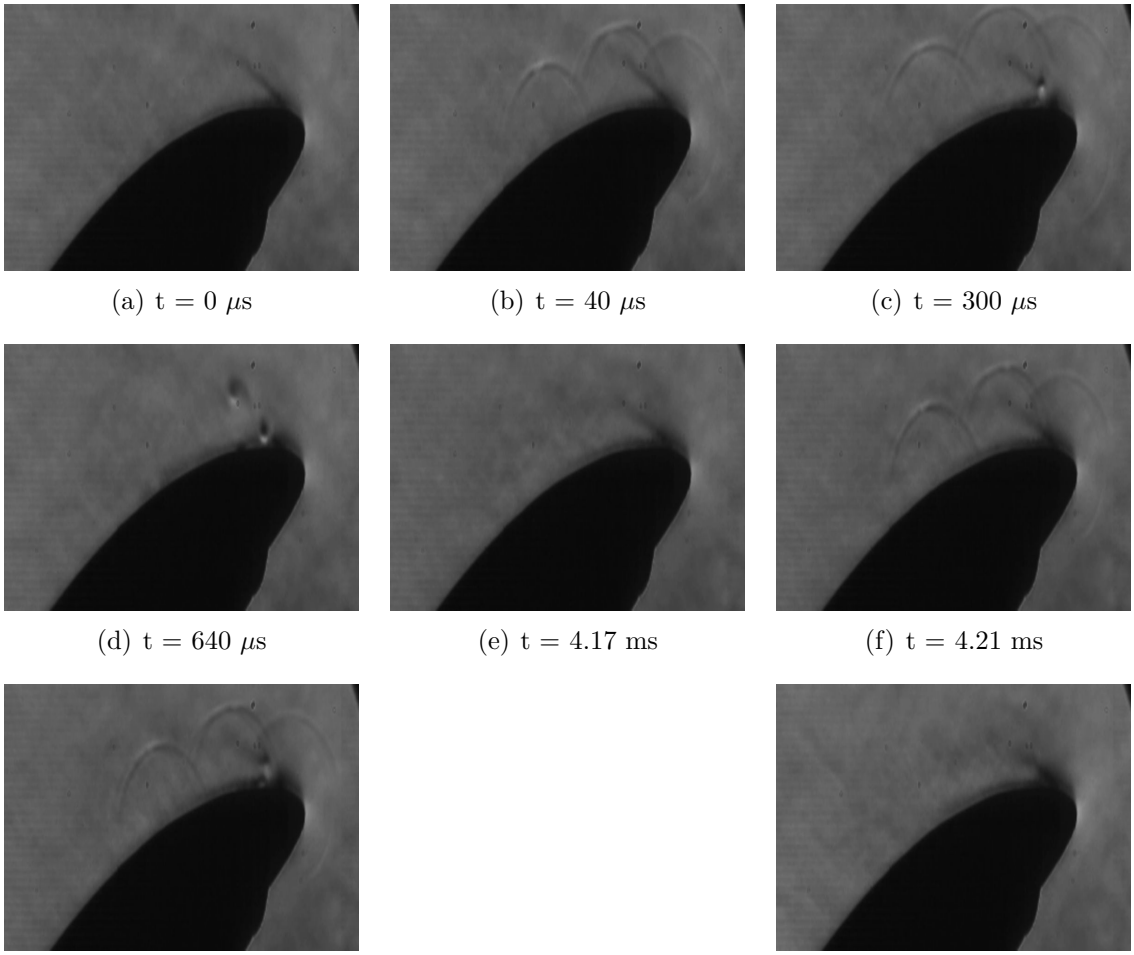

(a) t = 0 μs (b) t = 40 μs (c) t = 300 μs

(d) t = 640 μs (e) t = 4.17 ms (f) t = 4.21 ms

(g) t = 4.46 ms (h) t = 8.33 ms

Fig. D.17: AoA29.200hz.2p.300us.30ms.act 0-20-45 +0.2 0.15

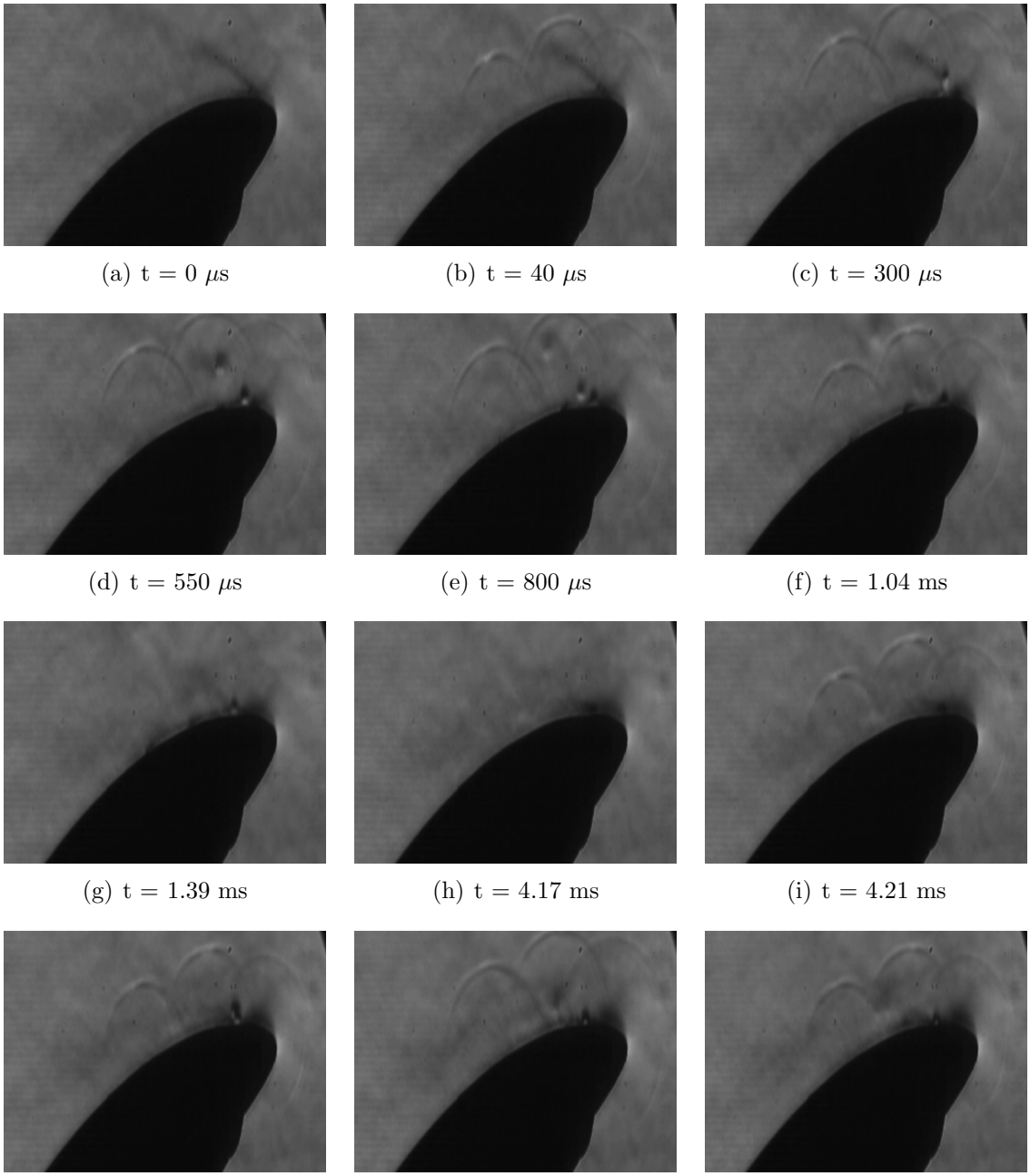

(a) t = 0 μs (b) t = 40 μs (c) t = 300 μs

(d) t = 550 μs (e) t = 800 μs (f) t = 1.04 ms

(g) t = 1.39 ms (h) t = 4.17 ms (i) t = 4.21 ms

(j) t = 4.46 ms (k) t = 4.72 ms (l) t = 4.96 ms

Fig. D.18: The figure continues on the next page

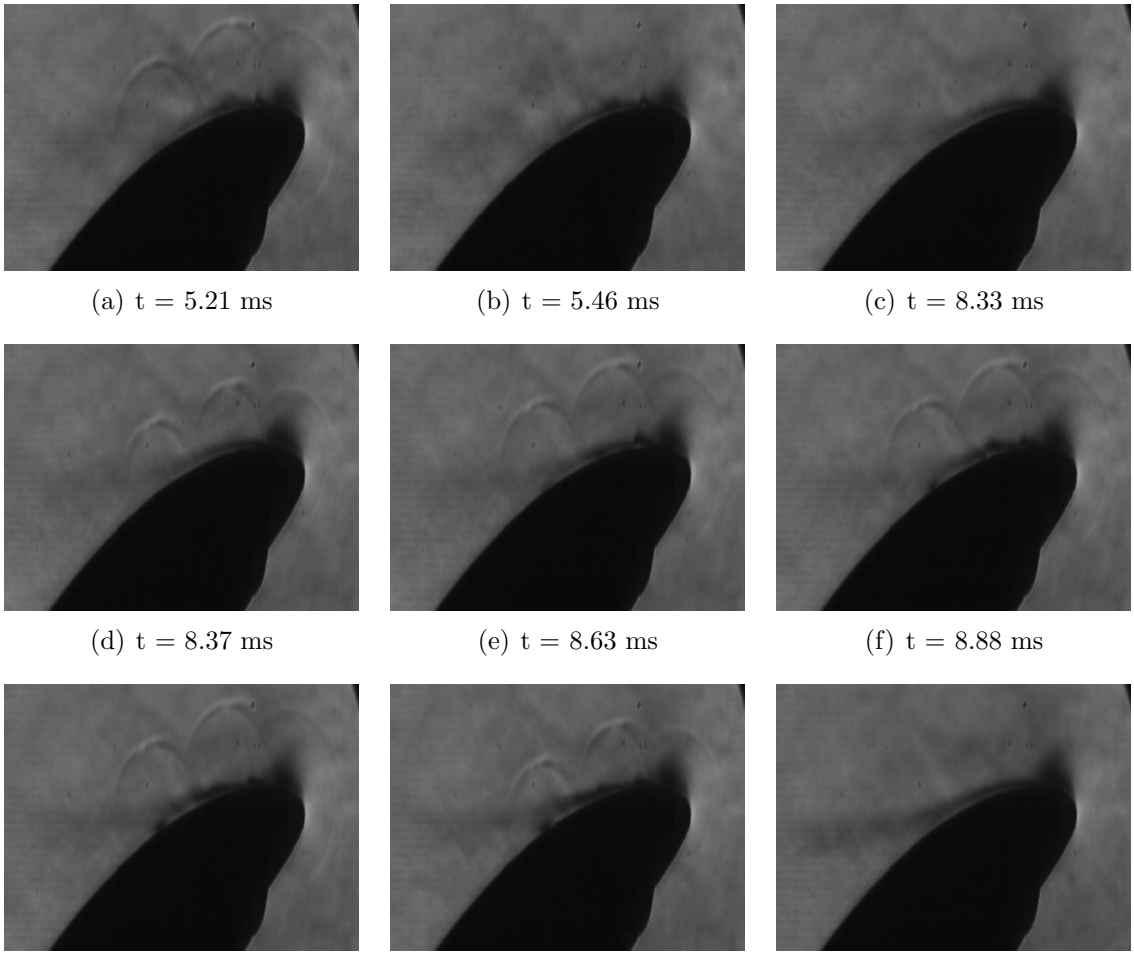

(a) t = 5.21 ms (b) t = 5.46 ms (c) t = 8.33 ms

(d) t = 8.37 ms (e) t = 8.63 ms (f) t = 8.88 ms

(g) t = 9.13 ms (h) t = 9.37 ms (i) t = 12.08 ms

Fig. D.19: AoA29.200hz.5p.300us.30m s.act 0-20-45 +0.2 0.15

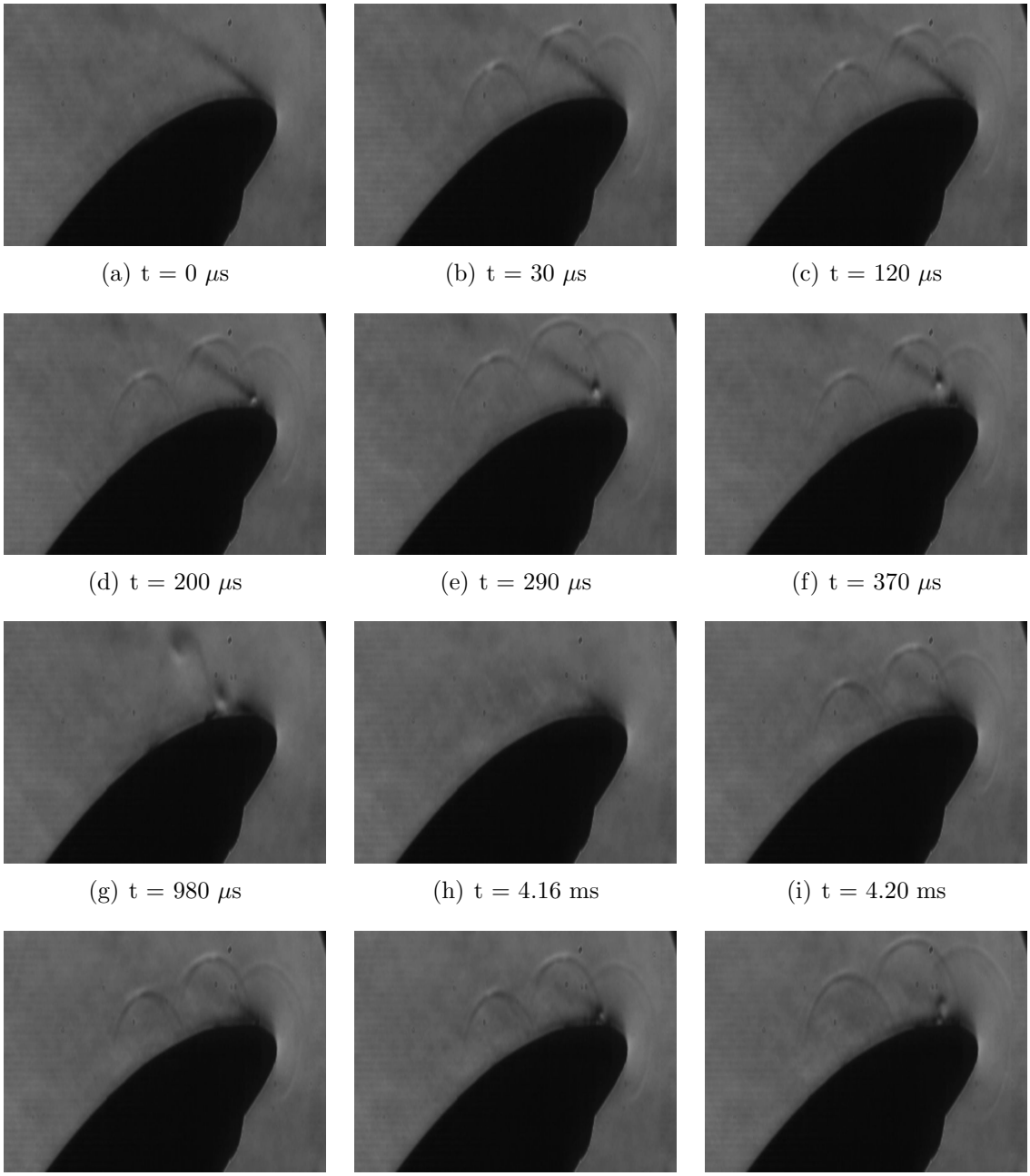

(a) t = 0 μs (b) t = 30 μs (c) t = 120 μs

(d) t = 200 μs (e) t = 290 μs (f) t = 370 μs

(g) t = 980 μs (h) t = 4.16 ms (i) t = 4.20 ms

(j) t = 4.28 ms (k) t = 4.37 ms (l) t = 4.46 ms

Fig. D.20: The figure continues on the next page

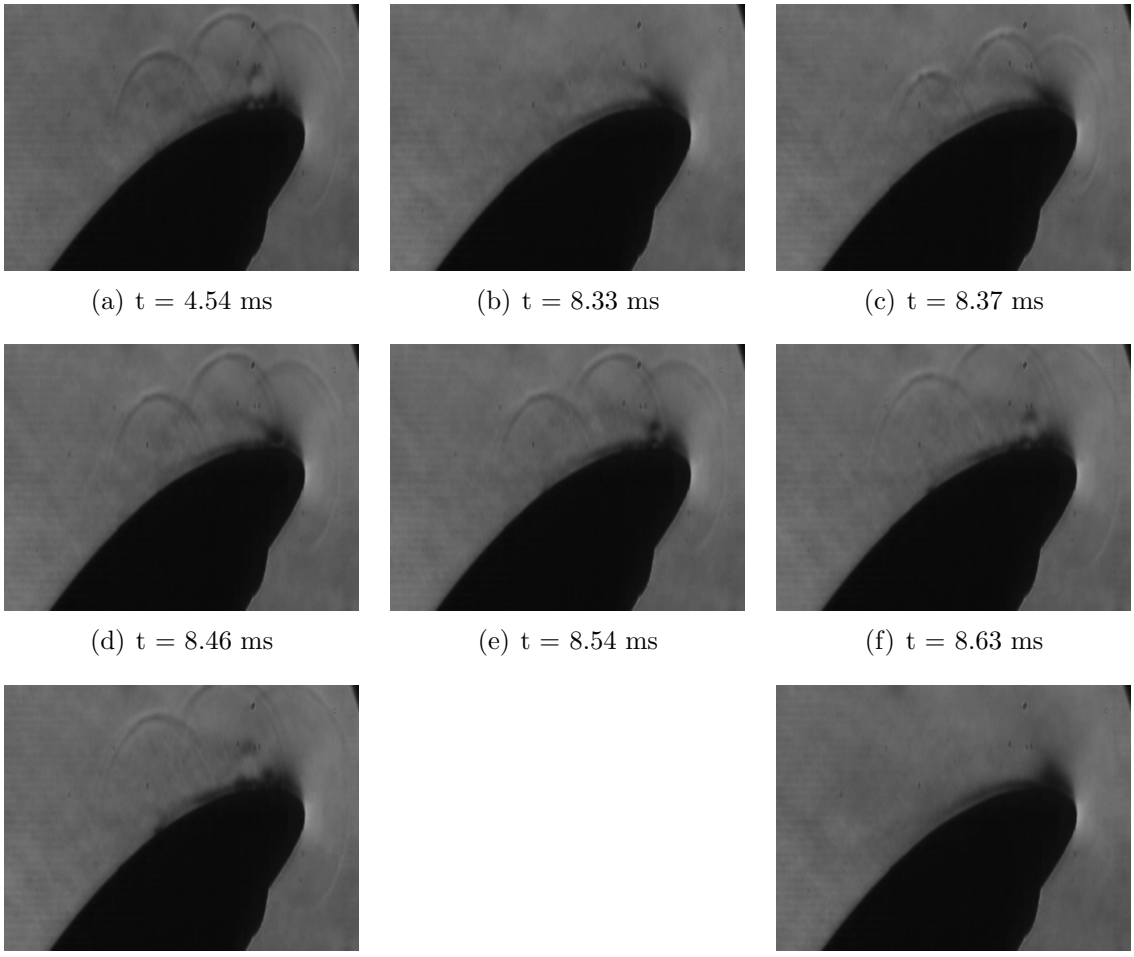

(a) t = 4.54 ms (b) t = 8.33 ms (c) t = 8.37 ms

(d) t = 8.46 ms (e) t = 8.54 ms (f) t = 8.63 ms

(g) t = 8.72 ms (h) t = 12.49 ms

Fig. D.21: AoA29.200hz.5p.100us.30m s.act 0-20-45 +0.2 0.15

Basically all the tests with different configuration of the actuator give results very similar to each other if only the mechanism of actuation is investigated. On the other hand, when the scalability is investigated it will be important to distinguish between the different configurations. For now, since the qualification of the mechanism of the actuation has been first investigated, there is not the need to make such a distinction. Firstly the tests for the Double actuator configuration are presented.

In the Fig.D.1 the result for an AoA26.50hz.30ms.act 0-20 +0.2 0.15 configuration is shown. In this test we could see two consecutive pulses with a frequency of 50 Hz and in this case the flow did not reattach.

In the Fig.D.3 the result for an AoA26.200hz.30ms.act 0-20 +0.2 0.15 configuration is shown. In this case the flow reattaches after 3 pulses.

In the Fig.D.5 the result for an AoA26.200hz.2p.300μs.30ms.act 0-20 +0.2 0.15 configuration is shown . In this case the flow is reattached after 2 bursts.

In the Fig.D.6 the result for an AoA26.200hz.2p.100μs.30ms.act 0-20 +0.2 0.15 configuration is shown. In this case the complete reattachment happen at the third bursts, but it is already partially reattached after the second one.

In the Fig.D.7 the result for an AoA29.200hz.30ms.act 0-20 +0.2 0.15 configuration is shown. In this case the actuation does not happen at all.

In the Fig.D.8 the result for an AoA29.200hz.2p.300us.30m s.act 0-20 +0.2 0.15 configuration is shown. Also in this case the actuation does not happen at all.

In the Fig.D.10 the result for an AoA29.200hz.5p.300us.30m s.act 0-20 +0.2 0.15 configuration is shown. In this case the actuator reattaches the separated flow after 2 bursts.

In the Fig.D.11 the result for an AoA29.200hz.5p.100us.30m s.act 0-20 +0.2 0.15 configuration is shown. In this case the flow is never fully reattached.

Secondly the results for triple actuator configuration as well are presented. The distinction between double and triple actuator has been made now in order to investigate the scalability property of the actuator. From a 'qualification of the actuation mechanism' point of view there are no many differences from the former presented set of results.

In the Fig.D.12 the result for an AoA26.50hz.30ms.act 0-20-45 +0.2 0.15 configuration is shown. Differently from the double actuator a complete reattachment of the flow (for the 25% of the chord) after the third pulse case is visible here.

In the Fig.D.13 the result for an AoA26.200hz.30ms.act 0-20-45 +0.2 0.15 configuration is shown. After 3 pulses the reattachment of the flow for the 25% of the chord is visible

In the Fig.D.14 the result for an AoA26.200hz.2p.300us.30ms.act 0-20-45 +0.2 0.15 configuration is shown. In this case the actuation happens already after 2 bursts (reattachment for the 25% of the chord).

In the Fig.D.15 the result for an AoA26.200hz.2p.100us.30ms.act 0-20-45 +0.2 0.15 configuration is shown. Here the reattachment is achieved after 2 bursts (again for the 25% of the chord).

In the Fig.D.16 the result for an AoA29.200hz.30ms.act 0-20-45 +0.2 0.15 configuration is shown. In this case a strange partial reattachment of the flow after 3 bursts has been achieved.

In the Fig.D.17 the result for an AoA29.200hz.2p.300us.30ms.act 0-20-45 +0.2 0.15 configuration is shown. In this case again a strange partial reattachment of the flow after 2 bursts has been achieved.

In the Fig.D.19 the result for an AoA29.200hz.5p.300us.30m s.act 0-20-45 +0.2 0.15 configuration is shown. Reattachment has been observed after 3 bursts(for about the 23% of the chord).

In the Fig.D.21 the result for an AoA29.200hz.5p.100us.30m s.act 0-20-45 +0.2 0.15 configuration is shown. Flow reattached has been observed here as well (for the 25% of the chord) after 3 bursts.

Acknowledgements

In order to make everyone understand how difficult and important it has been for me to get at this point today I need to say something about my story.

I came in the Netherlands in the January 2007 with the dream to enroll at Delft University of Technology in order to get a master degree. The first year I did not get enrolled since I was not able to fulfill the English level required. I failed the TOEFL test and this costed me the enrollment.

Unfortunately I did the English test other three times but I did not succeed in getting the required result, so I could not enroll also the year after, the 2008.

I started looking for a job, and I got a position at NEQLab Research BV, as experimentalist, it was the January 2009, two years later. One day I found in a drawer a project about Aerodynamics and I asked for taking over that research, hoping deeply inside to succeed in getting a Msc degree.

I actually did it, and thanks the support of my company I got enrolled, finally, as Master student at TUDelft, after three years.

Afterwards I did the TOEFL test for the fifth time, and eventually I got the required score.

The years between the 2009 and the 2011 have been very tough, being shared between a full time employment and a full time study.

The only reason why I have never given up on this dream is because I have been surrounded by incredible persons, and also by my family that even if far away from me, I always felt their love and their moral support.

I looked inside my heart and I found the force that made me struggle for my dream so hard.

And here I am today, and I need now to thank these people one by one. First of all I need to thank my friends Alessandro De Simone, Angelo Giuliano and Giovanni

Orlando. After I did not get enrolled the first year I moved back in Italy. I was very sad and depress. I did not have money and the university in Naples was not satisfying me. They, all of a sudden, surprised me buying me a one way ticket for moving back in Netherlands, in order to follow my dream. They believed in me so badly. I own everything to them. Thanks from the bottom of my heart.

I must thank my family, because they always believed in me, and today, when I go back home to visiting them, I can see the pride in their eyes, which thing makes me feel very happy. Thank you so much.

I want to thank my high school physics and math teacher, Maria Capone, which made get born in myself the love for the sciences. She is actually the first one who believed in me and if I am here today is because she put myself on the right path. Thank you.

I must thank Michiel Kruijff and Erik J van der Heide, they were my first bosses here in the Netherlands. They taught me so much, for me they are idols, and an example of life. Thank you guys.

I must thank my girlfriend for being so understanding. I have lived the last two years with about zero free time, and this must have been tough also for her. Thank you.

I want to thank friends like Fulviomaria Izzo, Davide Fezza, Serena Amendola and Giusy Tammaro for being always morally supporting me.

I must thank my colleagues at NEQLab Research BV. I have been growing up with these guys, they have been understanding, they helped me so much, and if I am here today is because such people believed in me. Thank to them I have been able to make this dream come true. Andrei Nikipelov, Paula Alonso, Cedric Boisdon, Sergey Pancheshnyi thank you for your support, you have been always cool with this my situation and I did appreciated it a lot. Ilia Popov for the great invaluable help. I will bring your teaching with me for ever. Thank you. Yury Leonov and Aleksandr Rakitin, they made everything begin. Thank you guys. And last but not least from NEQLab is professor Andrey Starikovskiy, the scientific advisor of NEQLab Research, who gave me precious teaching, and moral support.

I want to thank my friends Theo Michelis, Harry Kounenis and Siddharth Ravichandran for helping me during my study. Studying with them is actually fun. They helped me understanding very difficult things, and thank to their teachings I passed many exams. I will not forget that. Thank you.

I must thank all the people that worked around me at the university like: Nico van Beek, Stefan Bernardy, Frits Donker Duyvis, Peter J. Duyndam, Eric W. de Keizer and Leo Molenwijk. These persons are the one I must thank for helping me in carrying out my research, for all the precious teaching they gave me. Without them I would be the half of the researcher I am today. Thank you.

PhD students like Sina Ghaemi, Daniele Ragni and Marios Kotsonis gave me a big help as well performing tests, and actually helping with many ideas and suggestions.

Thank you.

I would like to thank my track supervisor, Dr. S.J. Hulshoff, who is the kindest person ever. He made me grow up with his advices and his moral support. He was the one replying to my request of starting a research project about Aerodynamics when I was working with NEQLab. He was one of the people that gave me the chance to get my dream come true. Thank you.

And last but not least I wish to thank my supervisor, Dr.ir. L.L.M. Veldhuis for all the energy he spent during the last two years for me. Always trying to make me do better and better. Leading me in this research with authority and honesty. For me he is an example to follow. I will be always grateful to him. I will bring his teachings always with me. Thank you professor.

FORZA NAPOLI !

...

Delft, The Netherlands
13th December 2011

Giuseppe Correale

Bibliography

[1] Prandtl L., "Über Flussigkeitsbewegung bei sehr kleiner Reibung", Proc.Third Int.Math.Congr.,Heidelberg, Germany, 484-491, 1904

[2] Mohamed Gad-el-Hak, "Flow Control: Passive, Active and Reactive", Cambridge University Press, chapter Introduciton, 2000

[3] Smith A.M.O., "Stratford's Turbulent Separation Criterion for Axially-Symmetric Flows". J.Applied Math & Physics 28, 929-939, 1977.

[4] Smith A.M.O., Stokes T.R.,Jr., Lee R.S., "Optimum Tail Shapes for Bodies of Revolution".J.Hydronautics 15, 67-73, 1981.

[5] Prandtl L., "The Mechanism of Viscous Fluids", Aerodynamic Theory,ed.W.F. Durand, vol.III, Springer-Verlag,Berlin, Germany, 1935.

[6] Truckenbrodt E., "Ein einfaches Näherungsverfahren zum Berechnen der laminaren Reibungsschicht mit Absaugung",Forschg. Ing.- Wes. 22, 147-157, 1956.

[7] Chang P.K., "Separation of Flow", Pergamon Press, Oxford, England, 1970.

[8] Schlichting H., Pechau.W., "Auftriebserhöhung von Tragflügeln durch kontinuierlich verteilte Absaugung". ZFW 7, 113-119, 1959.

[9] Illingworth C.R., "The Effect of Heat Transfer on the Separation of a Compressible Laminar Boundary Layer". Quart. J. Mech. Appl. Math. 7, 8-34, 1954.

[10] Morduchow M., Grape R.G., " Separation, Stability, and Other Properties of Compressible Laminar Boundary Layer with Pressure Gradient and Heat Transfer". NACA Technical Note No. TN-3296, Washington, D.C., 1955

[11] Gadd G.E., Cope W.F., Attridge J.L., "Heat-Transfer and Skin-Friction Measurements at a Mach Number of 2.44 for a Turbulent Boundary Layer on a Flat Surface and in Regions of Separated Flow". Aeronautical Research Council R&M No. 3148, London, England, 1958

[12] Lankford J.L., "Investigation of the Flow over an Axisymmetric Compression Surface at High Mach Numbers". U.S. Naval Ordnance Laboratory Report No. 6866, Corona, CA., 1960

[13] Rott N., "Unsteady Viscous Flow in the Vicinity of a Stagnation Point", Q.Appl. Math. 13,444-451, 1956

[14] Sears W.R., "Some Recent Developments in Airfoil Theory", J. Aeronaut.Sci. 23, 490-499, 1966

[15] Seifert A, Darabi A, Wygnanski I., "Delay of Airfoil Stall by Periodic Excitation". J. Journal of Aircraft 33[4] :691-698, 1996

[16] Glezer A, Amitay M, Honohan A., "Aspects of Low- and High-Frequency Actuation for Aerodynamic Flow Control".AIAA Journal 43[7]:1501-1511, 2005

[17] Darabi A, Wygnanski I., "Active Management of Naturally Separated Flow over a Solid Surface".Part 1. The Forced Reattachment Process. Journal of Fluid Mechanics 510:105-129, 2005

[18] Melton L, Schaeffler N, Yao C-S, Seifert A., "Active Control of Flow Separation from Supercritical Airfoil Leading-Edge Flap Shoulder".Journal of Aircraft 42[5]:1142-1149, 2005

[19] Corke T, Enloe C, Wilkinson S., "Dielectric Barrier Discharge Actuators for Flow Control". Annual Review of Fluid Mechanics 42:505-529, 2010

[20] Kotsonis M., Veldhuis L., "Experimental study on dielectric barrier discharge actuators operating in pulse mode", J. Appl. Phys. D: Appl. Phys. 108, 113304 (9pp), 2010

[21] Kotsonis M., Ghaemi S., Veldhuis L., Scarano F., "Measurement of the body force field of plasma actuators", J. Phys. D: Appl. Phys. 44, 045204 (11pp), 2011

[22] Seraudie A., Aubert E., Naude N., Cambronne J.P., " Effect of plasma actuators on a flat plate laminar boundary layer in subsonic conditions". Third AIAA Flow Control Conference, San Francisco, California, 5–8 January 2006.

[23] Jukes T.N., Choi K., Johnson G.A., Scott S.J., "Turbulent Drag Reduction by Surface Plasma through Spanwise Flow Oscillation". Third AIAA Flow Control Conference, San Francisco, California, 5–8 January 2006.

[24] Porter C.O., McLaughlin T.E., Enloe C.L., Font G.I., Roney J., Baughn J.W., "Boundary Layer Control Using a DBD Plasma Actuator". 45th AIAA Aerospace Sciences Meeting and Exhibit, Reno,Nevada, 8–11 January 2007.

[25] Post M, Corke T., "Separation Control on High Angle of Attack Airfoil Using Plasma Actuators". AIAA Journal 42[11]:2177-2184, 2004

[26] Mabe J.H., Calkins F.T., Wesley B., Woszidlo R., Taubert L., Wygnanski I., "On the Use of Single Dielectric Barrier Discharge Plasma Actuators for Improving the Performance of Airfoils". 37th AIAA Fluid Dynamics Conference and Exhibit, Miami,Florida, 25–28 June 2007.

[27] Forte M., Jolibois J., Pons J., Moreau E., Touchard G., Cazalens M., "Optimization of a Dielectric Barrier Discharge Actuator by Stationary and Non-Stationary Measurements of the Induced Flow Velocity": Application to Airflow Control. Experiments in Fluids 43:917-928, 2007

[28] Abe T., Takizawa Y., Sato S., Kimura N., "Experimental study for momentum transfer in a dielectric barrier discharge plasma actuator". AIAA Journal 46[9]:2248-2256, 2008

[29] Dong B., Bauchire J.M., Pouvesle J.M., Magnier P., Hong D., "Experimental study of a DBD surface discharge for the active control of subsonic airflow". J.Phys. D: Appl. Phys. 41, 155201, 2008[U+0352]

[30] Enloe C., McHarg M., McLaughlin T., "Time-Correlated Force Production Measurements of the Dielectric Barrier Discharge Plasma Aerodynamic Actuator". Journal of Applied Physics 103[073302]:1-7, 2008

[31] Hoskinson A., Hershkowitz N., Ashpis D., "Force measurements of single and double barrier DBD plasma actuators in quiescent air". Journal of Physics D: Applied Physics 41[245209]:1-9, 2008

[32] Thomas F., Corke T., Igbal M., Kozlov A., Schatzman D., "Optimization of Dielectric Barrier Discharge Plasma Actuators for Active Aerodynamic Flow Control". AIAA Journal 47[9]:2169-2178, 2009

[33] Schlichting H. and Gersten K., "Boundary Layer Theory". [U+0351]Springer, Berlin, 2000.

[34] Sturzebecher D. and Nitsche W., "Active cancellation of Tollmien–Schlichting instabilities on a wing using multi-channel sensor actuator systems". Int. J. Heat Fluid Flow 24, 572, 2003.

[35] Grundmann S. and Tropea C., "Active cancellation of artificially introduced Tollmien–Schlichting waves using plasma actuators". Exp. Fluids 44, 795, 2008.

[36] Grundmann S. and Tropea C., "Experimental damping of boundary-layer oscillations using DBD plasma actuators". Int. J. Heat Fluid Flow 30, 394, 2009.

[37] Post M.L. and Corke T.C., "Separation control using plasma actuators : Dynamic stall vortex control on oscillating airfoil". AIAA J. 44, 3125, 2006.

[38] Jukes T.N. and Choi K., "Flow control around a circular cylinder using pulsed dielectric barrier discharge surface plasma". Phys. Fluids 21, 084103, 2009.

[39] Gregory J.W., Enloe† C.L., Font G.I., McLaughlin T.E., "Force Production Mechanisms of a Dielectric-Barrier Discharge Plasma Actuator". 45th AIAA Aerospace Sciences Meeting and Exhibit 8-11, Reno, Nevada, January 2007

[40] Abe T., Takizawa Y., Sato S., Kimura N., "A Parametric Experimental Study for Momentum Transfer by Plasma Actuator". 45th AIAA Aerospace Sciences Meeting and Exhibit 8-11, Reno, Nevada, January 2007

[41] Roth J., Dai X., "Optimization of the Aerodynamic Plasma Actuator as an Electrohydrodynamic (EHD) Electrical Device". AIAA Paper 2006-1203, 2006

[42] Forte M., Jolibois J., Moreau E., Touchard G., and Cazalens M., "Optimization of a Dielectric Barrier Discharge Actuator by Stationary and Instationary Measurements of the Induced Flow Velocity, Application to Airflow Control," AIAA Paper 2006-2863, 2006.

[43] Bletzinger P., Ganguly B.N., VanWie D., Garscadden A., "Plasmas in High Speed Aerodynamics". Journal of Physics D: Applied Physics, Vol. 38, pp. R33–R57, 2005.

[44] Klimov A.I., Koblov A.N., Mishin G.I., Serov Y.L., Yavor I.P., "Shock Wave Propagation in a Glow Discharge". Soviet Technical Physics Letters, Vol. 8, pp. 192–194, 1982.

[45] Meyer R., Palm P., Ploenjes E., Rich J.W., Adamovich I.V., "Nonequilibrium Radio Frequency Discharge Plasma Effect on a Conical Shock Wave: M 2:5 Flow". AIAA Journal, Vol. 41, No. 5, pp. 465–469, 2003.

[46] Macheret S.O., Ionikh Y.Z., Chernysheva N.V., Yalin A.P., Martinelli L., Miles R.B., "Shock Wave Propagation and Dispersion in Glow Discharge Plasmas". Physics of Fluids, Vol. 13, No. 9, pp. 2693–2705, Sept. 2001.

[47] Khorunzhenko V.I., Roupassov D.V., Starikovskaia S.M., Starikovskii, A.Y., "Hypersonic Shock Wave Low Temperature Nonequilibrium Plasma Interaction". AIAA Paper AIAA2003-5048,2003.

[48] Opaits D.F., Roupassov D.V., Starikovskaia S.M., Starikovskii A.Y., "Shock Wave Interaction with Nonequilibrium Plasma of Gas Discharge". 42nd AIAA Aerospace Sciences Meeting and Exhibit, AIAA, Reston, VA, 2004.

[49] Shang J.S., "Plasma Injection for Hypersonic Blunt Body Drag Reduction". AIAA Journal, Vol. 40, No. 6, pp. 1178–1186, 2002.

[50] Kolesnichenko Y.F., Brovkin V.G., Khmara D.V., Lashkov V.A., Mashek I.C. , Ryvkin M.I., "Fine Structure of MW Discharge: Evolution Scenario". 2004 4th International Workshop on Thermochemical and Plasma Processes in Aerodynamics, Publisher, Publisher Location, July 2004.

[51] Opaits D.F., Roupassov D.V., Saddoughi S.G., Starikovskaia S.M., Zavialov I.N., Starikovskii A.Y., "Plasma Control of Boundary Layer Using Low-Temperature Non-Equilibrium Plasma of Gas Discharge". AIAA Paper 2005-1180, 2005.

[52] Roupassov D.V., Zavyalov I.N., Starikovskii A.Y., Saddoughi S.G., " Boundary Layer Separation Plasma Control Using Low-Temperature Non-Equilibrium Plasma of Gas Discharge". AIAA Paper 2006-373, 9–12 Jan. 2006.

[53] Patel M.P., Ng T.T., Vasudevan S., Corke T.C., Post M.L., McLaughlin T.E., Suchomel C.F., "Scaling Effects of an Aerodynamic Plasma Actuator". AIAA Paper 2007-635, 8–11 Jan, 2007.

[54] Roupassov D.V., Zavyalov I.N., Starikovskii A.Y., Saddoughi S.G., " Boundary Layer Separation Control by Nanosecond Plasma Actuators". AIAA Paper 2007-4530, 2007.

[55] Sidorenko A.A., Zanin B.Y., Postnikov B.V., Budovsky A.D., Starikovskii A.Y. , Roupassov D.V., Zavialov I.N., Malmuth N.D., Smereczniak P., Silkey J.S., "Pulsed Discharge Actuators for Rectangular Wing Separation Control". AIAA Paper 2007-941, 8–11 Jan. 2007.

[56] Roupassov D., Nikipelov A, Nudnova M, Starikovskii A., "Flow Separation Control by Plasma Actuator with Nanosecond Pulsed-Periodic Discharge". AIAA Journal 47[1]:168-185 , 2009

[57] Raizer Y.P., "Gas Discharge Physics". Springer–Verlag, Berlin, 1991.

[58] Little J., Takashima K., Nishihara M., Adamovich I., Samimy M., "High Lift Airfoil Leading Edge Separation Control with Nanosecond Pulse Driven DBD Plasma Actuators". 5th Flow Control Conference, Chicago, Illinois, 2010-4256, 28 June-1 July 2010.

[59] Correale G., Popov I.B., Rakitin A.E., Starikovskii A.Yu., Hulshoff S.J., Veldhuis L.L.M., "Flow Separation Control on Airfoil With Pulsed Nanosecond Discharge Actuator".AIAA Paper 2011-1079, 2011

[60] Rethmel C., Little J., Takashima K., Sinha A., Adamovich I., Samimy M., " Flow Separation Control over an Airfoil with Nanosecond Pulse Driven DBD Plasma Actuators". AIAA Paper 2011-487, 2011.

[61] Garner H.C. et al, "Subsonic Wind Tunnel Wall Corrections", AGARDograph 109, 1966

[62] Squire H.B. , "The lift and Drag of a Rectangular Wing Spanning a Free Jet of Circular Section", Philosophical Magazine, Series 7, Vol. 27, No. 181, Feb 1939

[63] Bakker P.,Van Leer B., "Lecture Notes on Gasdynamics",Delft, Feb 2005